

HIGH-ENERGY NEUTRINO ASTROPHYSICS

John G. Learned

*Department of Physics and Astronomy, University of Hawaii at Manoa,
 Honolulu, Hawaii 96822; e-mail: jgl@phys.hawaii.edu*

Karl Mannheim

*University Observatory, Geismarlandstrasse 11, D-37083 Göttingen, Germany;
 e-mail: kmannhe@uni-sw.gwdg.de*

Key Words neutrinos, neutrino astronomy, cosmology, cosmic rays, dark matter

■ **Abstract** High-energy (> 100 MeV) neutrino astrophysics enters an era of opportunity and discovery as the sensitivity of detectors approaches astrophysically relevant flux levels. We review the major challenges for this emerging field, among which the nature of dark matter, the origin of cosmic rays, and the physics of extreme objects such as active galactic nuclei, gamma-ray bursts, pulsars, and supernova remnants are of prime importance. Variable sources at cosmological distances allow the probing of neutrino propagation properties over baselines up to about 20 orders of magnitude larger than those probed by terrestrial long-baseline experiments. We review the possible astrophysical sources of high-energy neutrinos, which also act as an irreducible background to searches for phenomena at the electroweak and grand-unified-theory symmetry-breaking scales related to possible supersymmetric dark matter and topological defects. Neutrino astronomy also has the potential to discover previously unimagined high-energy sources invisible in other channels and provides the only means for direct observations of the early universe prior to the era of decoupling of photons and matter. We conclude with a discussion of experimental approaches and a short report on present projects and prospects. We look forward to the day when it will be possible to see the universe through a new window in the light of what may be its most numerous particle, the elusive neutrino.

CONTENTS

1. INTRODUCTION	680
1.1 Neutrinos in Astrophysics and Cosmology	682
2. NEUTRINO BACKGROUND EMISSION—KNOWN SOURCES	684
2.1 Atmospheric Neutrinos	684
2.2 Neutrinos Due to Cosmic Rays Hitting the Sun	691
2.3 Neutrinos from the Galactic Disk	692
2.4 Gamma-Ray Astronomy with Muons	693
3. BOUNDS ON DIFFUSE HIGH-ENERGY NEUTRINO RADIATION	693
3.1 Theoretical Bounds Based on Diffuse Gamma Rays and Cosmic Rays	694

3.2	Experimental Bounds	697
4.	CANDIDATE ASTROPHYSICAL SOURCES OF NEUTRINOS	698
4.1	Fermi Acceleration	699
4.2	Generic Models of Astrophysical Production of Neutrinos	702
4.3	Galactic Candidates	704
4.4	Extragalactic Candidates	707
5.	NEUTRINOS FROM DARK MATTER AND OTHER INTERESTING PHYSICS SIGNATURES	712
5.1	Cosmological High-Energy Neutrinos	712
5.2	Multiple Production of W Bosons and Such	716
5.3	Peculiar Features in the Neutrino Cross Section	716
5.4	Cosmological Neutrino Absorption (Weiler Process)	717
5.5	Tau Appearance in Astrophysical Long-Baseline Experiments	718
5.6	Neutrino Mass Measurement Using Time-Variable Astrophysical Sources	718
6.	EXPERIMENTAL APPROACHES	719
6.1	Survey of Techniques	720
6.2	Neutrino Telescope Design Principles	732
7.	EXISTING AND PROPOSED PROJECTS	738
7.1	Related Smaller and Lower-Energy-Threshold Projects	738
7.2	Second-Generation Projects	739
7.3	Future Projects	740
8.	SUMMARY AND CONCLUSIONS	742

1. INTRODUCTION

Compared with photon astronomy, neutrino astronomy is still in its infancy. We know that stars and supernovae emit neutrinos at roughly the level expected from the nuclear reactions going on in their centers. This can be concluded from observations of neutrinos emitted by the Sun and by the supernova SN1987A. However, the extremely low cross section of weak interactions and the poor angular resolution at nuclear energies represent major obstacles in advancing stellar neutrino astronomy much beyond targets like the Sun and a few nearby supernovae.

The prospects for initiating neutrino astronomy are much better at high energies for three major reasons: (a) the increase of the neutrino cross section, muon range, and angular resolution with energy; (b) the opportunity to use large natural target media (water, ice, atmosphere); and (c) the great potential for significant discovery. Neutrino telescopes will let us peer into the densest places of the universe (hidden to photon astronomy), will reveal unseen details of the ultimate energy release during the collapse of matter, and might even give crucial insights into the nature of dark matter. High-energy neutrino telescopes have been discussed in many reviews (1–5) documenting the rapid progress in this field. Following the pioneering experiments BAIKAL (6) and DUMAND (7), which demonstrated the detection technique, prototypes such as AMANDA (8), ANTARES (9), and NESTOR (10) currently explore the possibilities of using either the Antarctic ice or deep ocean water to build large telescopes reaching astrophysical

sensitivity. Cubic-kilometer-scale neutrino telescopes such as the proposed ICE-CUBE observatory (11) are now the main theme, and the prospects of finding celestial sources seem tantalizingly close. In this chapter, we hope to provide a global perspective on the recent developments in detector design and the rapidly moving frontier in high-energy astrophysics as it relates to future neutrino observations.

In the shadow of the well-known thermal inventory of the universe, as observed in the emissions of the stars, the gas, and the dust in galaxies, there is a dynamically important nonthermal inventory consisting of relativistic particles, turbulent plasma, and magnetic fields. The nonthermal universe is one of cataclysmic phenomena associated with stellar explosions and, possibly, out-of-equilibrium production of particles in the early universe.

Photon astronomy has recently made considerable progress at high energies, based on the successes of the Compton Gamma Ray Observatory (CGRO) (12) and imaging air Cherenkov telescopes such as Whipple and HEGRA (13–15). There have been striking discoveries of sources with extreme physical conditions, but the range for further gamma astronomical exploration is limited by the attenuation of gamma rays from very distant sources due to pair production in interactions with low-energy photons of the cosmic background radiation (16–22). At a few hundred TeV, gamma rays do not survive the journey from the center of our galaxy. At a few hundred GeV, gamma rays can reach us from other galaxies but not from the (bright phase) era of maximum quasar activity or across any other cosmologically interesting distance (see Figure 1). The view to the early universe is forever hidden from photon astronomy because of the photon-matter coupling barrier. In those regions from which both neutrinos and gammas can be observed, detection in both

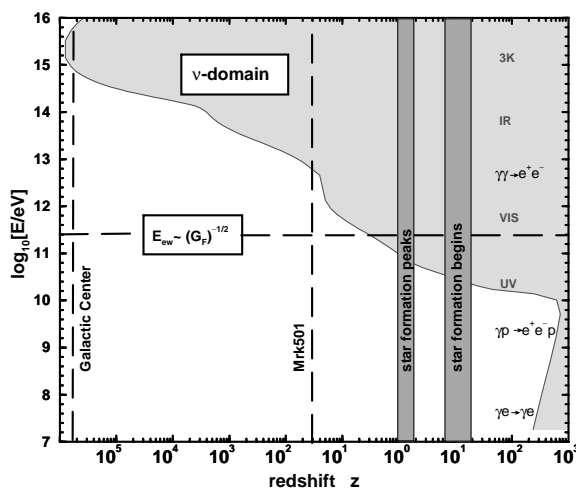


Figure 1 Gamma-ray horizon ($h = 0.6$, cold-dark-matter cosmology) due to various absorption processes (predominantly photon-photon pair production in the metagalactic radiation field) based on the work of Svensson & Zdziarski (17) and Kneiske et al (22). The shaded area is invisible for gamma-ray astronomy.

regimes can be a very powerful tool for understanding the most energetic objects seen in the universe.

After we elaborate on the potential of neutrino astronomy and elementary neutrino properties, Section 2 starts with an account of known sources of high-energy neutrinos producing an irreducible (and in itself interesting) background for neutrino telescopes. Other classes of sources are more speculative, and we discuss theoretical and experimental bounds on their total (cumulative) flux in Section 3. Section 4 summarizes important models of high-energy neutrino production and compares the expected fluxes from individual astrophysical sources. The fascinating realm of astrophysical particle accelerators entails the possibility of exotic sources of neutrinos involving non-standard-model physics, which is the subject of Section 5. In Section 6, we review neutrino detection techniques.

The main efforts of current experiments rely on the so-called optical Cherenkov technique, first suggested by Markov (23) and by Greisen (24) in 1960. Upward or horizontal muons produced by charged-current (CC) interactions of muon neutrinos produce optical Cherenkov light, which is easily detected by photomultipliers buried in an optically transparent medium such as water or deep ice. Other techniques reviewed here involve horizontal air showers, acoustic detection, and radio detection, some of which will be pursued in future experiments.

1.1 Neutrinos in Astrophysics and Cosmology

If the technical obstacles confronting cubic-kilometer detectors can be overcome, high-energy neutrino astrophysics can address a number of fundamental questions in astrophysics and cosmology. Among these are the nature of dark matter, the origin of the cosmic rays, and the extreme physics responsible for gravitational energy release in the most luminous objects in the universe.

Dark matter and its special relation with weak interactions has provoked many challenging speculations. Nonrelativistic particles that have frozen out of the thermal equilibrium in the early universe contribute a present-day density (in units of the critical density of the universe) proportional to the inverse of their annihilation cross section averaged over thermal velocities $\Omega_{\text{dm}} \propto \langle \sigma_A v \rangle^{-1}$, as described in detail in Kolb & Turner's classic textbook (26). This implies that weakly interacting particles should dominate the dark matter. Weakly interacting massive particles (WIMPs) with a mass near the electroweak-symmetry-breaking scale $E_{\text{ew}} = (\sqrt{2}G_F)^{-1/2} \simeq 246 \text{ GeV}$, such as those predicted by some supersymmetric theories, are therefore among the prime candidates for the cold dark matter. The known neutrinos appear to have mass, but a very small one (27). It has been estimated that the three known families of left-handed neutrinos and their antineutrinos contribute $\Omega_\nu < 0.15$ (28, 29). Even the maximally allowed contribution cannot obviate the need for a cold dark matter candidate with $\Omega_{\text{dm}} \sim 0.3$, since neutrinos are relativistic at decoupling, washing out small structures such as those that grow to become galaxies. If WIMPs are indeed the cold dark matter component, their possible annihilations or decays would lead to an observable flux of high-energy neutrinos at $E_\nu < E_{\text{ew}}$, allowing the determination of their mass and density.

A common source of neutrinos are the interactions of cosmic rays with various targets [see the books by Berezhinsky et al (30) and by Gaisser (31)]. Since the spectrum of cosmic rays extends from subrelativistic to ultrarelativistic energies (with individual particle energies reaching up to 50 J in the most energetic events), the corresponding spectrum of cosmic neutrinos has an extremely broad range, too. Almost 100 years after the discovery of cosmic rays, their origin is still not clear, mainly because the deflection of the charged particles in the magnetized interstellar medium washes out directional information.

Neutrinos and gamma rays propagate along straight lines, but the limited range of the gamma rays traveling through diffuse cosmic low-energy radiation fields (see Figure 1) highlights the importance of neutrinos as the only available long-range directional carrier of information about the origin of cosmic rays. The gamma-ray mean free path becomes as short as a few thousand light years in the hundred-TeV range, which is much too short to survey even our own galaxy for the places of cosmic-ray acceleration.

The spectrum of diffusing cosmic rays steepens during propagation, implying that the neutrino spectra produced at the sources of the cosmic rays must be flatter than the original cosmic-ray spectrum. At energies below 10 GeV, where the range of gamma rays does not pose a problem, the gamma-ray sky as seen by CGRO shows a very large number of potential sources of cosmic rays. Indeed, it is found that some sources emit most of their power in gamma rays, with the most luminous ones being among the most distant.

The production mechanism for nonthermal gamma rays is, however, not unique at energies where electron acceleration is not yet quenched by radiation losses. Thus, such gamma rays can be attributed either to accelerated electrons (synchrotron radiation, bremsstrahlung, inverse Compton scattering) or protons and ions (meson production). In the latter case, the gamma rays suffer electromagnetic cascading before escape, and it is impossible to infer the spectrum of the accelerated protons from the measured gamma-ray spectrum. Because cosmic-ray protons (and ions) carry almost two orders of magnitude more power than cosmic-ray electrons on top of the Earth's atmosphere, it is important to pinpoint the sources of proton acceleration and to clarify the particle acceleration mechanism behind the enormously efficient transfer of gravitationally released energy into these relativistic particles.

New windows to the universe have been opened up by the discovery of gamma rays from sources with extreme physical conditions, such as the supermassive black holes in the centers of active galaxies or the collapsing objects believed to be responsible for gamma-ray bursts, the most luminous cataclysmic events in the universe. Neutrinos emerging from such sources diagnose the in situ physical conditions inside the cauldrons, unaffected by the intervening scattering processes, and therefore carry the most crucial information about the nature of the most powerful energy-release processes that occur in strong gravitational fields.

Most putative astrophysical neutrino sources are thought to be too weak to be individually detected by the next generation of neutrino telescopes. However, these unresolved sources will produce a diffuse isotropic neutrino background at high

energies. The calorimetric measurement of this background is important because that background could provide the first evidence of neutrinos from hidden sources or neutrinos related to dark-matter interactions.

2. NEUTRINO BACKGROUND EMISSION—KNOWN SOURCES

We begin the discussion of possible natural neutrino sources with an exposition of the local background due to cosmic rays. We discuss the Earth as filter and the detectability of neutrinos. Thereafter we discuss several related guaranteed sources of neutrinos from the interaction of cosmic rays with the Sun and with matter in the galactic disk. We also mention the potential for large neutrino detectors to detect very-high-energy (VHE) gamma-ray point sources via muon signals underground.

2.1 Atmospheric Neutrinos

Neutrinos are produced in abundance by high-energy cosmic rays impinging on the Earth's atmosphere. These neutrinos, spanning energies from a few MeV to the highest-energy cosmic rays, provide a background against which one must discriminate to detect extraterrestrial sources, but they have been enormously useful as a test beam in which muon neutrino oscillations were discovered, providing the first convincing evidence for neutrino mass.

The atmosphere is constantly and uniformly bombarded with cosmic rays. These consist mostly of protons, but also heavy nuclei (9% alpha particles, 1% heavier nuclei), electrons, and even neutral particles. The neutrinos arise from the decay of pions and other mesons in the atmosphere and from the decay of muons (for a good introduction see Reference 31). The Earth's magnetic field and other magnetic fields cut off the lower-energy particles from the Sun and more distant sources, so that the mean incoming kinetic energy is around 1 GeV.

Particles in the multi-GeV range make showers in the atmosphere (which is roughly 10 interaction lengths thick), presenting an absorber of 1030 gm/cm^2 vertical column density. The density of the atmosphere decreases approximately exponentially with height, with a scale height of $h_o \simeq 8.4 \text{ km}$. The energies at which pion and kaon decay lengths equal the scale height h_o of the atmosphere are $\epsilon_\pi = \frac{m_\pi h_o}{c\tau_\pi} = 115 \text{ GeV}$ and $\epsilon_{K^\pm} = \frac{m_K h_o}{c\tau_{K^\pm}} = 850 \text{ GeV}$, respectively. The proton-air interaction length is about $\Lambda_{p\text{-air}} = 86 \text{ gm/cm}^2$ at 100 GeV, decreasing to roughly 43 gm/cm^2 at 1 EeV ($= 10^{18} \text{ eV}$). The secondary particles from cosmic-ray-air-nucleus interactions may interact themselves ($\Lambda_{\pi\text{-air}} = 116 \text{ gm/cm}^2$ and $\Lambda_{K\text{-air}} = 138 \text{ gm/cm}^2$ at 100 GeV) or decay. This competition between interaction and decay makes the spectrum for the decay products steeper by one power in the energy.

At energies below several GeV, the muons (produced mostly in charged pion decay) themselves decay. Starting with charged pions and averaging over the nearly equal numbers of positive and negative pions yields two muon neutrinos for each

electron neutrino. Moreover, the energy sharing in the decays is such that the resulting neutrinos are also of nearly equal energy. These decay kinematics are of course well-known, and so the ratio of muon neutrinos to electron neutrinos (<5 GeV) can be calculated with rather good accuracy, about 5%, almost independent of the cosmic-ray spectrum (32). Yet, the 20% absolute flux uncertainty for the low-energy atmospheric neutrinos constitutes a serious impediment to progress in untangling the oscillation parameters.

The higher-energy atmospheric muon neutrino (differential) flux can be approximated as a power law with a spectral index of about -3.7 up to 1 PeV and roughly -4.0 above 1 PeV. The electron neutrinos, which arise largely from muon decay, decline more swiftly above several GeV, decreasing to about 1% of the muon neutrino flux at the higher energies (TeV), where they arise mostly from kaon decay.

There is an angular variation in the neutrino flux, more prominent at higher energies, called the secant theta effect. This effect occurs because pions and muons that are produced nearly tangent to the Earth have more flight time in less dense atmosphere, so they have more chance to decay and make neutrinos. Hence there is a peak near the horizontal arrival direction in the atmospheric neutrino angular distribution. This peak is symmetric about the horizon for any location (except at the lowest neutrino energies, below around 400 MeV, where geomagnetic effects spoil the symmetry somewhat).

In this review, following a common convention in the cosmic-ray literature, we refer to the zenith angle as θ^* at production instead of the zenith angle θ at the detector. The connection is $\sin(\theta^*) = \sin(\theta)(R_e - D)/(R_e + h)$, where R_e = Earth radius, D = detector depth, and h = production altitude.

A simple analytic form suffices to describe the atmospheric muon neutrino ($\nu_\mu + \bar{\nu}_\mu$) flux at energies from about 10 GeV through 100 TeV (33):

$$\frac{d^2\Phi_{\nu_\mu}}{dE_\mu d\Omega} \simeq 0.0286 E_\mu^{-2.7} \left(\frac{1}{1.0 + \frac{6.0 E_\mu \cos(\theta^*)}{115 \text{ GeV}}} + \frac{0.213}{1 + \frac{1.44 E_\mu \cos(\theta^*)}{850 \text{ GeV}}} \right) / \text{cm}^2 \text{ s sr GeV}. \quad 1.$$

The cosmic-ray muon flux may be described by a similar form:

$$\frac{d^2\Phi_\mu}{dE_\mu d\Omega} \simeq 0.185 E_\mu^{-\gamma} \left(\frac{1}{1 + \frac{1.1 E_\mu \cos(\theta^*)}{115 \text{ GeV}}} + \frac{0.054}{1 + \frac{1.1 E_\mu \cos(\theta^*)}{850 \text{ GeV}}} \right) / \text{cm}^2 \text{ s sr GeV} \quad 2.$$

with $\gamma = 2.78 \pm 0.05$ (34).

The electron neutrino flux, similarly, is described by

$$\begin{aligned} \frac{d^2\Phi_{\nu_e}}{dE_{\nu_e} d\Omega} \simeq 0.0024 E_\nu^{-2.7} & \left(\frac{0.05}{1.0 + \frac{1.5 E_\nu \cos(\theta^*)}{850 \text{ GeV}}} + \frac{0.185}{1.0 + \frac{1.5 E_\nu \cos(\theta^*)}{194 \text{ GeV}}} \right. \\ & \left. + \frac{11.4/E_\nu}{1 + \frac{1.21 E_\nu \cos(\theta^*)}{115 \text{ GeV}}} \right) / \text{cm}^2 \text{ s sr GeV}. \quad 3. \end{aligned}$$

These formulas are good to about 5% in shape but are uncertain in absolute magnitude to perhaps 20% (35). The various atmospheric fluxes are illustrated in

Figure 2 (36). The top three panels show Monte Carlo-simulated spectra for μ , ν_μ , and ν_e , with contributions from π and K decays. While muons are dominantly the product of pion decay, muon neutrinos above 200 GeV arise dominantly from kaon decay. It is also apparent that electron neutrinos are suppressed by nearly two orders of magnitude relative to muon neutrinos.

A good approximation to the depth-intensity relation for muons is

$$I_\mu(x) = A \left(\frac{x_o}{x} \right)^\alpha e^{-\frac{x}{x_o}}, \quad 4.$$

where $A = (2.15 \pm 0.08) \times 10^{-6} / \text{cm}^2 \text{s sr}$, $\alpha = 1.93^{+0.20}_{-0.12}$, and $x_o = (1.155^{+0.060}_{-0.030}) \text{ kmwe}$, and where the depth is in kilometers water equivalent of “standard rock” (34).

2.1.1 Charm Decay

The three lower panels of Figure 2 show the spectra that arise from D and Λ decays and here are seen to yield flavor-independent fluxes. Because this “direct production” is not suppressed by competition between decay and interaction in the atmosphere, it has roughly the same spectrum as the primary cosmic rays. For the same reason, it lacks angular variation (no peaking near the horizon except above PeV energies). Many calculations have been carried out, but the results

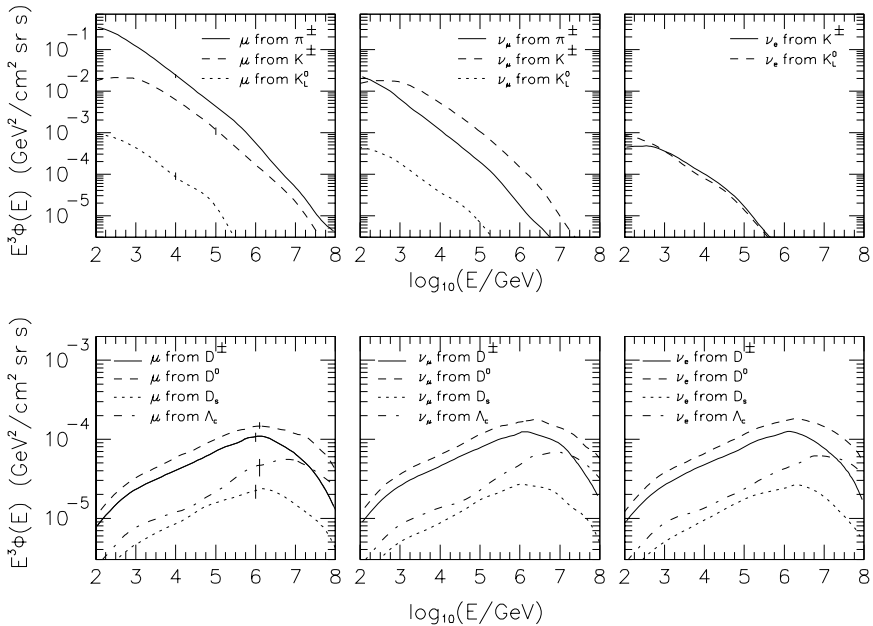


Figure 2 The vertical E^3 -weighted flux of muons ($\mu^+ + \mu^-$), muon neutrinos ($\nu_\mu + \bar{\nu}_\mu$), and electron neutrinos ($\nu_e + \bar{\nu}_e$) from decays of the specified particles. Error bars indicate the statistical precision of the Monte Carlo simulation. (From Reference 36 with permission.)

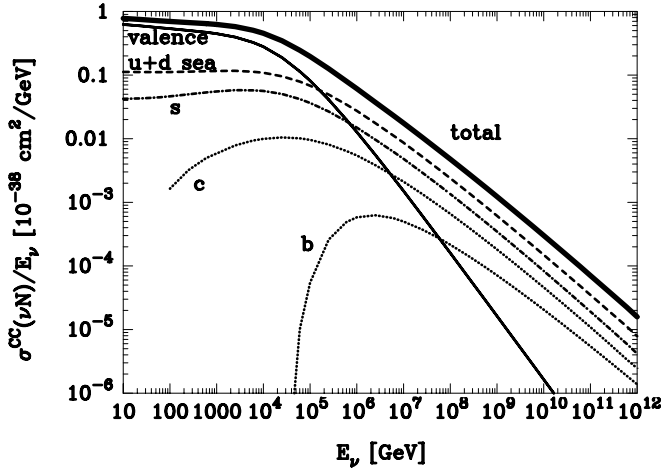


Figure 3 Components of the νN charged-current cross section as functions of the neutrino energy for the CTEQ3 distributions. (From Reference 38 with permission.)

remain imprecise. The expectation of the energy at which direct neutrinos become dominant ranges from about 20 TeV (for vertical neutrinos) to 1 PeV (for near-horizontal neutrinos), depending strongly on the model (37).

2.1.2 Neutrino Cross Sections

We cannot go into detail about the neutrino cross-section calculations here but mention the subject because it relates to all considerations of observations of neutrinos. Figure 3 shows the neutrino-nucleon (with the nucleon taken as half proton and half neutron) cross section divided by energy over a range from 10 GeV to the energy of the highest-energy cosmic rays. The cross section remains nearly linear with energy until ~ 10 TeV and then rises more slowly with $E^{0.41}$. One can observe the significant contribution of the sea quarks; the heavier quarks (s , c , and b) contribute at higher energies. The calculations are fairly reliable (error $< 20\%$) up through energies equivalently accessible at accelerators (e.g. HERA) around 1 PeV and are uncertain to perhaps a factor of two at the highest energies.

The featureless rise of the neutrino cross sections with energy is dramatically interrupted in the case of the $\bar{\nu}_e + e^- \rightarrow W^-$ (Glashow) resonance at 6.3 ± 0.7 PeV, where the integral cross section reaches $1/2 \mu\text{b}$, 300 times the $\nu_\mu N$ cross section (38). With an absorption length of $\simeq 60$ kmwe, the electron antineutrinos are restricted to arrival from the upper hemisphere at underground detectors in this energy range, with interesting (though perhaps not measurable) effects near the horizon. As discussed below, if we observe high-energy muons from $\nu_\mu N$ interactions, the $\bar{\nu}_e$ -induced cascade signature plus ν_τ flux observation via the double-bang signature may make it possible to decipher the incoming flavor mix in this energy range.

2.1.3 Underground Muons

The increasing range of muons with energy plus the growth of the $\nu_\mu N$ cross section with energy make muons an efficient means of detecting high-energy neutrinos. The effective target volume for an underground muon detector of area A_μ is $V(E_\mu) \simeq R(E_\mu)A_\mu$. With the muon energy-loss relation of $-dE_\mu/dx = a(E_\mu) + b(E_\mu)E_\mu$, a rough approximation to the muon range is $R(E_\mu, E_\mu^{\min}) = \frac{1}{b} \ln \frac{a+bE_\mu}{a+bE_\mu^{\min}}$, where $a \simeq 0.2$ TeV/kmwe and $b \simeq 0.39$ kmwe.

This leads one to contemplate the relative effectiveness of neutrino detectors that detect all events contained in some volume (volume arrays) versus detectors that register only traversing muons (area arrays), both of which have some threshold energy. A volume array senses all events above threshold inside that geometry and reconstructs the direction of the cascade, though usually with lower precision than muon trajectory reconstruction affords (typically 10° versus 1°). However, if we ignore the threshold question, then we can compare the relative effectiveness of volume and area array. If the volume is 1 km^3 and the surface area is 1 km^2 for a monoenergetic neutrino source, the effective volumes for muon and cascade detection will be equal at 240 GeV and muon detection will win at higher energies. Of course the advantage of volume detection is the better measurement of neutrino energy. Also, smaller initial arrays in water or ice may be first to detect the presence of high-energy neutrinos from cascades outside the array itself, although directional reconstruction will be poor.

Figure 4 illustrates an important point about the design of neutrino detectors, namely that increasing the muon energy threshold up to the order of 1 TeV greatly

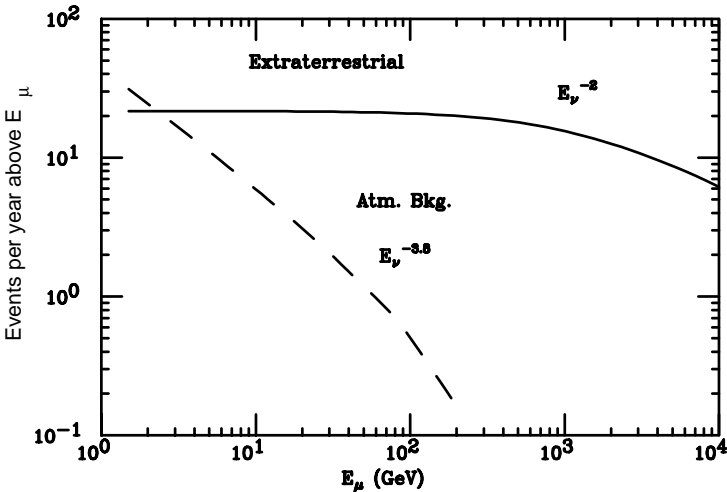


Figure 4 Muon spectrum at an underground detector for a hypothetical E^{-2} neutrino spectrum (of arbitrary normalization) compared with the spectrum of muons from atmospheric neutrinos. The signal-to-noise gain is approximately proportional to energy threshold and there would be negligible loss of signal if the threshold were raised to energies of around 1 TeV.

decreases atmospheric background at little cost to signal for a putative $1/E^2$ spectrum neutrino source. This circumstance creates some conflict in design goals for neutrino telescopes: Some interesting physics topics (e.g. dark matter and oscillations) are explored at muon energies below 1 TeV, yet the astronomy goal mandates higher thresholds to provide the necessary huge volume while controlling costs.

The point-spread function (PSF) for muons can act as signal for astrophysical point sources. The PSF is sharply peaked and non-Gaussian because a core of higher-energy muons is surrounded by lower-energy particles scattering near their end of range. The mean angle difference between neutrino and muon is about $0.7^\circ / (E_\nu/\text{TeV})^{0.7}$. This peaking and energy dependence of angular deviation from the original neutrino direction offer the possibility that neutrino telescopes could reach sub-arc-minute precisions in source location.

2.1.4 Effects of Neutrino Oscillations

For the purposes of this review, which focuses on high-energy neutrinos, the oscillations of terrestrial neutrinos do not have much impact. The effects of ν_μ oscillations, as Super-Kamiokande has shown, are most evident in muon neutrinos of energies close to 1 GeV. With a typical (near upper limit) value of $\delta m^2 = 5 \times 10^{-3} \text{ eV}^2$, 10% of ν_μ s from the other side of the Earth would oscillate into other species at energies as high as 800 GeV. Thus it is essential to account for ν_μ oscillation, which currently appears to occur almost exclusively into ν_τ ; there is little or no oscillation into ν_e at L/E values accessible through atmospheric neutrino experiments. We therefore expect a modest ν_τ flux in the energy range below ~ 100 GeV, well above the 10^{-4} fraction expected from prompt sources. Above 1 TeV, however, neutrino oscillations will lead to fewer ν_τ s in the atmospheric flux than from prompt sources. The effects of neutrino oscillations on astrophysical high-energy neutrino sources are discussed in Section 5. Figure 5 shows atmospheric neutrino spectra of all three flavors as expected under several assumptions of oscillations (two-flavor oscillations only).

There is an abundant literature on investigations of neutrino oscillations employing reactor neutrinos, neutrinos from accelerator beams, atmospheric neutrinos, and solar neutrinos (41). At present there is no evidence for any new (e.g. sterile) neutrinos beyond the familiar three flavors. Given what is known about standard oscillations, we can be sure that MSW resonant conversion will not be a factor for atmospheric neutrinos.

2.1.5 Earth Shadowing

Neutrinos are not absorbed by the Earth at energies below about 1 PeV, but at energies much greater the Earth is opaque to neutrinos, as illustrated by Figure 6.

Thus the strategy for neutrino astronomy changes in the range of around 100 TeV to 1 PeV. At lower energies it suffices to seek up-coming events, which will surely be neutrino-induced. The Earth functions as a filter, allowing only neutrinos through, but one must still discriminate against atmospheric neutrinos. For down-going events one must discriminate against cosmic-ray muons and the

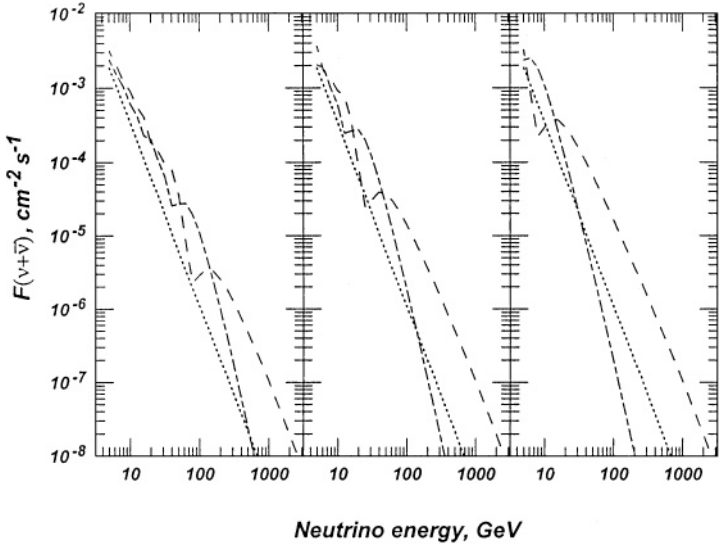


Figure 5 Atmospheric neutrino fluxes of all three flavors (dots: ν_e ; dashes: ν_μ ; long-short dashes: ν_τ) in the presence of $\nu_\mu \rightarrow \nu_\tau$ oscillations with maximal mixing and $\delta m^2 = 10^{-2}, 10^{-2.5}, 10^{-3} \text{ eV}^2$, from left to right. The fluxes are integrated over zenith angles beyond 120° . (From Reference 40 with permission.)

showers they create. However, atmospheric muons cannot reach a detector with more than 10–100 TeV (depending on depth), so one may shift strategy looking for down-going muons of sufficiently high (local, not initial) energy. For example, for $E_\mu^{\text{min}} > (1, 10, 100) \text{ TeV}$, the fluxes are $(7, 3 \times 10^{-2}, 6 \times 10^{-5}) \text{ km}^2 \text{ s sr}$ for a 3-kmwe-deep detector (39). The mean energy for atmospheric neutrino-induced muons is about 25 GeV, with flux $2 \times 10^{-3} \text{ km}^2 \text{ s sr}$, at any location, while the

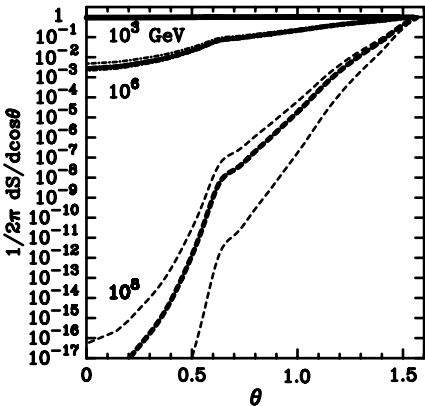


Figure 6 Differential shadow factor $(1/2\pi)dS(E_\nu)d\cos(\theta)$ versus nadir angle θ , for $E_\nu = 10^3 \text{ GeV}$ (solid line), 10^6 GeV (dot-dashed lines), and 10^8 GeV (dashed lines). The upper and lower curves represent various parton distributions. (From Reference 39 with permission).

down-going cosmic-ray–muon mean energy is about 300 GeV (at depth, increasing slowly with depth). Thus muons with energies beyond 100 TeV are essentially gone from either source at typical depths of several kilometers, and down-going events in the higher-energy regime can be interpreted as indicative of extraterrestrial neutrino origin.

It has been pointed out (42) that the Earth is not entirely opaque to ultra-high-energy (UHE) tau neutrinos, in that when a tau neutrino makes a CC interaction, the tau will then decay and 12.9% of the time will yield another tau neutrino, which proceeds with reduced energy and greater interaction length. In contrast, muon and electron neutrinos die after one CC interaction. All neutrinos have neutral-current interactions scattering them to lower energies, at which their probability of traversal is greater. Hence one may expect a slight spectral pileup of neutrinos, particularly taus, near the opaque energy limit for trajectories coming through the Earth from UHE neutrino sources. The effect does not, however, seem likely to enhance observations much (43). Observations of the tau neutrino via the double-bang signature are discussed later.

2.2 Neutrinos Due to Cosmic Rays Hitting the Sun

The Sun is a source of high-energy neutrinos created in cosmic-ray interactions in the solar atmosphere (44, 45). As for the cascades induced by cosmic rays in the Earth's atmosphere, mesons produced in the first interaction either decay or interact further depending on energy and the density at the point of the first interaction (see Figure 7).

Because of the scale height of the solar atmosphere, the density at the first interaction point is lower in the solar atmosphere than in the terrestrial one, and therefore a larger fraction of the mesons will decay instead of further interacting. As a consequence, the resulting neutrino spectra produced in the Sun's atmosphere have a slope similar to that of the original cosmic-ray spectrum, whereas the neutrino spectra due to showers in the Earth's atmosphere are steeper than the cosmic ray spectrum by approximately one power. Only above 10 TeV do shadowing effects due to interactions within the Sun become important. Adopting the

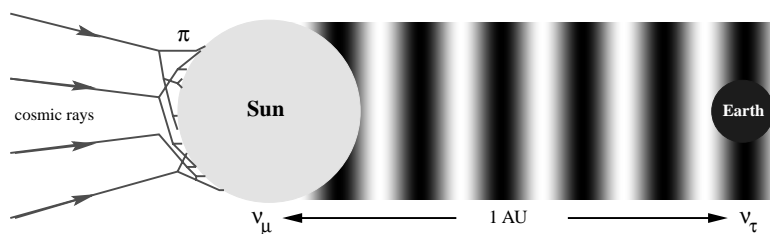


Figure 7 Cosmic rays hitting the Sun produce muon neutrinos that propagate to Earth. At an energy of 10 TeV the oscillation length for $\nu_\mu \rightarrow \nu_\tau$ oscillations is approximately equal to the distance between the Sun and the Earth.

local cosmic-ray flux $F_{\text{CR}} = 1(E/\text{GeV})^{-2.7} \text{ cm}^{-2} \text{ s}^{-1}$ (up to the so-called knee energy in the spectrum of cosmic rays, $E = 5 \times 10^6 \text{ GeV}$), the solar cosmic-ray-induced flux can be simply approximated by $EF_{\odot}(E) = EF_{\text{CR}}(E)\pi R_{\odot}^2/4\pi r^2 \sim 5 \times 10^{-6}(E/\text{GeV})^{-0.7} \text{ GeV cm}^{-2} \text{ s}^{-1}$, where $R_{\odot} = 6.960 \times 10^{10} \text{ cm}$ and $r = 1 \text{ AU} = 1.496 \times 10^{13} \text{ cm}$ denote the radius of the Sun and the distance between the Sun and the Earth, respectively.

The most recent calculations of the solar cosmic ray-induced neutrino flux use Monte Carlo codes based on the Lund model for particle interactions and include diffractive production processes (45) obtaining a high-energy neutrino flux from the Sun which significantly exceeds the atmospheric background above $\sim 10 \text{ TeV}$ in an experimental aperture of one square degree. Results are shown in Figure 10. The use of the Sun as a standard candle for the calibration of neutrino telescopes is hampered by the rather low expected event rate, which is of the order of 17 events per year above 100 GeV in a cubic-kilometer detector. A higher-than-predicted rate could indicate neutralino annihilation in the solar interior (46). Thus, despite the low cosmic-ray-induced flux, it is desirable to obtain statistics of solar high-energy neutrinos down to this conservative flux. Vacuum oscillations between the Sun and the Earth might be important in changing the received flavor ratios. Particular interest lies in a likely $\nu_{\mu} \rightarrow \nu_{\tau}$ oscillation for which Hettlage et al (47) compute a rate of 4–6 tau leptons above 100 GeV per year in a cubic-kilometer detector.

One could think of the moon as a similar source of high-energy neutrinos, but in the absence of an atmosphere, mesons generally interact before decaying, thereby generating very steep neutrino spectra that cannot compete with the atmospheric background from Earth.

2.3 Neutrinos from the Galactic Disk

The solar system lies at the outskirts of a lenticular system of stars, an ordinary spiral galaxy. When seen in projection, our galaxy appears as a brilliant band across the sky, the Milky Way. The interstellar medium has a density of $n_{\text{ism}} = 1 \text{ particle cm}^{-3}$ and a magnetic field of strength $B = (3\text{--}5) \mu\text{G}$. Cosmic rays diffuse through the interstellar medium and thereby give rise to gamma rays and neutrinos due to hadronic interactions. Most of the energy that is lost to secondary particles ends up in mesons, which decay freely in the low-density interstellar medium. Therefore the spectrum of the secondary gamma rays and neutrinos resembles the cosmic-ray spectrum in the interstellar medium: $dN/dE \propto E^{-2.7}$, as observed in the spectrum of the diffuse gamma-ray emission from the galactic disk. The characteristic symmetry of the differential spectrum about $E_{\gamma} \sim 70 \text{ MeV}$, due to the π^0 two-body decay kinematics, is not observed in the total spectrum, and this is interpreted as the effect of electronic bremsstrahlung and inverse Compton radiation dominating at lower energies. In some regions, the density is much higher than average and the neutral pion decay signature is visible, for instance in the molecular cloud $\rho\text{-Ophiuchus}$ (48). From the observed diffuse gamma-ray

emission, it is straightforward to compute the corresponding neutrino emission, as shown elsewhere (49–52). We show the latter flux in Figure 10 and compare it with the known background due to atmospheric neutrino production. The disk spectrum is significantly harder than that of the atmospheric background neutrinos and therefore wins at high energies. The reason for the steeper atmospheric spectrum is that the mesons produced in the atmosphere interact before decaying. The galactic center region shows up against the atmospheric background above 250 TeV with a flux of 160 neutrinos $\text{km}^{-2} \text{yr}^{-1}$ in an aperture of five square degrees. The flux may be higher if the cosmic-ray spectrum is harder than assumed in Reference 52, as the highest-energy bands of the EGRET data seem to indicate (53), or if unidentified hadronic point sources reside near or in the galactic center, as argued in Reference 54.

2.4 Gamma-Ray Astronomy with Muons

Another irreducible background for neutrino telescopes is the muon background due to meson production by extraterrestrial gamma rays. The typical muon energy in this case is $E_\gamma/50$ and the muon production probability is about 1% (55). Hence it follows that with an effective area larger by a factor of $\sim 10^4$, neutrino telescopes can become competitive with gamma-ray telescopes, provided that the muon energy is high enough to allow for an accurate determination of the muon direction. A neutrino telescope with an effective area of 10^4 m^2 and an angular resolution of 1° should thus be able to marginally detect the brightest gamma-ray sources, assuming that they emit energy fluxes at multi-TeV energies similar to those observed at EGRET ($\sim 1 \text{ GeV}$) energies. A pulsar-powered synchrotron nebula such as the Crab emits an order of magnitude less power at 1 TeV than at EGRET energies, and extragalactic TeV sources such as Mrk 421 and Mrk 501 are among the weakest EGRET sources, which discourages optimism about this window of opportunity for 10^4 m^2 neutrino telescopes. However, this becomes an interesting observational mode for effective areas an order of magnitude larger (see Section 6.1.8).

3. BOUNDS ON DIFFUSE HIGH-ENERGY NEUTRINO RADIATION

Neutrino astronomy explores the sky for unanticipated sources invisible in other channels. The properties of such sources can hardly be constrained, leaving a large parameter space open for exploration. On the other hand, there are well-known types of nonthermal sources with gamma-ray emission up to the multi-TeV range. In these sources, particle acceleration occurs in the tenuous shocked plasma associated with supersonic outflows, which are generally “thin” to the emission of gamma rays. The final fate of the escaping nucleons is less clear; they could escape straightaway without any losses, they could be trapped in surrounding large-scale

magnetic fields, and they could be degraded by energy losses. The cumulative neutrino flux associated with the high-energy sources represents an irreducible background for the exploration of the uncharted territory on the neutrino sky map. We discuss upper limits to this flux in this section.

3.1 Theoretical Bounds Based on Diffuse Gamma Rays and Cosmic Rays

A bound on the diffuse flux of neutrinos relies on the known diffuse fluxes of gamma rays and cosmic rays. The isotropic diffuse gamma ray background has an intensity of

$$E^2 I_E(E) = (1.37 \pm 0.06) \times 10^{-6} E^{-0.1 \pm 0.03} \text{ GeV cm}^{-2} \text{ s}^{-1} \text{ sr}^{-1} \quad 5.$$

above 30 MeV (83), where E is in GeV. There is a large ($\sim 20\%$) systematic error due to the subtraction of foreground emission. The slope of the spectrum is the same as the average slope of resolved extragalactic sources (blazars), which produce a combined flux of $\sim 15\%$ of the diffuse flux (57, 58). This suggests that unresolved extragalactic point sources are responsible for at least a large fraction of the background (59). The nonthermal spectrum extends down to approximately 1 MeV, where additional contributions are expected from supernovae in distant galaxies. At still lower X-ray energies, the background spectrum obtains a thermal shape and can be resolved almost entirely into active galactic nuclei (AGNs) at high redshifts (60).

It is not clear how far the diffuse gamma-ray spectrum extends to energies higher than ~ 100 GeV, but it appears plausible that the gamma-ray pair attenuation discussed in Section 1.1 and the source activity strongly increase with cosmological distance, which implies that one should expect a steepening of the gamma-ray background somewhat below 100 GeV (18). Most of the energy released at photon energies above 100 GeV and at high redshifts shows up in the gamma-ray band between 1 MeV and 100 GeV due to electromagnetic cascading in the metagalactic radiation fields (see References 61 and 62). The known bolometric gamma-ray background flux therefore limits the bolometric neutrino background flux. The flux ratio is solely determined by the branching ratios and kinematics at production (63, 64). For photoproduction of pions on a power-law target ($\alpha = 1$), one obtains

$$\int \Phi_\gamma(E_\gamma) dE_\gamma \simeq 2 \int \Phi_\nu(E_\nu) dE_\nu. \quad 6.$$

One can also compare with the flux of escaping nucleons to obtain an upper bound for neutrinos. This approach has been used to limit the blazar neutrino flux (Model A flux) (65), to test various models of extragalactic cosmic rays (ruling out some topological defect models) (61), and more recently assuming extragalactic sources emitting protons with a differential spectrum $dN/dE \propto E^{-2}$ (66). In using the experimental upper bound spectrum for extragalactic cosmic-ray protons instead of the model spectrum assumed above, Mannheim et al (67) corrected the bound

proposed by Waxman & Bahcall (66) and extended the analysis to include cases where the emitted protons suffer (a) adiabatic losses in large-scale magnetic fields or (b) absorption processes within the sources; the resulting set of more general bounds allows for much higher extragalactic neutrino fluxes.

To obtain an upper bound on the expected neutrino flux associated with extragalactic sources of cosmic rays, one must consider the neutrino production process with maximum efficiency (i.e. the largest number of neutrinos per escaping nucleon). Neutrons produced in hadronic interactions such as $p + \gamma \rightarrow \pi^+ + n$ can escape the cosmic accelerator, avoiding adiabatic energy losses, if they do not suffer further interactions and if the neutron energy is high enough to guarantee decay outside the magnetic field of the host galaxy. (If the nucleons all remain trapped or lose their energy, the gamma-ray limit is the only valid limit.) Production kinematics and branching ratios then determine a maximum possible neutrino flux; the escape of additional protons or ions would lead to a lower associated neutrino flux consistent with the logic inherent to an upper bound. The typical diameter of a bright galaxy is 10 kpc, which compares with a neutron decay length of $l_n = 10(E_n/10^9 \text{ GeV})$ kpc. UHE cosmic rays above $10^{9.5}$ GeV could therefore indeed be due to loss-free neutron escape, so that the neutrino flux is bounded by $E_\nu^2 \Phi_\nu(E_\nu) \leq 10^{-8} \text{ GeV cm}^{-2} \text{ s}^{-1} \text{ sr}^{-1}$ at $E_\nu = (10^{9.5})/25 \text{ GeV}$ using the observed cosmic-ray flux. An extragalactic origin of the UHE cosmic rays is suggested by the flattening of the cosmic-ray spectrum above $10^{9.5}$ GeV (the so-called ankle), the apparently light chemical composition (due to photodisintegration of heavy nuclei), and the isotropy. Extragalactic sources generally show strong evolution with cosmic time in the sense that they were much more active in the past than they are today (68); therefore the expected neutrino contribution today will be larger than the above estimate. Neutrinos are received from the entire cosmic volume (including the more active sources in the past), whereas cosmic rays suffer energy losses traversing the microwave background, so the volume from which their sources contribute to the present-day diffuse background is reduced. This increases the maximum neutrino flux at $E_\nu \sim 10^8 \text{ GeV}$ to $(3-7) \times 10^{-8} \text{ GeV cm}^{-2} \text{ s}^{-1} \text{ sr}^{-1}$ (depending moderately on cosmology). At energies below $\sim 10^{9.5}$ GeV it is difficult to say which fraction of the cosmic rays might be extragalactic or might have escaped their accelerators without losses. If the cosmic-ray nucleons escape their sources, decay into protons, and then travel through their host galaxies, galaxy clusters, and superclusters unaffected by large-scale magnetic fields, one can apply the observed cosmic-ray proton flux for the bound. The slope of the cosmic-ray proton spectrum above the ankle closely resembles $\Phi_{\text{cr,ex}} \propto E^{-2.75}$, and the composition measurements are consistent with extrapolating this spectrum down to the lower energies (see references in 67). At neutrino energies below $E_\nu \sim 10^6 \text{ GeV}$ (which are relevant for optical Cherenkov detectors), the bolometric gamma-ray flux becomes the more stringent limit. The maximum neutrino flux (including effects of evolution) relevant for sources that are thin to the emission of nucleons is shown in Figure 8 as the curved upper boundary of the grey-shaded area of confidence. The straight-line upper boundary indicates the bound relevant for the thick

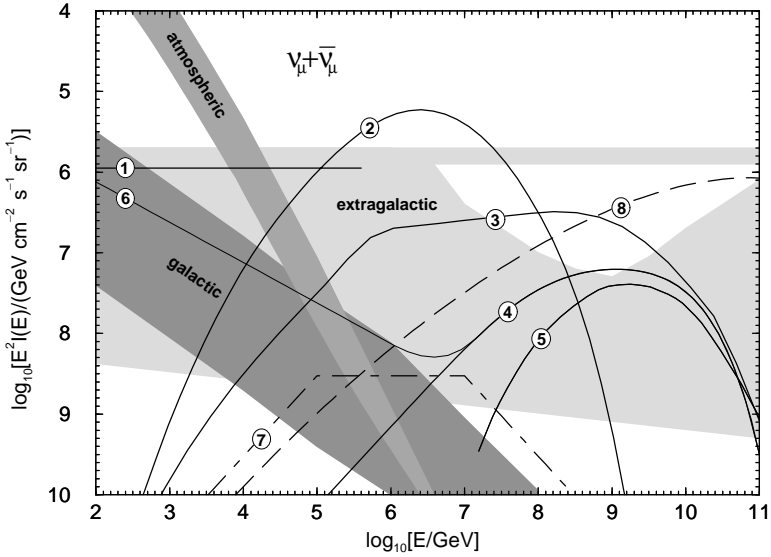


Figure 8 Summary of expected $\nu_\mu + \bar{\nu}_\mu$ intensities for diffuse emission from various sources. *Shaded regions:* *Foreground*, terrestrial atmosphere in the horizontal (upper boundary) and vertical (lower boundary) directions including prompt neutrinos from charm production (69); *Intermediate*, galactic disk toward the center (upper boundary) and the poles (lower boundary) (52); *Background*, unresolved extragalactic sources from which gamma rays and cosmic-ray nucleons escape freely (curved upper boundary) and from which only gamma-rays escape (straight upper boundary) (67), cosmic-ray storage in galaxy clusters (lower boundary) (70). *Numbered lines:* (1) Nellen et al model for pp interactions in the core of AGNs (71), (2) Stecker & Salamon model for $p\gamma$ interactions in the core of AGNs (from which nucleons cannot freely escape) (72), (3) Mannheim et al model for $p\gamma$ interactions in extragalactic photoproduction sources (maximum model) (67), (4) Mannheim model A for $p\gamma$ interactions in blazar jets producing ultra-high-energy (UHE) cosmic rays through neutron escape (65), (5) $p\gamma$ interactions due to UHE cosmic rays escaping from radio galaxies and traveling through the 2.7-K background according to the model of Rachen & Biermann (73, 61), (6) pp interactions in host galaxies of blazar jets as assumed in the model of Mannheim (65), (7) gamma-ray burst model by Waxman & Bahcall (157), (8) decaying XY gauge bosons of mass 10^{16} GeV created at topological defects, as in the models of Sigl et al (75) and Birkel & Sarkar (182).

case, in which nucleons are degraded in the surroundings of their sources or the sources themselves. We consider as a benchmark flux for high-energy neutrinos in the TeV to PeV regime the logarithmic mean of the minimum and maximum bounds shown in Figure 8, which amounts to

$$E_\nu^2 \Phi_\nu(E_\nu) \approx 10^{-7} \text{ GeV cm}^{-2} \text{ s}^{-1} \text{ sr}^{-1}. \quad 7.$$

The atmospheric background flux is up to two orders of magnitude larger at 1 TeV, but it drops rapidly, meeting the benchmark flux at about 100 TeV. With the following probability of detecting a TeV neutrino,

$$P_{\nu \rightarrow \mu} = 1.3 \times 10^{-6} \left(\frac{E_\nu}{\text{TeV}} \right)^{0.8}, \quad 8.$$

for $1 \text{ TeV} \leq E_\nu \leq 1 \text{ PeV}$, the benchmark flux corresponds to a muon rate of

$$R_\mu = \int_{\text{TeV}}^{\text{PeV}} AP(E_\nu, E_{\mu, \min}) \Phi_\nu(E_\nu) S(E_\nu) dE_\nu \approx 200 A_{\text{km}^2} \text{ yr}^{-1} \text{ sr}^{-1}, \quad 9.$$

where A_{km^2} denotes the telescope area in square kilometers and $S(E_\nu)$ denotes the Earth shadowing factor, which always remains close to unity below 100 TeV. At energies approaching 100 TeV, the atmospheric background rate becomes small compared with the benchmark rate, demonstrating that a square kilometer is the natural scale at which to achieve astrophysical sensitivity.

3.2 Experimental Bounds

Interpreting experimental bounds on what was not seen is a tricky business because unstated assumptions often influence the limits produced. The essential problem is that one must calculate backwards from the observed quantity, typically either a muon flux or some high-energy cascade rate, and in order to do that one must postulate a neutrino flux spectral function. Thus if one assumes a rather flat $1/E^2$ power-law spectrum and makes a low-energy measurement, as with underground detectors, this will imply rather stringent limits at very high energies. Clearly this is not a valid procedure, although some experimenters claim to have established limits using this logic.

We suggest that experimenters restrict the flux limit to the neutrino energy region of the sensitivity of their detectors. Also, if the flux is quoted at the mean source neutrino energy, the resulting limit will be reasonably independent of spectral index. (For example, in the past, the underground detectors have usually quoted a flux limit at their threshold energy, typically around 1 GeV, whereas the neutrino sensitivity region is nearer to 100 GeV.) This still assumes a power-law spectrum, which may not be applicable, though it is indeed what is typically observed in the cosmic rays.

The Glashow resonance is a special case because the cross section is so much larger than the muon CC reaction. From the absence of a bump in the rate of showers at this energy, one can infer a dip in the limits at 6.4 PeV, or even argue for a lower power-law spectrum limit, at least for a $\bar{\nu}_e$ flux. Again, we advise caution in interpretation. Nonetheless there are some limits, and they are not far above the more optimistic predictions.

Figure 9 shows the experimental upper limits on the diffuse high-energy neutrino fluxes obtained by the Baikal (79), SPS-DUMAND (80), AMANDA (81),

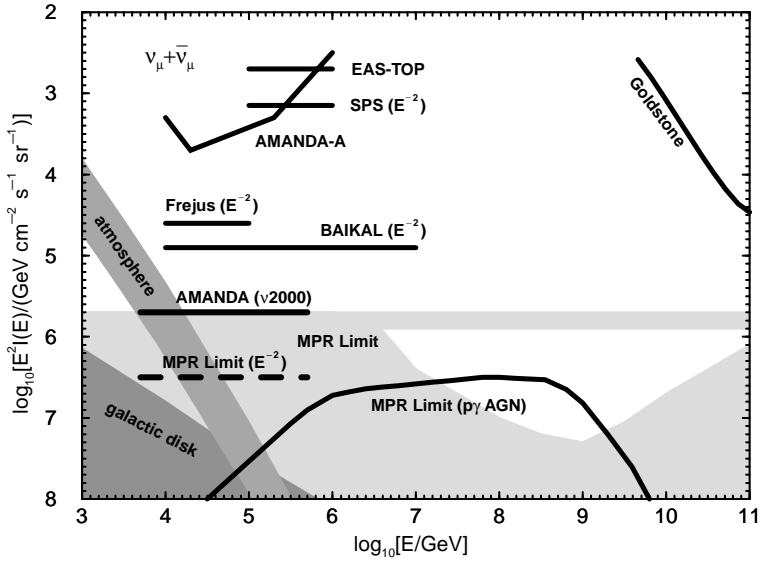


Figure 9 Upper limits on the differential flux of high-energy neutrinos obtained by different experiments compared with some theoretical upper bounds (see text).

EAS-TOP (82), Fréjus (77), and Goldstone (78) experiments. Also shown is the model-independent upper limit for the extragalactic neutrino intensity (MPR Limit), and an upper limit for neutrinos from AGNs (MPR Limit— $p\gamma$ AGN) within the framework of photoproduction models, as obtained by Mannheim et al (67). For comparison with the only observed neutrino signal, Figure 9 also depicts the atmospheric neutrino flux (69) (the flux obtained in Reference 84 is very similar). Current experimental bounds are still far from the level at which astrophysical sources might come into play, and arrays on the kilometer scale are needed to launch a breakthrough.

4. CANDIDATE ASTROPHYSICAL SOURCES OF NEUTRINOS

There are many potentially interesting astrophysical sources of high-energy neutrinos. All sources with nonthermal emission qualify as such sources in the widest sense. We have already discussed some of them because of their guaranteed neutrino emission. In other sources, the evidence for hadronic emission processes is less convincing, and the range of possible ways to model their neutrino fluxes is wider. In the following, we describe some current models for galactic and extragalactic sources that may be relevant for the next generation of large neutrino telescopes (see Figure 10). It has proven very useful to discuss the neutrino fluxes in terms of highly simplified “generic models” by adapting only a few parameters

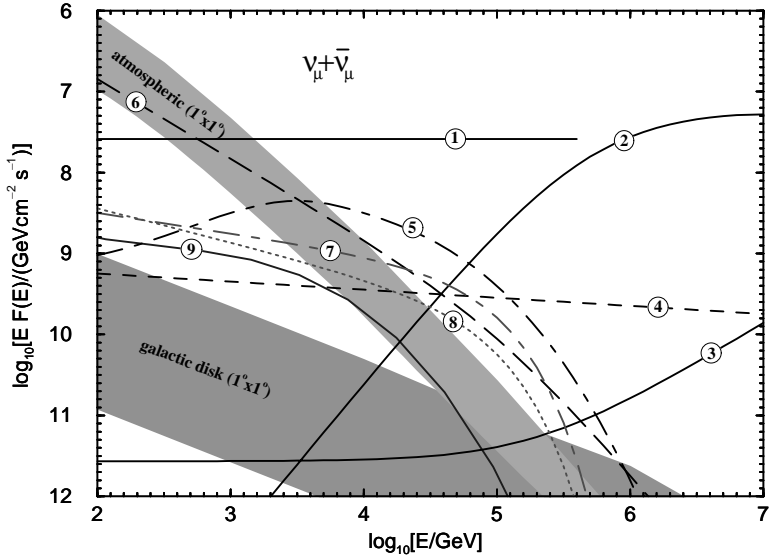


Figure 10 Summary plot for the expected $\nu_\mu + \bar{\nu}_\mu$ fluxes from candidate cosmic-ray accelerators. *Numbered lines:* (1) Nellen et al (71) model for the core emission from 3C273 due to pp interactions (or similarly Mrk501 during its outburst in 1997 if it emits half of its TeV gamma-ray flux in neutrinos); (2) Stecker & Salamon model for the core emission from 3C273 due to $p\gamma$ interactions (72); (3) Mannheim (87) model for the relativistic jet of 3C273 including pp and $p\gamma$ interactions; (4) coma cluster according to the model of Reference 70; (5) Crab nebula, Bednarek & Protheroe, Model I (88); (6) Cosmic-ray-induced neutrinos from the Sun from Ingelman & Thunman (45); (7) supernova remnant (SNR) IC444 according to the model of Gaisser et al (89); (8) SNR γ Cygni (89); (9) CasA according to the model of Atoyan et al (90) (adopting $L_\nu = L_\gamma$ and $E_\nu = 0.5E_\gamma$).

to the astronomical input data relevant to the sources under discussion. One common assumption is that Fermi acceleration is at work in the known high-energy gamma-ray sources, and we start with a brief discussion of this mechanism.

4.1 Fermi Acceleration

Many astrophysical objects exhibit spectra characteristic of conditions far from thermodynamic equilibrium and indicate highly efficient particle acceleration. Typically, the nonthermal emission is associated with powerful supersonic outflows, such as those seen in supernova remnants, gamma-ray bursts, or galactic and extragalactic radio jets. Particle acceleration is known to occur at shock waves in the solar system, too, where in situ measurements of the particles can be obtained. Thus, although theories for particle acceleration in the astrophysical plasma have some empirical foundation (91), the models would benefit greatly from neutrino astronomy, which provides crucial information about the accelerated proton (ion) spectra at the sources, unaffected by propagation effects.

A theory of diffusive shock acceleration was developed by Krymskii (92) and by Axford et al (93). The theory can be traced back to Fermi's original suggestion of repeated scattering between magnetic mirrors (94, 95), which gained new importance after Parker's discovery that shock waves in the interstellar medium (96) increase the efficiency of the mechanism. Shock acceleration provides a plausible scheme for understanding the observed spectra from nonthermal astrophysical sources (see References 97–99 for reviews). The energy gain is achieved at the expense of the kinetic energy of the shocked bulk flow, and the mechanism of energy conversion is based on the repeated scattering of particles on both sides of the (collisionless) shock wave. Owing to the velocity difference across the shock wave, there is a net energy gain associated with closed trajectories, analogous to the energy gain of a tennis ball scattering elastically off a pair of approaching walls. However, the analogy is only partial, since there is no rigid boundary resembling a wall on the downstream side. Some particles are advected away from the shock with the flow rather than returning, and the spectral slope of the stationary distribution of particles reflects the statistical equilibrium between escape and acceleration.

The microphysical description of the scattering involves plasma waves in resonant interaction with the particles. The interaction leads to a change of the pitch angle with the average magnetic field direction, and repeated scattering leads to spatial diffusion with length scale $\lambda_D = \xi r_g$ with $\xi \geq 1$, where $r_g = pc/(ZeB)$ denotes the Larmor radius of a particle of charge Z and momentum p . The corresponding diffusion coefficient is $D = \frac{1}{3}\lambda_D c = \xi Ec/(3ZeB)$, and in general ξ and D are both energy-dependent, reflecting the spectrum of the magnetic field fluctuations responsible for the scattering. Biermann & Strittmatter (100) argue for a Kolmogórov spectrum of the plasma turbulence.

Diffusive shock acceleration only operates for particles that can cross the shock front without scattering in it, which means that their Coulomb mean free path must be much larger than their gyroradius, which in turn must be much larger than the shock thickness. Under collisionless conditions, a shock wave can form because of the short-range (shorter r_g) interactions of the low-energy particles with the magnetic field and the plasma waves. An important corollary of the statistical nature of the Fermi acceleration mechanism balancing energy gains and escape losses is the power-law shape of the resulting particle energy spectra (far away from limiting energies). The energy spectra giving the number of particles with energy between E and $E + dE$ per volume have the form

$$dN = N_0 E^{-s} dE, \quad 10.$$

with

$$s = 2 + \frac{4}{M^2} \quad 11.$$

where $M^2 = v/c_*$ denotes the square of the Mach number and c_* the sound (Alfvén) speed of the plasma. For strong nonrelativistic shocks with $M \rightarrow \infty$, the asymptotic index is $s = 2$. Cosmic rays are observed with a slope $s = 2.7$ and a slight steepening with $\Delta s = 0.3$ – 0.6 is due to energy-dependent leakage from the

galaxy. The inferred injection spectral index $s = 2.1\text{--}2.4$ is in fair agreement with the prediction for finite Mach numbers. It is important to note, however, that the most efficient nonthermal sources in astrophysics involve relativistic and oblique shocks, e.g. in the jets emerging from accreting black holes and gamma-ray bursts. There seems to be some dependence on the microphysical details of the scattering and shock obliquity for moderately relativistic shocks (101). At ultrarelativistic shock speeds, however, there is convergence toward an index $s = 2.2\text{--}2.4$, as shown elsewhere (102, 103). Another caveat is the effect of the pressure of the accelerated particles on the shock, which causes so-called modified shock structures with somewhat different particle spectra (104).

Fermi acceleration ceases to operate when the energy-loss timescale becomes shorter than the acceleration timescale, when the scattering length becomes larger than the shock radius, when the sideways diffusion timescale becomes shorter than the acceleration timescale, or simply after the shock decays. As an example, consider the maximum energy in the case of limitation by energy losses, which one expects to be relevant for variable sources in which the magnetic field strength is high (and therefore the acceleration timescale short). The first-order Fermi acceleration rate for a shock with velocity v and a relativistic particle of charge Ze and mass m is given by

$$\dot{E} \approx \frac{\Delta E}{\Delta t} = \frac{E(\frac{v}{c})}{D/(vc)} \approx \frac{3ZecB}{\xi} \left(\frac{v}{c}\right)^2. \quad 12.$$

The synchrotron energy loss rate is

$$-\dot{E}_{\text{syn}} = \frac{4}{3}\sigma_{\text{T}}c \left(\frac{m_e}{m}\right)^2 \left(\frac{Z}{A}\right)^4 \frac{B^2}{8\pi} \gamma^2, \quad 13.$$

where A denotes the mass number of the particle. Equating these rates, one obtains the characteristic maximum Lorentz factor

$$\gamma_{\text{max}} = 2 \times 10^8 \xi^{-\frac{1}{2}} B^{-\frac{1}{2}} Z^{\frac{1}{2}} \left(\frac{A}{Z}\right)^2 \left(\frac{m}{m_e}\right). \quad 14.$$

At $\xi = 10$ (very rapid diffusion), the maximum energy for protons is $E_{p,\text{max}} \approx 10^{20} B^{-\frac{1}{2}}$ eV and for electrons $E_{e,\text{max}} \approx 30 B^{-\frac{1}{2}}$ TeV for B measured in Gauss. If photo-production energy losses dominate over synchrotron energy losses, the maximum energies are lower by the factor $(1 + u_\gamma/u_B)^{-1/2}$ in the case of electrons and $(1 + 240u_\gamma/u_B)^{-1/2}$ in the case of protons, where u_γ denotes the energy density of the radiation field and $u_B = B^2/8\pi$ the energy density of the magnetic field. Of course, in sources where the magnetic field strength is low (e.g. supernova remnants) other limitations, such as the lifetime or radius of curvature of the shock, bound the maximum energy.

Applied to supernova remnants, diffusive shock acceleration theory successfully explains the observed cosmic rays in that it accounts for energetics, power-law shape, maximum energies, and chemical composition, although the nondetection of many remnants at TeV energies remains a concern (106, 107). The basic assertions of the theory of the origin of cosmic rays can be used to construct generic

models of astrophysical neutrino production due to particle acceleration at shock fronts. Non-ideal processes in magnetohydrodynamics that can produce electric fields are receiving increasing attention (see Reference 108), since much of the nonthermal energy release on the surface of the Sun appears to be governed by the reconnection of magnetic field lines (differential rotation twists lines of opposing polarity) and since much of the high-energy activity in cosmic nonthermal sources seems to be produced in an explosive manner. However, because these processes typically occur in high-density regions, they are believed to operate as preacceleration mechanisms accelerating the bulk of the particles to moderate energies. This could drive supersonic outflows in which shock acceleration to ultrahigh energies occurs as a secondary process. Ordered electric fields arising from unipolar induction (109) in accreting compact sources could also accelerate particles to high energies. However, this possibility is not favored by current observations.

4.2 Generic Models of Astrophysical Production of Neutrinos

Generic models for astrophysical neutrino production assume that a beam hits a target, which results in pion production and subsequent meson decay. The aim is to estimate neutrino fluxes within an order of magnitude under the most general assumptions. Generic models are important for prioritizing the large number of potentially interesting sources in the astronomical zoo. The beam is usually assumed as a power-law distribution of protons, Equation 10, with spectral slope s and normalizing constant N_0 . The proton spectra are further characterized by a lower cutoff energy E_{\min} , which determines the total number density $N(>E_{\min}) = \int_{E_{\min}}^{E_{\max}} dN$ of nonthermal protons, and an upper cutoff energy E_{\max} from the limitations of shock acceleration. The two target substrates typically found in astrophysical sources are ambient matter and low-energy photons, which produce different neutrino fluxes.

4.2.1 Interactions With Matter

The volume emissivity of the produced pions is given by

$$Q_{\pi}^{(pp)} = \int n_t c N_{\pi} \frac{d\sigma_{pp}(E_{\pi}, E)}{dE_{\pi}} \frac{dN}{dE} dE, \quad 15.$$

where $d\sigma_{pp}(E_{\pi}, E)/dE_{\pi}$ denotes the differential inclusive cross section for pion production on a proton target of density n_t and pion multiplicity N_{π} . A solar abundance of elements in the target increases the effective proton density by the factor 1.14. A simple estimator can be obtained by putting $d\sigma_{pp}(E_{\pi}, E)/dE_{\pi} \approx \sigma_{pp} \delta[E_{\pi} - \kappa_p E / N_{\pi}]$, where κ_p denotes the inelasticity. The proton-proton inelastic cross section is given by $\sigma_{pp} \approx 30$ mb, and at TeV energies (lab frame) $N_{\pi} \approx 15$ and $\kappa_p \approx 0.4$ are appropriate. Since N_{π} , κ_p , and σ_{pp} are all only weakly energy-dependent, the pion emissivity carries practically the same energy dependence as the initial proton spectrum, namely

$$Q_{\pi}^{(pp)}(E_{\pi}) \approx n_t \sigma_{pp} c \frac{N_{\pi}^2}{\kappa_p} \frac{dN}{dE} \left(\frac{N_{\pi} E_{\pi}}{\kappa_p} \right) \quad 16.$$

for energies well above 1 GeV. At many astrophysical accelerators it is possible to compute the neutrino emissivity from Q_π assuming decay in free flight, since the prevalence of a collisionless plasma is the condition for the particle acceleration mechanism to work. In this case, the two muon and one electron neutrinos each carry 1/4 of the charged pion energy. Assuming isospin symmetry, 2/3 of all produced pions are charged ones, and

$$Q_v^{(pp)} \approx \frac{1}{2} Q_\pi^{(pp)} (4E_v) \propto E_v^{-s}. \quad 17.$$

In very compact and rapidly variable sources, or in sources in which a beam of accelerated particles dumps onto a thick target, pions interact before decaying, giving rise to a neutrino spectrum steeper than the pion spectrum (see Section 2.2 and Reference 63). The source flux $\Phi_v(E_v)$ (neutrinos per unit area and time) can be obtained by integrating the emissivity over the spatial extent of the source, $d\Phi_v/dE_v = \int Q_v dr$.

4.2.2 Interactions With Photons

Blackbody Target Spectrum Suppose the photon frequency distribution is strongly peaked, as in the case of a blackbody radiation field. It is possible to compute the emissivity, as in the material target case, by inserting the photon density n_γ for n_t , by replacing the cross section σ_{pp} with the (smoothed) photo-hadronic cross section $\sigma_{p\gamma} \approx 120 \mu\text{b}$, and by using $\kappa_p \approx 0.3$ and $N_\pi \approx 3$ well above threshold ($\sqrt{s} \geq 3 \text{ GeV}$) (for exact numbers, see Reference 64). The neutrino emissivity thus obtained has the same energy dependence as in Equation 17. Photoproduction of pions occurs above the threshold energy,

$$E_{\text{th}} = \frac{m_p m_\pi c^4}{2\epsilon} \left(1 + \frac{m_\pi}{2m_p} \right) \simeq 7.5 \times 10^6 \left(\frac{\epsilon}{10 \text{ eV}} \right)^{-1} \text{ GeV}, \quad 18.$$

in head-on collisions between protons and low-energy photons of energy ϵ . The value $\epsilon = 10 \text{ eV}$ is representative of ultraviolet radiation fields characteristic of many stars and supermassive accreting compact objects. Interactions with photons from the microwave background, where $\epsilon \approx 7 \times 10^{-4} \text{ eV}$ and $n_\gamma \approx 420 \text{ cm}^{-3}$, occur at $E_{\text{th}} \approx 10^{11} \text{ GeV}$ and should produce the so-called Greisen-Zatsepin-Kuzmín cutoff in the spectrum of extragalactic cosmic rays.

Power-Law Target Spectrum If the photon density is given by $n_\gamma(\epsilon) = n_0 \epsilon^{-\alpha}$ (where α is called the spectral index), the energy dependence of the target shows up in the final expression for the emissivity. One can easily infer this from Equation 15 when using the threshold condition of Equation 18 to replace ϵ in $n_\gamma(\epsilon)$, which yields

$$Q_\pi^{(p\gamma)} = n_0 \left(\frac{m_p m_\pi c^4}{2} \left(1 + \frac{m_\pi}{2m_p} \right) \right)^{-\alpha} \int_{E_{\text{th}}(\epsilon_{\text{min}})}^{E_{\text{max}}} E^\alpha \frac{d\sigma_{p\gamma}(E_\pi, E)}{dE_\pi} c \frac{dN}{dE}(E) dE. \quad 19.$$

Inserting the delta-function approximation for the differential cross section and assuming free-flight decay of the pions, one obtains a neutrino emissivity with

$$Q_{\nu}^{(p\gamma)} \propto E_{\nu}^{-(s-\alpha)}. \quad 20.$$

The power-law target photons in a generic model would be the synchrotron photons produced by the accelerated electrons. Two cases can arise: (a) The electron and proton spectra are the same or (b) the electron spectrum is loss-steepened by one power. In the former case $s = 2\alpha + 1$, and in the latter case $s = 2\alpha$. Inserting these relations into Equation 20 yields the neutrino emissivities $Q_{\nu} \propto E_{\nu}^{-(\alpha+1)}$ and $Q_{\nu} \propto E_{\nu}^{-\alpha}$. Since power-law target spectra often arise in sources expanding with Lorentz factor Γ , it is important to apply proper Lorentz boosts to obtain the energy of the target photons dominating the interaction rate for the production of neutrinos with observed energy E_{ν} :

$$\epsilon = 4 \times 10^4 \left(\frac{\Gamma}{10} \right)^2 \left(\frac{E_{\nu}}{10^4 \text{ GeV}} \right)^{-1} \text{ eV}. \quad 21.$$

This shows that interactions with photons in the hard X-ray band, where the spectral slopes typically range between $\alpha = 0$ and $\alpha = 1$, are of particular importance for neutrino astronomy in the TeV range. It must be noted that generic models generally assume quasi-stationary conditions whereas neutrino experiments integrate over time intervals much larger than the typical flux variation timescales of the observed astronomical sources.

4.3 Galactic Candidates

We discussed in Section 2.3 the diffuse flux of neutrinos that arises from interactions of cosmic rays diffusing through the interstellar medium in the galactic disk. Here we focus on point sources of various types superimposed on this diffuse emission. Generally, such sources tend to cluster strongly around the galactic center, where the stellar density is highest. Thus, in order to maximize the number of targets, it is advantageous to design neutrino telescopes with the galactic center in their field of view.

4.3.1 Pulsars and Pulsar-Driven Nebulae

Pulsars are rapidly spinning neutron stars with radii $r_{\text{ns}} \approx 10^6$ cm, with rotation periods $P_{\text{ns}} \geq 1$ ms, and with strong magnetic fields $B_{\text{ns}} \approx 10^{12}$ G. Owing to the rotation, there is a potential drop from the magnetic pole region of the neutron star to infinity (110), which could lead to electrostatic particle acceleration up to

$$E \simeq 3 \times 10^{18} Z \left(\frac{P_{\text{ns}}}{1 \text{ ms}} \right)^{-2} \left(\frac{B_{\text{ns}}}{10^{13} \text{ G}} \right) \left(\frac{R_{\text{s}}}{10^6 \text{ cm}} \right)^3 \text{ eV} \quad 22.$$

for ions of charge Z . Thus, very young pulsars could be a source of cosmic rays (as discussed in Reference 30), but their lifetimes are less than a few years, and SN1987A observations do not support the suggestion. There remains the possibility

to connect UHE cosmic rays with ions accelerated in accretion-borne millisecond pulsars distributed in an extended halo or nearby galaxies (111).

At later times during the pulsar evolution, the potential drop decreases as the rotation slows down and the surface cools below the temperature at which thermionic emission of iron nuclei is important. During later phases, electron-positron pairs from vacuum discharges in the inner magnetosphere probably dominate the outflowing particle flux. The pulsar wind powers the environment of the pulsar with magnetic flux and relativistic particles, which leads to very strong unpulsed synchrotron emission, as observed from the Crab nebula. Pulsars embedded in such a synchrotron nebula (plerions) are generally assumed not to be responsible for the acceleration of cosmic rays, since they should provide mainly electron-positron pairs and since cosmic rays would suffer adiabatic losses expanding the synchrotron nebula around the pulsar.

Neutrons at very high energies can, however, escape the plerion without adiabatic losses, since they do not couple to the magnetic field inside the plerion. The decay length is $l_n \simeq 10(\gamma_n/10^6)$ pc at the knee energy. Neutrons well below the knee energy would be trapped doing thermodynamic work and expanding the nebula, but also to some extent suffering inelastic energy losses (due to collisions with matter in filaments). As shown in Figure 10 for the case of the Crab nebula, this would be an interesting source of high-energy neutrinos (88), and a more important source than β -decay, since neutrinos from β -decay carry only $\sim m_e/m_p$ of the initial neutron energy. Pulsed neutrinos from the magnetosphere also arise from muon pair production and deep inelastic electron-nucleon scattering caused by the accelerated electrons or positrons hitting the polar cap.

4.3.2 Shell-Type Supernova Remnants

Supernova remnants (SNRs) are powerful blast waves driven into the interstellar medium (or into a progenitor wind, as pointed out in Reference 112) by the collapses of the cores of massive stars (supernovae). The supernovae themselves are powerful sources of gamma rays and neutrinos at nuclear energies, as demonstrated by the discovery of neutrinos from SN1987A. No high-energy gamma ray or neutrino flux associated with SN1987A has been discovered, although high-energy emission associated with particle acceleration at the shock forming in the expanding blast wave in its early phases could be possible (30). A possible reason for this nonobservation of a young SNR is that, in the initial phase of the explosion, very little energy is contained in the blast wave. During later phases, the shock wave carries a significant amount of the total kinetic energy of the ejecta.

As discussed in References 118 and 105, SNRs represent the leading candidate for the origin of the bulk of cosmic rays up to $\sim 10^6$ GeV, since (a) they show strong nonthermal power-law spectra indicating the presence of relativistic electrons (113, 114), (b) they inject enough power to be able to sustain the cosmic-ray flux for a reasonable particle acceleration efficiency of ~ 1 –10%, and (c) they have the chemical abundances found in cosmic rays (after correcting for spallation, and assuming injection of dust grains to explain the overabundance of

volatile elements). Nevertheless, few-TeV gamma-ray emission at the level expected from π^0 production in SNRs has not been found (106), except possibly in Cas A (115, 90). TeV gamma rays have been observed from the Crab nebula and from SN1006, but in both cases these gamma rays seem to originate from inverse-Compton scattering of low-energy photons by accelerated electrons rather than from π^0 production by accelerated protons. Furthermore, in the case of the Crab nebula, the TeV gamma-ray emission is most likely pulsar-wind-driven and due to the acceleration of electron-positron pairs in the plerion (see Section 4.3.1).

There are several theoretical ways around the problem of the missing strong hadronic TeV sources (89, 116). The most compelling arguments invoke steeper source spectra ($\propto E^{-2.4}$) than originally assumed ($\propto E^{-2.1}$). Biermann (118) points out that the steepening due to energy-dependent diffusive transport through the galaxy and its halo would then have to be less pronounced at energies approaching 100 TeV than estimated from the ratio of beryllium isotopes at GeV energies, i.e. closer to $\propto E^{-0.3}$ than $\propto E^{-0.6}$, reflecting the Kolmogorov nature of the plasma turbulence spectrum in the interstellar medium. In fact, continued steepening $\propto E^{-0.6}$ would lead to anisotropies at knee energies, which are not observed. It could also be a selection effect that the SNRs accessible to observation have steeper than average spectra (e.g. due to their age). Protheroe & Stanev (119) argue that the spectra could turn up approaching the knee energy while remaining below the observational limits at TeV due to pile-up effects.

Figure 10 shows the expected neutrino fluxes inferred from model fits to the gamma-ray spectra of the SNRs γ -Cygni and IC443 observed with EGRET (89) (see also Reference 117), and of CasA [which has a weak HEGRA/IACT detection (115)], according to the model of Atoyan (90). The models demonstrate that SNRs could dominate over the atmospheric background (in a square-degree aperture) above 20 TeV with fluxes similar to that of the Sun, as discussed in Section 2.2.

4.3.3 Black Hole Candidates and Microquasars

Accreting black holes with masses $M \geq 3M_\odot$ are commonly believed to be responsible for galactic hard X-ray transients such as GRO J1655-40 and GRS 1915+105. These sources have many similarities with AGNs, particularly superluminal jets and complex X-ray variability and are therefore called the “microquasars” (see Reference 120). It is often stated that microquasars are the ideal laboratories to probe the physics of AGNs, since they are so much closer to us. This is not quite true. The fluxes from AGNs are of the same order as those from microquasars, but the ratio of the spatial scales in units of the Schwarzschild radius $r = R/R_S$ that can be probed with a fixed angular resolution $\theta = R/d$ are given by $r_{\text{micro}}/r_{\text{AGN}} = (d_{\text{micro}}/d_{\text{AGN}})(M_{\text{AGN}}/M_{\text{micro}}) \sim 10^3$ using the distances $d_{\text{AGN}} = 100$ Mpc and $d_{\text{micro}} = 10$ kpc and the masses $M_{\text{AGN}} = 3 \times 10^8 M_\odot$ and $M_{\text{micro}} = 3M_\odot$. Hence, relatively smaller scales can be probed in AGNs for a given flux limit and angular resolution.

Microquasars are useful for studies of variability, since all timescales are shorter by the factor $M_{\text{micro}}/M_{\text{AGN}} \sim 10^{-8}$ than in AGNs. If the strong daily variations of the TeV emission observed in some AGN jets indicate a transient phenomenon close to the light cylinder radius ($\sim 100R_S$), one would expect very short TeV bursts in microquasars on a timescale of milliseconds.

To estimate neutrino fluxes, one would have to scale hadronic AGN jet models to microquasars. The optical depth for interactions with the radiation field inside the jet is proportional to the compactness L/R , which is independent of the black hole mass. However, the maximum possible proton energy arising from the gyro-limitation of Fermi acceleration scales as $E_{\text{max}} \propto RB \propto M^{1/2}$. It is therefore a factor of 10^4 smaller than in the comoving frame of relativistic AGN jets, where $E_{\text{max}} \sim 10^{10}$ GeV, and is therefore comparable to the knee energy of the local cosmic-ray spectrum. The hadronic luminosity relative to the synchrotron luminosity is proportional to the maximum proton energy, so intense hadronic emission seems unlikely, with two exceptions. The first exception is during the early phase of the evolution of an outburst, when particle acceleration occurs in the X-ray radiation field of the accretion disk. The other is in the late phase, when escaping accelerated protons (with energies up to knee) interact with dense clouds in the vicinity of the microquasar. Searching for neutrino emission from microquasars will thus shed light on their possible contribution to the flux of cosmic rays and the physical processes occurring near the putative black holes.

4.4 Extragalactic Candidates

4.4.1 Cosmic Rays in Other Galaxies

The cosmic-ray-induced luminosity of the Milky Way in diffuse gamma rays is about $L_\gamma \approx 10^{39} (E/0.1 \text{ GeV})^{-0.7} \text{ erg s}^{-1}$, which compares to its stellar luminosity of $L_* \approx 10^{44} \text{ erg s}^{-1}$. By adopting the gamma-ray-to-stellar-luminosity ratio of $10^{-5} (E/0.1 \text{ GeV})^{-0.7}$ as a universal value for all galaxies and putting $L_\nu \approx L_\gamma$, we can compute the neutrino background due to cosmic rays in galaxies from the known present-day cosmic energy density of stellar (infrared to ultraviolet) light, $u_* \approx 6 \times 10^{-3} \text{ eV cm}^{-3}$ (121). The corresponding neutrino energy density is $u_\nu \approx u_* (L_\nu/L_*)$, which leads to

$$E^2 I_E(E) = \frac{c}{4\pi} u_\nu \approx 10^{-7} \left(\frac{E}{0.1 \text{ GeV}} \right)^{-0.7} \text{ GeV cm}^{-2} \text{ s}^{-1} \text{ sr}^{-1}. \quad 23.$$

The flux at TeV energies is far below detectability and that expected from other sources. It must be noted, however, that the slope $\propto E^{-2.7}$ could be much flatter ($s = 2.4$) for Kolmogorov interstellar turbulence. The slope is certainly flatter ($s = 2.1\text{--}2.4$) in galaxies at high redshifts, due to a higher target matter density (122). The cosmic-ray density is higher in starburst galaxies (123), but the ratio of gamma-ray and stellar luminosity is probably the same, since both are driven by massive stars, and therefore the contribution from these galaxies is accounted for by the normalizing factor u_* in the above estimate.

4.4.2 Active Galactic Nuclei

AGNs have received considerable attention as possible powerful sources of high-energy neutrinos, since their bolometric nonthermal energy release far exceeds that of any other known population [such as SNRs or gamma-ray bursts (124, 125)]. Roughly 1% of all bright galaxies [possibly many more at high redshifts (60)] possess an active nucleus in which the equivalent of the radiation power of more than the entire stellar inventory of our galaxy is radiated from a small region, less than the size of the planetary system.

The only known mechanism that could provide and sustain this luminosity for at least 10^8 years is the gravitational energy release associated with accreting supermassive black holes of mass $M = 10^8 M_\odot$ lurking in the centers of galaxies (126). The maximum luminosity for spherical accretion onto a black hole of mass $M = 10^8 M_\odot$ is the Eddington luminosity, $L_E = 1.3 \times 10^{46} M_8 \text{ erg s}^{-1}$, at which the radiation force and the gravitational attraction balance each other. By equating the radiation energy density at the radius of the last marginally stable orbit around the black hole $r_{\text{ms}} = 6GM/c^2$ with that of a black body emitter $L_E/(4\pi r_{\text{ms}}^2 c) = aT^4$ with $a = 7.56 \times 10^{-15} \text{ erg cm}^{-3} \text{ deg}^{-4}$, one obtains the temperature $T \approx 10^5 M_8^{-1/4} \text{ K}$ corresponding to a Wien peak in the ultraviolet (127). Such an ultraluminous and short-term variable “big blue bump” is in fact characteristic of AGN spectra and is taken as evidence for the presence of black holes (129). Doppler-broadened and gravitationally redshifted iron K_α fluorescence lines strengthen this interpretation (130) and further suggest the presence of an accretion disk, which is also revealed on larger scales by the maser lines emitted by molecular clouds embedded in it (131). The accretion flow could be shocked and, in the presence of magnetic fields, initiate shock acceleration of protons (132).

Since the early work of Berezinsky (see references in 30), it has several times been noted that if the matter density is low enough, proton acceleration could continue until saturation with photo-pair and photo-meson production (e.g. in References 100, 133–135). If the radiation field is the thermal radiation field of the accretion flow, this leads to ample neutrino production peaking around the energy $E_{\text{th}}/20 \approx 10^6 \text{ GeV}$, as strongly emphasized in Reference 135. Below this energy, the neutrino spectrum is essentially the flat decay spectrum of the pions until the neutrino flux due to pp collisions begins to dominate (136, 71). Due to the high photon density near the black hole, gamma rays from pion decay are reprocessed by electromagnetic cascades into the X-ray band below $m_e c^2 \sim 500 \text{ keV}$, where photons emerge with a nonthermal spectrum (137). The observed X-ray spectra of AGNs as well as the spectrum of the diffuse X-ray background indicate, however, that AGN X-rays are thermal in origin, have a peak at around 100 keV, and cannot be explained by electromagnetic cascades (138).

Stecker & Salamon (139) circumvented this problem by lowering the normalization of the neutrino spectrum to a value corresponding to an electromagnetic fraction of only 30% of the diffuse X-ray background, which is somewhat arbitrary. Another possible escape from this problem (71) assumes a very high matter density of the accretion flow so as to thermalize the gamma rays. This has the additional effect of causing pp -interaction energy losses to dominate over

photo-pion production, which changes the energy spectrum of the emerging neutrinos, as discussed in Section 4.2. A higher target matter density would quench Fermi acceleration, which requires collisionless conditions, unless the particle acceleration zone is located away from the accretion flow. This is possible in AGNs, in which a jet emerges from the accretion disk, transporting some of the released energy (and angular momentum) away from the black hole. These jets can be highly supersonic and therefore a convenient environment for shock acceleration.

Jets in radio-loud AGNs emit strong nonthermal radiation at all wavelengths and show evidence of apparent superluminal motion, indicating relativistic bulk motion as described in the model of Blandford & Königl (140). This jet emission is strongly beamed around the jet axis (the rotation axis of the supermassive black hole). Beamed radio-loud AGNs in which the jet axis is close to the line of sight (the so-called blazars) have recently received increasing attention, since they are very strong gamma-ray emitters (57). Gamma rays from one source, Mrk501, have detected up to $E_\gamma \simeq 20$ TeV (141). This observation supports hadronic emission models and casts doubt on models based on accelerated electrons, as pointed out in Reference 142.

Unresolved blazars contribute up to $\sim 25\%$ of the diffuse isotropic gamma-ray background (59). The remaining fraction could be due to the unbeamed counterparts (radio galaxies), which are much more numerous. Since the resolved AGNs produce a cumulative flux that is 15% of the diffuse flux, the total flux provided by AGNs should be 115% of the observed diffuse gamma-ray background (83). Choosing $L_\nu \approx 0.5L_\gamma$, as appropriate for photo-pion production (63), we estimate that the sources could produce a muon neutrino energy flux of $E^2 I_E \approx 2 \times 10^{-6}$ GeV cm $^{-2}$ s $^{-1}$ sr $^{-1}$, which is plotted as the upper bound in Figure 8.

Depending on the distance from the shocks in the jet to the accretion disk, either the synchrotron photons produced by the accelerated electrons in the jets (143) or the thermal ultraviolet photons from the disk (144) provide the dominant target for pion production. The electron and photon targets lead to different expected neutrino spectra. The pp energy losses are generally very small, since the density of the jet material is very small. A viable possibility is that the jets hit some higher density clouds with either associated particle acceleration (145) or higher initial Lorentz factors of the jet particles (146). In Mannheim's Model A (65), the photoproduction of pions and pairs is assumed to dominate, and the spectral slope over a wide energy range is therefore given by $E^2 I_E \propto E^{2-\alpha} \propto E$, adopting $\alpha = 1$ (see Section 4.2). The spectrum is assumed ad hoc to become steeper by one power above 10^8 GeV due to the (unknown) distribution of maximum energies in the sources. When integrated over its broad energy range, this model produces a sizeable fraction of the diffuse gamma-ray background, and ultrahigh-energy cosmic rays above 3×10^{18} eV. Such a model could easily be modified to generate much higher neutrino fluxes at TeV energies, to reproduce the maximum model in Figure 8, as shown in Reference 67.

Maximum proton energies of up to 10^{20} eV require shocks with field strengths of the order of $B \sim 1$ G at scales $r \leq r_g(E_{\max}) = 0.1 B^{-1} (E_{\max}/10^{20} \text{ eV})$ pc. Adopting the equipartition magnetic field determined from $B^2/8\pi = L_{\text{edd}}/(4\pi r^2 c)$ for

which $B = 10^4(r/6 \times 10^{13} M_8 \text{ cm})^{-1} \text{ G}$, the magnetic field at 0.1 pc is indeed of the order of 1 G. The smallest scales for particle acceleration are of the order of the asymptotic jet radius, $r_j \approx 100$, $r_s \approx 3 \times 10^{15} M_8 \text{ cm}$. At these scales, the magnetic field strength should be of the order of $B \approx 100 \text{ G}$. This corresponds to $E_{\text{max}} \approx 10^{18} \text{ eV}$, which demonstrates why the AGN model neutrino flux peaks between $E_{\text{max}}/20 \approx 5 \times 10^{16} \text{ eV}$ and $5 \times 10^{18} \text{ eV}$.

It is important to note that these models compute the neutrinos produced at the acceleration site only. Further neutrino production occurs in the storage volume of the accelerated protons and ions, that is, either the AGN host galaxy or the galaxy cluster. It is impossible to predict the slope of the cosmic rays stored in the host galaxies, for it depends on the escape probability. Assuming conditions similar to those in our galaxy, one obtains a steepened spectrum $I_E \propto E^{-2.5}$, and the bolometric flux is still bounded by the diffuse gamma-ray background flux.

A remarkable property of the predicted AGN neutrino fluxes is that they are highly beamed; the most luminous sources, such as the quasar 3C273, should contribute about 1% of the expected diffuse neutrino background. This is not just theory; the flux of the brightest 50 gamma-ray AGNs detected by EGRET is 15% of the diffuse gamma-ray background. Thus, a neutrino telescope should have good angular resolution to reduce the background at energies in the TeV region, where the isotropic atmospheric background is bolometrically still dominant.

4.4.3 Galaxy Clusters

As shown in Section 4.4.1, the neutrino emission due to cosmic rays in other galaxies is generally expected to be rather low. One reason is the rapid leakage of cosmic rays out of the galaxies as a containment volume, which leads to spectral steepening. However, the galaxies themselves are embedded in the much larger containment volume provided by the ionized gas in galaxy clusters, which acts as a target for the escaping cosmic rays and leads to generic pp neutrino production. Taking into account a formation scenario of the clusters and assuming a nonthermal energy input from galaxies of $3 \times 10^{40} \text{ erg s}^{-1}$ per galaxy and from AGNs of $10^{44} \text{ erg s}^{-1}$ per AGN, Colafrancesco & Blasi (70) conclude that the clusters do not contribute more than a few percent to the diffuse gamma-ray background and, consequently, that the diffuse neutrino background produced by them would be about two orders of magnitude below the maximum allowed value (147–150). A higher flux would indeed lead to conflicts with EGRET flux limits for individual nearby galaxy clusters.

4.4.4 Gamma-Ray Bursts

Gamma-ray bursts (GRBs) are the most luminous known cataclysmic phenomena. From general physical considerations, Meszáros & Rees (151) derived a consistent and physically plausible model for relativistic fireballs that can explain the observed properties of GRBs rather well (allowing for beaming). In this model, the observed radiation originates from electrons accelerated at shock waves

associated with the relativistically expanding ejecta with typical bulk Lorentz factors $\Gamma \approx 300$. The nature of the cataclysmic event that releases a large fraction of the binding energy of a solar mass in the observed radiation is under dispute. For example, mergers of neutron stars or collapses of very massive stars (hypernovae) have been considered. The cosmological fireball model is consistent with the most recent finding of the GRBs' cosmological distances and the occurrence of lower-frequency afterglows. Neutrinos at nuclear energies are certainly associated with the collapse during a merger or hypernova (152), but high-energy neutrinos associated with hadronic interactions of accelerated protons and ions should also occur (153, 154). Milgrom & Usov (155) were the first to note the possible association of UHE cosmic rays and GRBs (although the argument has been invalidated by the discovery that most GRBs seem to be too far away for emitted protons to survive energy losses traversing the microwave background; see References 67 and 156 for discussion), and this observation gave rise to the models by Waxman & Bahcall (157) and Vietri (158) for neutrino emission due to accelerated protons in GRBs. Rachen & Mesz  ros (63) point out important corrections to these models. Plaga (159) suggests, instead, that superconducting cosmic strings are the source of GRBs, and predicts associated neutrino emission.

From our outline for generic models in Section 4.2, it is easy to understand the shape of the expected neutrino spectrum. As in the case of AGNs, the dominant targets for protons at high energies are the photons produced by the accelerated electrons, and their spectral index is $\alpha \approx 0$ below MeV and $\alpha \approx 1$ above. Considering the effect of the threshold condition for hadronic interactions with accelerated protons, this spectral break for the photons translates into one for the protons at the energy

$$E_{pb} = \frac{\Gamma^2 E_{th}}{\epsilon_{\gamma b}} = 1.3 \times 10^7 \Gamma_{300}^2 \left(\frac{\epsilon_{\gamma b}}{1 \text{ MeV}} \right)^{-1} \text{ GeV}, \quad 24.$$

where $\Gamma_{300} = \Gamma/300$.

For energies above this break, $\alpha = 0$ is the relevant target index, and below it is $\alpha = 1$. The corresponding spectral slopes of the neutrino spectrum are $E^2 dN_\nu/dE_\nu \propto \text{const.}$ above $E_{\nu b} \approx E_{pb}/20 \approx 10^5 \text{ GeV}$ and $E^2 dN_\nu/dE_\nu \propto E_\nu$ below $E_{\nu b}$, assuming a proton spectrum $dN_p/dE_p \propto E_p^{-2}$. Another break by one power occurs above $10^7 \Gamma_{300}^2 (\Delta t/\text{ms}) \text{ GeV}$ because of the adiabatic losses of muons when their decay length exceeds the emission-zone radius. Note, however, that a slope of $s = -2$ is not expected from theoretical studies of particle acceleration at relativistic shock waves [some authors (see e.g. 101–103, 160) favor values $s = 2.2\text{--}2.4$], and that the observed synchrotron spectrum does not support this slope for the electron. (The spectral index connected with it is $\alpha = 0.5$.) On other hand, the reverse shock or internal shocks could be only mildly relativistic in the frame of the expanding fireball and the local spectrum of the target photons could be different from the spatially averaged spectrum.

The flux normalization of GRB neutrino spectra requires the knowledge of their proton luminosity, which follows from the assumption that they produce the observed UHE cosmic rays. Assuming that GRBs are cosmologically distributed

but not evolving with redshift, one obtains an energy flux of $E^2 dN_\nu/dE_\nu \sim (f_\nu/0.1) 10^{-8} \text{ GeV cm}^{-2} \text{ s}^{-1} \text{ sr}^{-1}$, where f_ν denotes the ratio of proton power converted into neutrinos. If the luminosity density of GRBs increases in the same way as that of galaxies and AGNs with redshift [e.g. $\propto(1+z)^{3.8}$ in a frame co-moving with the Hubble flow], the present-day neutrino and (isotropic diffuse) gamma-ray fluxes should be much larger (see the discussion in Section 3 and Reference 161).

A signature of proton acceleration in GRBs would be high-energy tails in their spectra (162). There is a small chance of detecting TeV emission from the nearest GRBs, and the possible detection of a GRB using the MILAGRITO detector has been announced (163). However, high-energy gamma rays emitted from bursts at large cosmological redshifts inevitably suffer pair attenuation (164) whereas neutrinos do not, and thus only neutrino astronomy can decide the issue.

5. NEUTRINOS FROM DARK MATTER AND OTHER INTERESTING PHYSICS SIGNATURES

The previous sections have dealt with guaranteed and potential sources of cosmic neutrinos of high energy. A great many more speculative possibilities have been discussed over the years. These have to do with the decay or annihilation of Big Bang relic exotica. We also discuss several unique signatures for neutrinos.

5.1 Cosmological High-Energy Neutrinos

Here we discuss the various possibilities for neutrinos arising from some cosmological relics.

5.1.1 WIMPs in the Earth, Sun, and Galaxy Cluster

Weakly interacting massive particles (WIMPs) have been proposed as a generic class of particles that could solve the riddle of the missing dark matter in the universe. If these WIMPs are massive and are sufficiently long-lived and weakly interacting (but not as weak as gravity), then they may become trapped by elastic scattering in the core of astronomical bodies, such as the Earth and Sun. If, furthermore, these WIMPs exist as both particles and antiparticles, or as Majorana particles (which are their own antiparticles), then they may annihilate as they reach sufficient densities. This annihilation may lead to interesting fluxes of neutrinos at energies typically $1/3$ the mass of the WIMP. Detection of such neutrinos could provide indirect evidence for WIMPs, in contrast to the more direct detection that is pursued by very-low-background detectors in deep mines seeking the $\mathcal{O}(\text{KeV})$ signals produced by elastic scattering of the WIMPs. There has been debate about the relative merits of the search methods, but both should be pursued, since in some situations one might succeed where the other would fail. Surely the search for dark matter is one of the most important quests in science at this time. The

problem is that we are really groping in the dark, and without clues it is hard to justify spending huge resources on such investigations.

Because the subject is complex and there are many calculations, and because it relates mainly to lower-energy neutrinos, we review the subject only briefly here. Most of the calculations have to do with a specific realization of WIMPs in supersymmetry. Here the number of unknowns is daunting. The minimal supersymmetric standard model (MSSM) contains 105 parameters plus 19 from the standard model. These may be reduced to about 7 by various debatable but essential assumptions. If supersymmetric particles must be produced in pairs, the lightest supersymmetric particle (LSP) should not decay. It may be the needed WIMP, but it is not clear which particle in the MSSM is to be identified with the LSP. Since charged LSPs are ruled out over a large range of parameter space, the favorite candidate is among the four neutralinos, the superpartners of the two neutral Higgs bosons, the Z^0 and photon. The trouble is that the mixing that generates the mass eigenstates depends on the MSSM parameters, and a range of masses from ~ 1 GeV to ~ 1 TeV is permissible, with 10 GeV to 500 GeV favored (165).

Figure 11 shows one example from the several useful plots in Reference 166. Existing best limits from Baksan, MACRO, IMB, Kamiokande, and (soon) Super-Kamiokande are at the level of 10^3 muons/km²/yr for through-going muons. A 1-km² array could thus make significant progress, although it would by no means cover all of the phase space for possible models. It is important to note that the calculations are for a muon threshold energy of 25 GeV, whereas the optimal muon threshold would be even lower, down to several GeV. This can be translated directly into cost in designs of cubic-kilometer arrays: to first order, a given budget

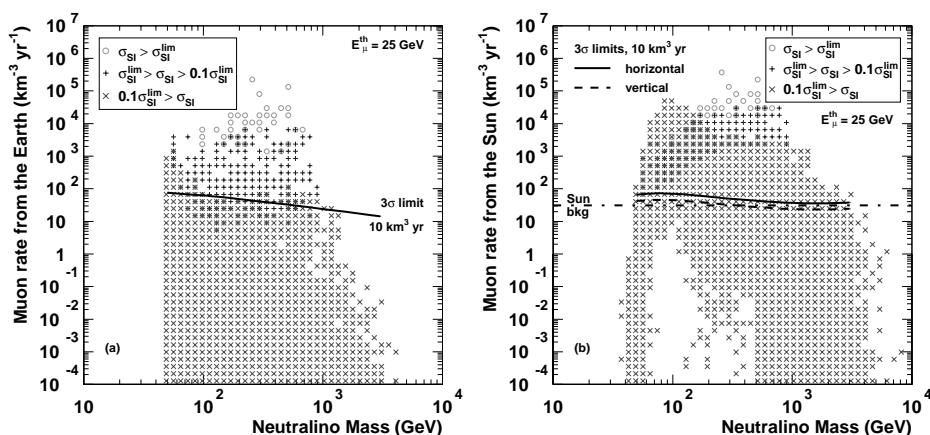
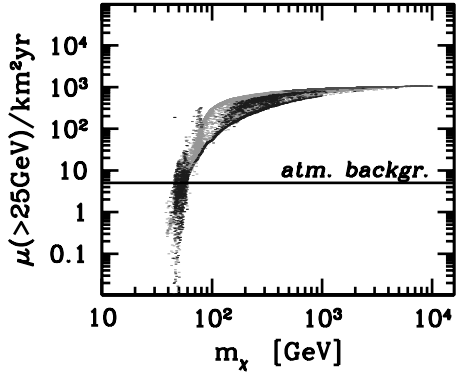


Figure 11 Contained-event rates in a 1-km³ detector for neutrinos generated by WIMP annihilation in (a) the Earth and (b) the Sun, with a muon energy threshold of 25 GeV. The best 3σ limits with an exposure of 10 km³/year are also shown, as well as the background from the Sun's corona. (From Reference 166 with permission.)

Figure 12 Maximal flux of neutrino-induced muons in a neutrino telescope from neutralino annihilations at the galactic center, after imposing the current constraints on the neutrino emission. (From Reference 167 with permission.)



purchases a certain light-collector area, and the ratio of muon detection area to threshold energy is constant.

Another place to search for WIMP signals may be the galactic center. Recent simulations (167) have shown that the dark matter halo of galaxies may be sharply “cusped” toward the center. This is the case with our galaxy; there is growing evidence that it harbors a $(2.6 \pm 0.2) \times 10^6 M_{\odot}$ black hole. In this region, WIMPs, or neutralinos specifically in the numerical example, may annihilate, making substantial fluxes of neutrinos (more efficiently than within dense matter, as well, since all secondary particles decay prior to absorption). Existing limits (as no peaking is seen) on neutrinos from the direction of the galactic center, as measured by underground detectors, significantly constrain the density slope of the inner halo (167). Figure 12 illustrates the rate of muons expected with various selections of neutralino models and density profile slopes. The current constraints (≈ 1000 muons/km²/yr) from underground detectors have already been taken into account, and a cubic-kilometer detector can improve on this result by several orders of magnitude. Ultimately the atmospheric background line shown is not an impenetrable limit in sensitivity; going below that line is a matter of statistics, so that with patience, one may reach a greater sensitivity.

In summary, neutrino telescopes can make significant contributions to the search for dark matter and supersymmetric particles. The searches are in several ways complementary to direct searches. For maximal sensitivity, the neutrino telescopes need a muon energy threshold of a few GeV. Searching for neutrinos from the Sun and galactic center could produce significant results, whereas the sensitivity regarding the Earth as a source more nearly overlaps with the sensitivity of direct searches.

5.1.2 Evaporating Black Holes

Ever since the famous realization by Hawking (168) that black holes (BH) radiate, and may radiate elementary particles at fierce rates as they evaporate, people have

speculated on black holes as sources of cosmic rays. Since the temperature of the black hole goes as $T_{\text{BH}} = M_{\text{P}}^2/8\pi M_{\text{BH}}$, with the Planck mass $M_{\text{P}} = 1.22 \times 10^{19}$ GeV, the radiation winds up in a flash increase of temperature to energies where there is much debate about exactly what may take place. Black holes evaporate only if their temperature is above the cosmic background radiation temperature, so the limit of M_{BH} is $<0.8\% M_{\odot} = 4.8 \times 10^{25}$ gm. This excludes those black holes expected from gravitational stellar collapse, which would have masses greater than the Sun, because the lifetime for evaporation is on the order of $10^{64} (M_{\text{BH}}/M_{\odot})^3$ years. Such black holes never evaporate. The lifetime for evaporation is on the order of the age of the universe for $M_{\text{BH}} \simeq 4.4 \times 10^{14} (H/100 \text{ km/s/Mpc})^{0.3}$ gm, assuming $\Omega = 1$ (170). (That is only about 440 megatons!) Hence the small evaporating black holes under consideration are primordial black holes (PBHs), formed during the Big Bang.

The integral of PBH density times mass is restricted by the contribution to the total mass density of the universe. Moreover, one would expect that the black holes would be clustered in the galaxy, or perhaps the halo. The initial mass function is not known and could vary a great deal depending on the time of formation. Given the expected evaporation temperature of about 100 MeV, there are fairly strict limits on the local evaporation of PBHs from observations of cosmic gamma-ray backgrounds, of the order of $10^{-8} \Omega_{\text{crit}}$ (169). This means that local observations are unlikely.

The possible role for neutrino astronomy here is in the detection of UHE neutrinos that might arise from the last instant of decay of these PBHs, and there is great uncertainty about that process as the hole reaches the Planck mass. Most models and limits derived with these models disfavor PBHs as the explanation for cosmic-ray events beyond the GZK cutoff (171).

5.1.3 Monopoles and Other Ultrahigh-Energy Relic Particles

Magnetic monopoles and similar massive relic particles may also produce neutrinos through decay or annihilation, as discussed above for WIMPs. (These particles may be considered WIMPs for search purposes.) However, direct detection of such particles as monopoles, supersymmetric Q-balls, quark nuggets, and the like may be possible. The signature varies according to the object and interactions. For example, an incoming monopole at galactic velocities ($10^{-4} < \beta < 10^{-3}$) may produce a string of (Rubakov) nucleon decays (172). This would create a slow-moving, intense, and fluctuating source of Cherenkov radiation, which should be observable in most large detectors. Indeed, limits have been set by most of the underwater and underground detectors (IMB, Kamioka, Baksan, MACRO), with Baikal having the current strongest bound (173). Baikal also set limits on relativistic monopoles with velocities $\beta > 0.75$ (173).

Supersymmetric models allow for stable nontopological solitons, Q-balls, which could have been produced in the early universe and contribute to dark matter. The experimental signature of electrically neutral Q-balls is similar to that expected

for superheavy magnetic monopoles that catalyze baryon decay. The Baikal group reports a limit of $3.9 \times 10^{-16} \text{ cm}^2/\text{sr/s}$ (90% CL) on such a flux (174). AMANDA has reported similar results. This could be improved by two to three orders of magnitude in a cubic-kilometer neutrino detector.

Other searches involve seeking a nonrelativistic light source traversing the array, perhaps generating light by heating along the path. Limits are similar and no hint of such events has been seen.

5.1.4 Other Topological Defects

One of the most ambiguous areas of suggested sources of UHE neutrinos comes from various “top-down” scenarios that produce the highest-energy cosmic rays by cascading from unification-scale energies (175–178). Such processes must necessarily produce significant fractions of neutrinos, with energies up to perhaps 10^{25} eV. In any case, concerns have been raised that the seemingly unavoidable cascading of the gammas to lower energies around 1 GeV constrains these models, depending strongly on the (not well-determined) intergalactic magnetic fields (179–182).

5.2 Multiple Production of W Bosons and Such

It has been suggested that giant neutrino detectors might shed light on such phenomena as multiple W production, sphaleron processes, quark compositeness, and leptoquark production (183). In the case of multiple W production, the idea is that at some point the nonperturbative production of $\mathcal{O}(1/\alpha_W) \simeq 30$ bosons may occur. In the down-going cosmic radiation seen by underground detectors, this could lead to unusual three-muon events from the prompt decay of the W bosons. This signature will be heavily obscured by normal down-going extensive air showers. However, the close clustering of the muons could be a signal, although detectors on the cubic-kilometer scale may not be able to resolve close multiples. A potentially clearer signal could come from neutrino interactions, and here the tipoff would be incoming multiple muons from near the horizon or upward (for which there is currently no evidence).

The LHC will have an opportunity to seek many- W events, though it may be difficult to separate signal from background. The calculations, being nonperturbative, are very unreliable, so the experimenter can only look. Since past underground experiments have shown hints of multiple down-going muon clusters, there is reason for hope.

5.3 Peculiar Features in the Neutrino Cross Section

The standard calculations of the neutrino-nucleon cross section lead to a smoothly rising cross section increasingly dominated by the sea quarks of heavier varieties with higher energy. We have already mentioned one variation of this pattern with the resonance of $\bar{\nu}_e + e^- \rightarrow W^-$ at 6.4 PeV, where the cross section rises to 300 times the normal CC value. In a similar vein, it may be that neutrinos of sufficient energy will encounter resonances with quarks, perhaps through a scalar leptoquark as

proposed in Reference 184. These would be signaled by multi-TeV cascades with $E_{\text{cas}} \simeq m_{s_0}^2/2m_p$. With increased limits on a leptoquark mass, this possibility fades, as it would require large VHE fluxes (as from optimistic AGN models) to observe. Still, cubic-kilometer detectors will be probing the neutrino interactions at energies not soon accessible by accelerators, so surprises could arise. An example would be rapid cross-section growth due to extra dimensional effects (185).

5.4 Cosmological Neutrino Absorption (Weiler Process)

Weiler (186) realized that if there are abundant UHE neutrinos from the early universe, and if neutrinos have some mass and are now moving slowly, there will be a resonance energy,

$$E_{\nu_j}^R = M_Z^2/2m_{\nu_j} = 4 \left(\frac{\text{eV}}{m_{\nu_j}} \right) \times 10^{21} \text{ eV}, \quad 25.$$

at which the absorption cross section will be important,

$$\langle \sigma_{\text{ann}} \rangle \equiv \int \frac{ds}{M_Z^2} \sigma_{\text{ann}}(s) = 4\pi G_F / \sqrt{2} = 4.2 \times 10^{-32} \text{ cm}^2, \quad 26.$$

where s is the square of the energy in the center of momentum frame, with peak width of $\Gamma_Z/M_Z = \pm 3\%$. UHE neutrinos from a great distance may thus be attenuated by the relic neutrinos, causing a notch in the neutrino spectrum incident on the Earth. Such an observation would be marvelous on both scores, detecting the UHE neutrinos and making probably the first observation of the relic neutrinos. However, as the neutrino mass limits have crept downward, the resonant energy $E_{\nu_j}^R$ has moved upward to energies formerly considered implausible.

A quandary has emerged in recent years, with a total of six different extensive air shower arrays having detected more than 24 events near or above $10^{20} \text{ eV} = 100 \text{ EeV}$, well above the GZK cutoff. Many proposals have been put forward to solve this problem.

Weiler and others have revived the idea of UHE neutrino interaction on relic neutrinos, with a new twist (187–189). The idea is that perhaps that superhigh-energy neutrinos of distant origin are scattering from the relic neutrinos somewhere within the GZK cutoff distance of about 50 Mpc, where they produce a Z that decays to around 30 gammas, 2.7 nucleons, and 84 neutrinos, plus 28 electrons and positrons. The rate of these “ Z bursts” may be significantly increased by the local accumulation of neutrinos with mass in our supercluster, and estimates are in the range of 1% for conversion of neutrinos within the GZK distance. By this means, nucleons and gammas above the GZK cutoff may arrive at Earth and produce the observed extensive air shower. One must worry about the non-observation of the (degraded in energy but multiplied in number of) electromagnetic particles, though it is claimed that this constraint is satisfied by the model presented (189). Of course, this raises the question of how such superheavy-element (SHE) neutrinos could be generated in the first place. One source could be cosmic rays from early bright-phase galaxies, or AGNs. As discussed above, AGNs may well possess

hidden neutrino sources. There is the possibility of acceleration in a dense plasma up to energies on the order of 10^{25} eV (Y Takahashi, T Tajima, article in preparation; 190). One may invoke essentially all the proposals for top-down production of high-energy particles, but with the improvements that they are not restricted to be anywhere near us in space-time and that constraints due to photons and anisotropy are eased (191).

5.5 Tau Appearance in Astrophysical Long-Baseline Experiments

Identification of the appearance of tau leptons from ν_τ CC interactions with terrestrial sources poses a terrific challenge to experimentalists because the flight distance before decay is $c\tau E/m_\tau = 86.93 \mu\text{m} (E/1.777 \text{ GeV})$. However, for a 2-PeV tau, the flight distance before decay will be of the order of 100 m, and the decay will be spectacular. Moreover, the initial cascade induced by the momentum transferred to the target quark will typically be half the energy of the decay burst (192). Since the tau will travel with relatively little showering compared with the muon, the intervening track will be fairly clean. At lower energies this signature will not be as clean (due to muons and cascade “punch-through”), whereas at higher energies both events may not be recorded, even in a cubic-kilometer detector. Of course, at higher energies, any entering track that suddenly ends in such a tremendous cascade (say 10 PeV) is probably a tau, since the radiation length for a 10-PeV muon is of the order of 20 cm).

In this energy range, given enough neutrino events (as from AGNs), one may determine the ratios of the neutrino flavors by detecting the muon CC events, the $\bar{\nu}_e$ resonant events, and the tau double-bang signature. As pointed out previously (192–194), the ability to discern the neutrino flavor mix in the PeV region provides an excellent opportunity both to look for neutrino mixing not otherwise accessible [$\delta m^2 \sim \mathcal{O}(10^{-16} \text{ eV}^2)$] and to learn about the production environment. The observation of point sources in this region provides the ultimate “long-baseline” neutrino experiment.

The double-bang signature may also be useful at energies in the EeV range, where the shower separations may be $\mathcal{O}(100 \text{ km})$. In this instance, the observation is restricted to the atmosphere, with the neutrinos arriving near tangent to the Earth, as may be observed with extensive air shower arrays such as the HiRes, the LTA, the atmospheric fluorescence detector associated with the Auger Project, or the proposed space-based OWL/Airwatch detectors. Other possibilities may be via radio detection of the cascades (195) or radar observation of the ionized wake of such events (196).

5.6 Neutrino Mass Measurement Using Time-Variable Astrophysical Sources

The neutrino mass makes a slight and at least potentially measurable difference in the arrival time relative to photons, gravity waves, and various flavors of differing

masses. The time difference from a massless particle is only

$$\Delta t(E) = 0.515 \text{ s} \left(\frac{m}{1 \text{ eV}} \right)^2 \left(\frac{1 \text{ MeV}}{E} \right)^2 \left(\frac{D}{10 \text{ kpc}} \right). \quad 27.$$

Thus, for a typical supernova neutrino with an energy of 20 MeV, a mass of 0.1 eV, and an optimistically small distance of 1 kpc, the time shift is only 0.7 ms. For cosmological distances, the time difference is about the same for a neutrino of energy 20 GeV and distance near 1000 Mpc.

People have long discussed the potential of making direct neutrino mass determinations from supernova neutrinos, and the work has been updated as detectors have improved (197). It appears that mass determinations are limited to several tens of eV via this method. Other indirect neutrino mass measurements via large-scale structure, the cosmic microwave background, weak lensing, and the Lyman-alpha forest may yield summed mass measures in the same range of 1–10 eV.

Stodolsky (198) has pointed out that despite the formidable obstacles to direct time difference measurement, the payoff would be great, since the time difference from a distant source (at redshift z) depends on the Hubble constant H and the acceleration parameter q as

$$\Delta t \approx \frac{z}{H} \left(1 - \frac{3+q}{2} + \dots \right) \frac{1}{2} \left(\frac{m_1^2}{P_1^2} - \frac{m_2^2}{P_2^2} \right). \quad 28.$$

Thus, for sharply impulsive sources, one could in principle measure the Hubble constant and acceleration parameter and avoid the problems of evolution, absorption, etc that arise in other methods. This may not be so hopeless in the future if it becomes possible to detect periodic sources (as with pulsars).

6. EXPERIMENTAL APPROACHES

In this section we discuss the design of high-energy neutrino telescopes to observe neutrinos with energies ≥ 100 MeV, and especially above 1 TeV. From the earlier sections one sees that the size of device needed is in the range of a gigaton effective target volume and a square kilometer of muon detection area in order to surely begin neutrino astronomy.

For the detection of solar neutrinos or neutrinos from gravitational stellar collapse, the appropriate technology is distinct. It includes radiochemical detection and large underground instruments. For the foreseeable future, costs for adequate sensitivity will limit such detectors to about a megaton at most. The next section briefly reviews the relevant underground instruments currently in operation or planned.

We start with general design considerations, short discussions of the various techniques proposed, and a discussion of the effects of size and threshold on sensitivity. We offer some remarks about detection of muons versus cascades of

TABLE 1 Techniques proposed for large neutrino detectors

Radiation	Medium	Detect muon	E_ν Threshold	Attenuation length	Spectral region
Cherenkov	Filtered H ₂ O	Y	GeV	100 m	300–500 nm
	Natural lake	Y	GeV	~20 m	400–500 nm
	Deep ocean	Y	GeV	~40 m	350–500 nm
	Polar ice	Y	GeV	~20 m	300–500 nm
Cherenkov radio	Polar ice	N	>5 PeV	~1 km	0.1–1 GHz
Cherenkov radio	Moon	N	>100 EeV		1–2 GHz
Acoustic	Water	N	>1 PeV	~5 km	10–20 kHz
	Ice	N	>PeV	?	10–30 kHz
	Salt	N	>PeV	?	10–50 kHz
EAS* particles	Air	N	10 PeV	1 km	100 MeV
N ₂ fluorescence	Air	N	EeV	10 km	337 nm
EAS radar	Air	N	>EeV	(~100 km)	30–100 MHz

* EAS, extensive air shower.

particles and conclude by noting design principles that have emerged from various workshops and field experience.

6.1 Survey of Techniques

Table 1 summarizes the detection techniques that have been explored. We discuss each one below, particularly the much-studied water Cherenkov technique.

6.1.1 General Considerations

In designing high-energy neutrino detection experiments, the primary considerations are target volume and threshold energy. Fortunately, the “detectability” of neutrinos rises with energy, as does the interaction cross section; we have intrinsically more energy deposition to work with than, say, for solar neutrinos. At high energies, there is a tradeoff between energy threshold and sensitivity, as we illustrate for water Cherenkov detectors below.

A detector of appropriate size for high-energy neutrino detection requires sensitivity over an area of 10^6 m². Covering this large area with detectors that intercept the particles would be extremely costly. An instrument similar to fixed-target accelerators, consisting of layers of particle ionization sensitive devices, that provides tracking over a reasonable solid angle for through-going muons, would require at least 10^7 m² of detection planes. Even the least expensive tracking detectors, which cost more than US \$100/m², would place the total cost for detectors alone (excluding other substantial costs for the total system, such as environmental housing and deployment) beyond the budgets of today’s typical large-scale instruments. (The biggest present-day natural neutrino experiment, Super-Kamiokande, cost close to US \$100 million.)

Accordingly, the particle-sensing method chosen must detect tracks at some substantial impact parameter from the sensor. Cherenkov radiation in a transparent medium has this capability. Commercially available photomultipliers with $\sim 0.1 \text{ m}^2$ area can “see” minimum ionizing muons out to approximately 100 m in the clearest natural water or ice. This leads to area gain of about 10^5 , at the price of spatial resolution, of course.

Other means of sensing at a distance are variations on Cherenkov radiation such as radio detection (exploiting the transparency of water to radio waves at frequencies below 100 MHz) and acoustic detection. Acoustic detection depends on the fact that acoustic waves propagate with little loss through homogeneous solid or liquid media. At typical frequencies (10 kHz), sound waves easily travel kilometer distances in water.

One interesting variation on this rule occurs at sufficiently high (EeV) energies in sufficiently tenuous media, such as the atmosphere. Here the secondary particles are numerous enough (typically one particle per GeV at shower maximum) and the medium thin enough that showers spread over substantial distances, allowing a single detector to sample events up to about a kilometer away from the core axis. Because of the high energies and resulting high particle densities, one can place detectors on a small fraction of the area (typically $< 1\%$). This is the classic extensive air shower technique. Neutrinos can be uniquely recognized by finding EASs arriving from near the horizontal direction and interacting at atmospheric column depths too large for ordinary incoming cosmic rays (protons and heavier nuclei) to have survived.

Another type of radiation from interactions that may be sensed at a distance is scintillation of the medium, which radiates light isotropically. Owing to the cost of manmade scintillating materials ($> \text{US } \$1000/\text{ton}$), only natural scintillators may be considered for present purposes. So far, the only practical source of natural scintillators is atmospheric nitrogen, whose output light has enabled remote optical tracking of extensive air showers, as realized by the Fly’s Eye and similar instruments. This trick does not work in the only naturally available transparent solid (ice) or liquid (water) because they apparently scintillate little.

In sum, high-energy neutrino astronomy requires a remote sensing technique for the neutrino interactions and requires a very low-cost target/detection medium. The only means yet identified that satisfy these requirements are listed in Table 1. We discuss each in turn in the following sections.

6.1.2 Optical Cherenkov Technique

Cherenkov radiation has been known since 1934 and understood since 1937. This classical electromagnetic phenomena is simply the delta function polarization and relaxation of atoms along the route of a particle where the charged particle velocity exceeds the velocity of light propagation in the medium. The Cherenkov angle (θ_c) is thus given by

$$\theta_c = \cos^{-1}(1/n\beta), \quad 29.$$

where n is the index of refraction in the medium and $\beta = v/c$ is the velocity of the particle divided by the speed of light. Fast charged particles will radiate as long as $\beta > c/n$. Particles with relativistic energies leave a light wake of constant angle until close to Cherenkov threshold, which involves only the last few centimeters of range. The spectrum is that of the Fourier transform of a delta function in time (thus flat in frequency space) and $1/\lambda^2$ in wavelength. The radiation per unit length x and wavelength λ is given by the Frank-Tamm formula (200),

$$\frac{d^2N}{dx d\lambda} = \frac{2\pi\alpha z^2}{\lambda^2} \left(1 - \frac{1}{\beta^2 n^2}\right), \tag{30}$$

where z is the particle charge. The optical dispersion of water is slight within the useful wavelength range, it is a good approximation to take the index of refraction to be roughly constant. The effective wavelength interval for water and detectors is typically 310–500 nm and the effective number of radiated quanta per unit distance is

$$\frac{dN_{\text{eff}}}{dx} \simeq 200 \text{ photons/cm}. \tag{31}$$

Given the energy loss rate of 1.991 MeV/cm in pure water for a minimum ionizing particle, this means that Cherenkov radiation accounts for only 5.9×10^{-5} of the ionization energy loss. Yet this still allows a powerful detection tool, depending on the optics of the medium, since very sensitive detectors permit sensing from tens of meters of lateral distance from the particle trajectory.

Table 2 compares measurements in the three different situations—ice, lake, and ocean—as represented specifically by measurements from AMANDA, Baikal, and NESTOR (201). It is possible to find natural water and ice that are marvelously clear. The water in Lake Baikal is typical of the clearest near-surface waters, which have absorption and scattering lengths of 10–20 m. The clarity of the deep oceans, with an attenuation length of 40–50 m, was a pleasant surprise. This clarity is not altogether understood but apparently exists throughout the world’s oceans, including the Mediterranean Sea, below about 2 km depth. An even greater surprise

TABLE 2 Comparison of optical properties in various venues as related to optical Cherenkov detection in H₂O [see explanation in text (201)]

Venue	Ice	Ocean	Lake
Absorption length (m)	90–100	50–60	20–30
Scattering length (m)	3–5	~200	18
$\langle \cos(\theta_{\text{scatt.}}) \rangle$	0.88	0.88	0.95
Effective scattering length (m)	25–30	~2000	380
Effective attenuation length (m)	~25	40–50	~20
Distance to collect 1 photoelectron from a 100-TeV source (m)	95	200	105

was the discovery that the deep ice at the South Pole has absorption lengths comparable to ultrafiltered water, around 100 m. On the other side of the balance sheet, the deep ice was found to have significant scattering despite predictions to the contrary.

It is noteworthy that laboratory measurements of pure water have not been very good, so the first indications of the surprising blue transparency of pure water and ice have really been from measurements in the large underground detectors (IMB and Super-Kamiokande), and in the natural environs for the other experiments.

The important factor for the instruments in question is not the total scattering cross section but only that which scatters light significantly out of the direct path. This is an important distinction because there is typically a good deal of near-forward scattering (Mie regime) in such media. Optical oceanographers define a quantity called the diffuse attenuation coefficient, whereas physicists tend to employ the effective scattering length, which is

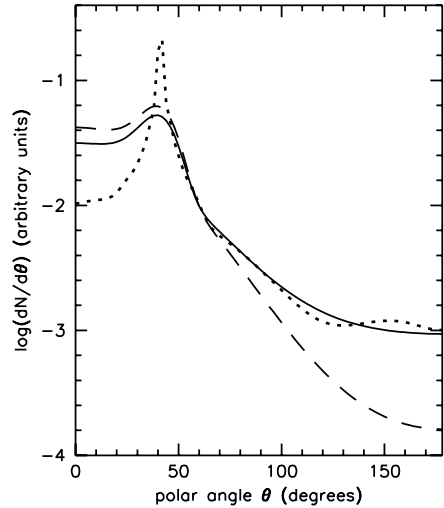
$$\Lambda_{\text{eff}} = \frac{\Lambda_{\text{scatt}}}{1 - \langle \cos(\theta_{\text{scatt}}) \rangle}. \quad 32.$$

As indicated in Table 2, the ocean and deep ice are in opposite optical regimes, the ocean being absorption-limited and the ice being scattering-limited. The ocean scattering has not been well measured because the length is so great, but it is thought to be near the Rayleigh scattering limit in the deep ocean, with the effective scattering length greater than 2 km. In the case of deep (2 km) Antarctic ice, the current speculation is that the source of the scattering involves the nucleation centers for the snow crystallization. Price (202) presents a model for scattering and absorption in the ice depending on the concentrations of minerals, salt, acid, and soot, at levels of the order of 10^{-7} . This model fits the available optical data, but it predicts significant depth-dependent variations and that the ice near 2 km depth should have poor optical properties. The model predictions suggest that the proposed ICECUBE should be placed at a depth of 1400–2000 m.

The last entry in the table (like most of the others) is from Djilkibaev's calculations (201) comparing the three locations. He presents calculations for the different media, taking into account the preferred detectors for each application (20-cm phototubes for AMANDA, 40-cm for NESTOR, and 37-cm for Baikal), as well as optics. The calculation also accounts for time of arrival of the photons, as only the nearly prompt photons are useful for event location. The example in the table involves photons within 25 ns of the light cone and a source energy of 100 TeV. It is thus apparent that the effective volume per module is about eight times greater in the ocean than in the ice and lake situations. This picture reverses somewhat if one considers the total photon collection, independent of arrival time; the total collection is about twice as great in ice as in the ocean (202).

The deep oceans appear to be better suited for the detection of large neutrino-induced cascades. Detection is possible at distances out to hundreds of meters before directional information is lost. Deep ice has the advantages of smaller background light and greater absorption lengths, and thus offers better calorimetry if one knows the vertex.

Figure 13 Several calculations of the expected angular distribution of Cherenkov light from a 6.4-PeV energy particle cascade in water. The dotted curve is an analytic form for an electromagnetic cascade (Belyaev). The other curves show results from a GEANT simulation by Hauptman: dashed for electromagnetic showers and solid for hadronic showers. (From Reference 231 with permission.)



6.1.3 Muon and Cascade Detection

Figure 13 illustrates the expected angular distribution of light from a 1-PeV cascade at a distance of 100 m in water. The vertex is taken as the center of the projection sphere for this figure. Since the extent of the cascade in water is about 10 m, the source is not entirely pointlike.

Nonetheless, the figure illustrates two points. First is that the cascade results in a conical light source, but with significant light in other directions. The shape of this angular distribution allows for the distant determination of cascade directions, which obviously is difficult compared with muon track direction registration. Estimates for the angular resolution depend on detector spacing and sensitivity, but typical angular resolutions are not expected to be better than a few degrees, compared to a degree or less for high-energy muons.

The second interesting point is that the light in the backward direction distinguishes between hadronic and electromagnetic sources. If real, this distinction could prove very useful in the future, determining for example that a cascade is due to the “Glashow resonance” in the (11% branching ratio) case of

$$\bar{\nu}_e + e^- \rightarrow W^- \rightarrow \bar{\nu}_e + e^-. \quad 33.$$

In ice, optical scattering appears to limit the range of detection of such cascades to less than 200 m, whereas the range in deep ocean water is approximately twice as great (and thus the target volume is eight times as great). However, in ice the directional information is quickly lost due to scattering. At very deep installations it would still be possible to search for the total diffuse neutrino flux down to the 10-TeV energy range (in the upper hemisphere anyway). At less deep installations, such as the one at the South Pole (which is limited to about 2 km depth), one must

be wary of backgrounds due to electromagnetic cascades from VHE down-going muons. Still, there appears to be a useful window allowing the search for cascades above roughly 100 TeV.

For the application of Cherenkov radiation to detect muons in water or ice, the situation is somewhat different. Here the range of detection in water is largely determined by the size of the light detector (the photomultiplier, as no other device is as yet competitive). The ocean has inescapable optical background light due to its radioactivity, which is mostly due to K^{40} decays. The ambient ocean light (which depends linearly on the optical absorption coefficient) is about $\phi_n = 200$ photons/cm².

6.1.4 Muon Versus Cascade Detection

If a simple cubical array of length L on a side contains N_d detection elements, each of area A_d , then an estimate of the number of signal photoelectrons from a through-going muon is

$$\langle n_{\text{pe}}^s \rangle \sim \frac{\eta \frac{dN_{\text{eff}}}{dx} A_d N_d}{L^2 \alpha}, \quad 34.$$

where η is the detector's effective quantum efficiency (averaged over wavelengths) and $1/\alpha$ is the effective optical attenuation length. The number of struck detectors will be a little smaller. As expected, the signal scales with the total photocathode area and the attenuation length and scales inversely with the array projected area. If we take $\eta = 20\%$, $A_d = 0.125$ m², $N_d = 1000$, and $L^2 = 1$ km², then the number of collected photoelectrons will be about 25.

In a coincidence time window Δt , the array will also collect

$$\langle n_{\text{pe}}^n \rangle = \eta \phi_n A_d N_d \Delta t, \quad 35.$$

which amounts to roughly 0.48 pe for the conditions above and $\Delta t = 10$ ns. The number of noise hits in the time interval required for the muon to traverse the array is 300 times larger, around 150 pe. Triggering such an array is not trivial and the noise cannot be eliminated until a rather good track fit has been achieved. For ice the situation is different: There is little photomultiplier noise but most hits are late because of optical scattering.

The latter point has incited much discussion about strategies to improve an unacceptable situation (150 pe noise with only 25 pe signal, in this example) to achieve a fitted track with little background. Strategies range from physically clustering the detectors and making local coincidences between adjacent units to beat back the noise on the local level (Baikal), to software triggers following light cones through the array (DUMAND). Nearest-neighbor triggers are generally effective, whatever the geometry.

One can do a similar calculation for cascades. Let us make the simplifying assumption that the light emission is isotropic. Then, if we take the probability of detection to be

$$P_{\text{det}} = 1 - e^{-m} \simeq m \quad 36.$$

in the small signal (small- m) limit where

$$m = \frac{N_\gamma \eta A_d e^{-\alpha r}}{4\pi r^2} \quad 37.$$

and where

$$N_\gamma = \frac{E_{\text{vis}} \frac{dN_{\text{eff}}}{dx}}{\frac{dE}{dx}}, \quad 38.$$

then this can be integrated over the volume surrounding the hypothetical vertex, giving an effective volume for the cascade,

$$V_{\text{eff}}^{\text{cas}} = \frac{N_\gamma \eta A_d}{\alpha}. \quad 39.$$

Using the same values as before for an estimate (for an ocean array), we arrive at the amazingly large volume of 1 km³ for a 10-TeV shower. However, this is now an overestimate, since the implied detection range is out to 625 m, at which range scattering must be taken into account even in the clearest waters.

We can estimate the sensitivity for such arrays as

$$S = \frac{0.1\text{pe}}{\text{GeV}} \frac{N_d}{10^3} \frac{10^9\text{m}^3}{L^3} \frac{A_d}{0.125\text{m}^2}. \quad 40.$$

This estimate works reasonably well from the scale of the underground instruments to cubic-kilometer arrays.

Two points should be made. First, in the hypothetical cubic-kilometer array in our example, a 10-TeV cascade occurring within the array would be detected by a large fraction of the array elements. Clearly the cascade would be well fitted in energy and angle. At around 100 GeV, about 10 detectors would sense the cascade, close to trigger threshold. The necessity of rejecting down-going muons would raise the useful threshold, depending on depth.

Second, one can use a very small number of detectors to make a search for UHE neutrinos over a significant volume, with much greater search power than using muons, but with much poorer pointing ability.

The situation in ice is interestingly different. The scattering length is short and the absorption length is long in comparison to deep ocean water. Moreover, in ice the optical background is nil, which cuts the required photodetector area in half. A reconstruction strategy, worked out by the AMANDA group, is to use the earliest hits for the vertex or track reconstruction and the full set of (straggling) hits for energy measurement. In principle one needs to fit for only seven parameters: three for a space point, two for direction, one for energy, and one for time. Thus at least seven good hits (i.e. on the light cone) are needed. Actually, the three space points and the single time point are overdetermined, and one may not care about the energy loss rate for muons, so the requirement can be reduced to a minimum of five detector hits to reconstruct a track.

The reduction to five hits is profitable because the probability for a direct hit goes as

$$P_{\text{direct}} = e^{-\beta x}, \quad 41.$$

where β is the effective scattering length. Thus, with $1/\beta \simeq 25$ m, one has about a 2% chance of recording a direct hit from a 100-m-distant source. If the source is bright enough to provide 100 pe at 100 m, then one photon would nearly always arrive promptly. Thus the calculations for the ocean apply for ice as well, except that we should use the effective scattering length instead of the attenuation length for the prompt hits.

Of course, one can create as large a neutrino detector as one wishes, whether in lake, ocean, or ice, if one can afford to deploy optical detectors on a sufficiently fine grid. From the optics standpoint it appears that the deep ocean represents the best choice; practical matters may dictate otherwise.

The idea of using Cherenkov radiation for large neutrino detectors arose shortly after the neutrino was discovered. Many years passed before it was possible to build a large detector, the earliest being the IMB instrument (10^4 m³), followed shortly by the HPW and Kamiokande detectors (10^3 m³). All three use (or used) photomultipliers in a tank of pure water located in deep mines and were built to search for nucleon decay, with neutrino astronomy as only a secondary goal. Of course it was the observation of SN1987A that paid off spectacularly for Kamiokande and IMB. The DUMAND project set out to apply the technique in the deep ocean and the Baikal project to do the same in Lake Baikal, both starting in about 1980. Although the DUMAND project was cancelled in 1995, three new projects have arisen to follow the quest in the ocean (NESTOR near Pylos, Greece; ANTARES near Marseilles, France; and NEMO near Sicily, Italy). Meanwhile, the AMANDA project began at the South Pole in 1992, utilizing the deep ice.

All the present arrays are of the order of 10^4 m² in size. As explained in previous sections, arrays of the order of 10^6 m² are needed for neutrino astronomy. Many things improve with array size. The muon energy threshold for traversing muons goes up roughly linearly with array size, and is about 200 GeV for a cubic-kilometer array. The atmospheric neutrino background falls fast with energy ($E^{-2.7}$), and probably at least one power of the energy faster than anticipated sources, so a higher threshold energy gains in signal-to-background for neutrino astronomy, while losing little in signal (for expected flat spectrum sources). Another gain lies in angular resolution, as the leverage due to the size of the array increases. For a cubic-kilometer array the muon trajectory resolution should reach well under a degree, where it becomes limited by multiple scattering of the muon itself. Also, the bigger the array, the better the trajectory fit, the more the time window can be squeezed down, the more background can be eliminated, the better the fit, etc. This is simply to say that the gains with size are faster than linear.

6.1.5 Coherent Radio-Pulse Technique

The coherent radio-pulse technique has been recognized for a long time, but it has been underused because of its dauntingly high apparent threshold. Here the

problem is simply that most of the low-frequency (wavelength large compared with shower dimensions) Cherenkov radiation from the particles cancels out, since the radiation formula depends on the square of the net charge. Still there is some radiation because there is some net electron charge (more than positron charge) traveling with cascades, and the particle distribution has asymmetries (due to the difference in scattering of electrons and positrons, and the Compton scattering of photons from electrons in the medium).

A problem is the transparency of the medium to electromagnetic waves. The ocean is conductive, and fresh water is not useful in the high-frequency regime. A unique environment seems to be the South Pole region, where ice is pure enough and cold enough for reasonable transmission. The resulting cascades detection threshold for a range of 1 km, under ideal noise conditions, appears to be ~ 5 PeV (204).

A Russian Institute of Nuclear Research group studied the noise temperature in the deep ice at the Antarctic Vostok Station, where the ice temperature is -56°C (245). They have operated an array of seven antennas placed 15 m deep and found an equivalent noise temperature of 1500 K, though it is expected to be less than 500 K deeper into the ice. A problem is that the refraction index changes down to a depth of about 100 m, the extent of the firn (uncompressed granular snow) layer. Also the ice must be cold for long attenuation lengths, and the ice becomes warmer with depth. At Vostok Station, then, the range is limited to about 1 km for 1 GHz.

The economic upheavals in the former Soviet Union ended research at Vostok Station, but a new group (RICE) from the United States has undertaken work at the South Pole station. Their new idea is to employ antennas directly in the ice (as AMANDA deploys photomultipliers). This avoids the index of refraction problem near the surface; more important, RICE claims that it enables detection of neutrinos with energies down to the TeV energy regime. This means that they can detect guaranteed signals of atmospheric neutrinos. Tests are under way for a cubic-kilometer class array. Co-location of such a radio array with a Cherenkov array is quite attractive, since they should have some overlapping region of sensitivity, and the radio array can take the neutrino search to far higher energies.

Another application of the radio technique involves sensing the radiation from cascades passing through the limb of the moon. The solid angle is small, but the target mass is large. Explorations of backgrounds are under way (78), and useful limits on SHE neutrino flux have been produced.

6.1.6 Acoustic Technique

Another category of techniques makes use of the acoustic pulse produced by expansion of the medium when heat is deposited by the particle cascade, an inefficient process with energy transfer efficiency of about 10^{-9} . When a particle cascade is generated from a neutrino interaction (or any other cause), the energy is deposited into the medium via ionization losses and other processes, and within a fraction

of a nanosecond is converted to heat. The heat dissipates only very slowly, so the bulk effect is a step-function expansion of the region in which the energy was deposited. This in turn generates a bipolar acoustic pulse with leading compression. Transverse to the cascade, typically 10 m long in water and a few centimeters wide, the radiation is coherent and adds, much like a stack of dipole antennas. The speed of sound in water is 1.5 km/s, so typical maximum frequencies are of the order of 20 KHz. The beam pattern is a disk transverse to the neutrino direction with angular thickness of about a degree.

The magnitude of the pulse depends on the bulk coefficient of thermal expansion, the density and specific heat of the medium, and the speed of sound. The expansion coefficient of fresh water has a minimum at 4°C, so no output should be present at that temperature, but in the ocean the zero-expansion temperature is lower. Warmer is better in most media. People have considered the use of other media, such as salt domes, which should work rather well. One necessity is that the medium be homogeneous, since even microscopic cracks kill waves of tiny amplitude. The acoustic attenuation coefficient of water is known to be small; it is typically about 1 km in the ocean at 20 KHz and scales with frequency squared over the range relevant for this subject. The lack of dispersion and the shape of the attenuation function allow the pulse to maintain its shape with distance, though its duration lengthens. The amplitude falls with distance as a power law, not an exponential. The beam width of the radiation disk also becomes wider with distance.

In the ocean, the noise background scales approximately as $1/f$ up to frequencies in the tens of kilohertz, but is highly variable because there is much added noise from surface wave-wind interactions. Above ~ 20 kHz, thermal noise dominates and the background increases with frequency. In the deep ocean there is some shielding from surface noise, which is not isotropic, due to the increasing sound velocity with depth. In fact, deep-ocean noise levels are not far above thermal noise in the range of interest. This fact helps compensate for the small energy-transfer efficiency from particle kinetic energy to acoustic energy and makes the method interesting.

Acoustic detection was first proposed by Askaryan in the 1960s and has been talked about since the reinvention of the notion by Bowen in the mid-1970s, following which experimental work took place in the United States and the Soviet Union. In particular, an American group measured acoustic pulses in water at Brookhaven National Laboratory in 1978, finding that the temperature dependence was largely as predicted by the thermo-acoustic mechanism, except for an unexplained tripolar pulse present at the temperature of greatest density of water (4°C) (208). In any case, the experimental results and calculations pointed to a threshold energy for detection of the order of 1 PeV or more (206), so the idea was dropped in favor of Cherenkov detection. With the new AGN models suggesting that many PeV neutrino interactions may occur per year in a cubic kilometer of water, there has been some revival of interest.

The Russian INR group that is involved with NESTOR has been working steadily for a few years to develop an acoustical array near Pylos in the Mediterranean

Sea, which they call SADC0 (209). They plan three initial 100-m strings, with 384 hydrophones located 100–200 m apart, for deployment with autonomous recording packages. They claim a threshold of 6 PeV over 10^9 m^3 . The Mediterranean is much warmer than the open oceans; the temperature at a depth of 3.5 km near Pylos is 14°C , which improves the threshold by a factor of three over the ocean.

A group of Russian and US scientists are attempting to use existing deep ocean sonar arrays that were built for submarine detection (209). These arrays unfortunately are aimed at low frequencies (hundreds of Hertz) but have some capability up to several kiloHertz depending on the installation. Calculations for a particular phased array located off the Kamchatka Peninsula indicate the potential for discovering neutrinos in the range of the highest-energy cosmic rays at ranges up to many kilometers. However, field studies employing realistic bipolar-pulse noise distributions are required. This technique could allow exploration for neutrino interactions in the range beyond 10^{20} eV in volumes of the order of hundreds of cubic kilometers, and in much larger volumes as development progresses.

Some members of the AMANDA collaboration have discussed the possibility of acoustic detection in the Antarctic ice as well (207). There are some sure advantages in pulse production, but the attenuation remains unmeasured. A further advantage is that ice, being a solid, supports shear waves (210). Observing both compressional and shear waves gives range in one record. Tests are required, particularly studies of background noise, including noise from glacial scraping and shearing, since the ice at the South Pole moves about 10 m per year.

6.1.7 Shower Detection

A rather different method of neutrino detection has been found for energies near the end of the cosmic-ray spectrum, in the range from $1 \text{ EeV} = 10^{18} \text{ eV}$ to around 100 EeV, the upper end being determined by simply running out of expected rate. To put this in context, recall that the optical Cherenkov method generally dominates the lower energies; the radio and acoustic methods may take over beyond $\sim 10 \text{ PeV}$, but with an effective volume of a few cubic kilometers, they too run out of possible rate at or below the EeV range. (An exception is the speculative acoustic technique described above, which may allow sonar systems to search a huge ocean volume for signs of SHE neutrinos.) Three things mitigate the seeming impossibility of neutrino detection at the highest energies. First, the cross section for neutrino interactions continues to rise, faster than for other interactions, so neutrinos interact more often; the interaction length is $115 \pm 25 \text{ kmwe}$ at 10^{20} eV . Second, as shown in previous sections, many models for neutrino production indicate that neutrino fluxes may be similar to primary cosmic-ray fluxes at these energies (and in some cases not). Third, the deposited energy (Joules) becomes macroscopically detectable, as is the case with extensive air showers produced by ordinary charged cosmic rays of these energies. Such SHE showers extend over kilometer distances and are easily detected with a few simple particle counters at the Earth's surface (although to get a usable rate one needs to cover 1000 km or more for 10^{20} eV).

Alternatively, the showers can be “seen” by pixelated optical detectors monitoring the dark night sky. The light arises from nitrogen fluorescence, isotropic de-excitation of nitrogen atoms along the shower path (dominantly at 337 nm). The excitation becomes greater at lower altitudes due to higher density while the competing collisional de-excitation rate becomes greater, making the light output insensitive to atmospheric depth (to first order anyway). This technique has been developed over several decades by the Fly’s Eye group and is now being carried onward by at least three other groups.

The method for discriminating neutrinos from ordinary cosmic rays is to seek events that must have originated (given that one cannot see the incoming primary particle) too far into the atmosphere to be due to photons or strongly interacting particles (protons, nuclei, or neutrons). Straight downward, the atmosphere constitutes about 1000 gm/cm^2 , or more than 10 strong interaction lengths. However, near the horizon (say at 85°) it is 30 times thicker. Hence, one may seek events that originated well inside the atmosphere, near the horizon or even slightly upcoming, and be sure that any events seen are of neutrino origin. The effective area is large, about $30,000 \text{ km}^2$, but the solid angle is small, about 0.1 sr. Nonetheless, useful limits have been set (as indicated in Section 3), and better ones—or even detections—will be obtained within a few years.

The extensive air shower arrays may also be used to seek near-horizontal neutrino-induced showers, but they must discriminate against electromagnetic showers initiated deep in the atmosphere by muons themselves from extensive air showers originated by ordinary cosmic rays of large energy. We do not go into detail here, but the shape and thickness of the shower front discriminate ν -induced and μ -induced showers. Shower discrimination poses no problem for setting upper limits, but it may be hard to establish a signal. Fluorescence detection is a bit more robust, as one may examine the longitudinal shower development.

Slightly further in the future are plans for space-based versions of the nitrogen fluorescence detectors, OWL and AirWatch. The idea is simply to fly large mirrors with light detectors that look down on the atmosphere. A much larger area can be searched from this vantage point than from a single point on the Earth’s surface. There will be a tradeoff, however, for higher energy thresholds, and the associated costs of space activities.

As mentioned above, the fluorescence detectors may have a chance to see double-bang events initiated by CC tau neutrino interactions, in which the second and larger burst is separated by a distance of tens of kilometers in the EeV energy range. It seems that the characteristically large and well-separated bursts, without much other shower activity, should constitute a fairly clean signature.

If tau neutrinos are detectable, then there may also be muon and electron neutrino events, since the neutrino oscillations presently indicated in the atmospheric and solar neutrino fluxes seem to imply that cosmic sources are well mixed. These flavors may be distinguishable if the cascades due to electron and neutral current events are seen as distinct from tau and muon CC events, the muon being signaled by multiple downstream showers. Interesting physics might thus be done in

learning the flavor mix, and hence something of the nature of the source, at these energies.

A recently proposed variation would use radar to detect the ionization trail left by EASs, in the same way that meteorites are detected (196). Tests are planned soon.

6.1.8 Gamma-Ray and Muon Astronomy with Neutrino Telescopes

Of course, the high-energy neutrino telescopes discussed here have applications for other kinds of particle astronomy. In particular, down-going muons may be studied, as they have been in the past, for signs of astrophysical sources. There have been some claims for signals due to Cyg X-3, for example, in multiple-muon events observed in deep mine experiments and some other circumstances. These signals have not been confirmed by later and larger detectors, so they may be in error. The episodic nature of such sources, however, allows some possibility that the early signals were correct. The mechanism for such point sources appearing in the down-going muon flux would be unusual, but one can certainly make studies of the sidereal and seasonal variation of the cosmic rays, which are worthwhile subjects.

More likely to prove fruitful is the use of the down-going events as tags for VHE gamma rays (see Section 2.4).

6.2 Neutrino Telescope Design Principles

There have been numerous neutrino telescope workshops, beginning in the mid-1970s with the series of DUMAND Workshops (212–226) and continuing with many others, including NESTOR Workshops (227), the Neutrino Telescope Workshops in Venice in recent years (228), the Zeuthen 1998 Workshop (230), and several KM3 Workshops (229). The earlier workshops focused more on techniques, array design, and experimental goals, whereas the later ones have tended to focus more on the physics as many of the technical issues have been sorted out.

Here we review, for the reader new to the field, some general considerations about designing and constructing high-energy neutrino telescopes. We have already stated the principle that such telescopes must use natural (free) targets and detection media, and we have noted that these must be “open” detectors (i.e. not enclosed in the costly tanks used at lower energies). We have also discussed the merits of the several techniques so far investigated. The greatest effort has gone into the study of water and ice Cherenkov detectors, so we focus here on those arrays. Some of the conclusions apply to the other techniques, but not generally.

6.2.1 Site Choice

Deeper Is Better, but Near Surface Is More Practical Down-going cosmic rays, although they provide a calibration beam and some interesting physics possibilities, limit high-energy neutrino telescopes in several ways. First, near the surface there is the problem of total rate: A 1-km² array would have a cosmic-ray muon entering

the array every 3 ns, which would make triggering and reconstruction potentially overwhelming problems. As depth increases, the total rate improves exponentially, with a decrease of 10^{-5} by a depth of 2 km, for example. Sparse arrays, which attempt to cover the largest possible area for high energies, are particularly vulnerable to misreconstructing down-going multiple-muon events (present about 4% of the time) as up-coming muons. Nonetheless, near-surface arrays were proposed [the GRANDE (238), LENA (239), NET (240), and PAN (241) projects, the Blue Lake projects (242), and SINGAO (243)], and the proponents claimed they could deal with the problems by having several layers of directional detectors. [A spinoff to this activity is the present MILAGRO (244) experiment, which uses a 5000-m² pond for TeV gamma-ray-induced extensive air shower measurements.]

Another gain with depth comes from the increasing solid angle, in which up-coming, side-going, and even slightly down-going muons dominate the inescapable down-going cosmic-ray muons (seen even in the deepest mines at 10 kmwe). The gain is slow, however. Near the surface, one may utilize events arriving from 20° below the horizon; 2 km deep, near-horizontal events come into play, and at the deepest locations the useful zenith angle moves up to 30° above the horizon. The total range of solid angle is a factor of three or so.

Offsetting the solid-angle effect somewhat for UHE neutrinos in the PeV energy range and beyond is the attenuation of the neutrinos through the Earth. For these energies, one wants enough absorber to kill off the ordinary cosmic rays but not so much as to annihilate the neutrinos of interest. For the extensive air shower technique (EeV), these competing desires result in a narrow window near the horizon where one can look for deeply originating showers. For underground detectors, it means seeking depths greater than roughly 2 km, which is enough to filter out hundred-TeV down-going cosmic-ray muons.

Finally, of course, there are practical economic matters. Deeper is better but more expensive in every venue. The increasing pressure in water or ice demands sturdier housings, more care with connectors, and so on. Deployment costs escalate with depth, particularly in ice, where drilling costs are said to scale with the cube of the depth. In the ocean, problems with the self-weight of cables, winching tensions, and such also increase nonlinearly with depth. Other factors tend to favor great depths in the ocean, as we discuss below.

Latitude and Longitude Perhaps the ideal location for a neutrino telescope is near the Earth's equator, so that the sky is swept over once per day. For the range below 1 PeV, the telescope looks through the Earth; for higher energies, it scans the heavens in the opposite direction. A location such as AMANDA's at the South Pole has the advantage of looking down continuously at the well-studied Northern hemisphere sources. Northern hemisphere telescopes have the advantage of looking through the Earth at the galactic center. In the end, as in optical astronomy, more telescopes with various fields of view are better, and cross-checking and confirmation will be important for the first source detections.

Another criterion which may become more important is location relative to a neutrino factory, now much discussed (247). Some claim that detection in a large array located roughly 3500 km from the accelerator is ideal for neutrino oscillation studies. However, unless a more fine-grained detector is co-located with the type of high-energy neutrino telescopes discussed here, this may not be relevant; the energy of the muon beams seems likely to be <50 GeV, so the neutrinos would generally be below threshold for the instruments we have discussed.

Optical Backgrounds The ocean- and lake-based optical Cherenkov detectors have similar background light to deal with, about 200 quanta/cm²/s. In deep ice, this problem is nonexistent, and the photomultipliers have only their intrinsic noise rates (roughly a factor of a hundred lower). In the ocean, further optical background can arise from bioluminescence (see below). The light in Lake Baikal has not been satisfactorily explained, but claims have been made that it is due to triboluminescence of dust settling in the lake.

Biology and Sedimentation Biological activity in the ocean is to be avoided on two grounds. First, growth on optical surfaces will surely be a problem for any array more shallow than about 1 km anywhere in the ocean. Bioluminescence, which appears to be universal with benthic creatures, is known to decrease exponentially with depth, with a constant of 800–1000 m. The amount of light increases by an order of magnitude or more in the presence of mechanical disturbance of the water, perhaps triggered by pressure fluctuations. Studies of the depth dependence indicate that the bioluminescent background is roughly equal to the radiogenic light background at 4 km depth for stationary detectors (detectors hanging from a ship are almost always in motion due to ocean swell). The bioluminescent light tends to arrive in bursts about 1 s in duration and can generate roughly 1% dead time, which is not correlated between photomultipliers separated by more than a few meters (i.e. the flashes are typically weak and detected only near the photomultiplier). Sedimentation is partly related to biological activity and partly to dust settling. This depends highly on the location but appears not to be a serious problem for sites investigated so far for downward-facing surfaces. Significant sedimentation on upward-facing surfaces has been reported from 2 km depth near Marseilles in the ANTARES tests.

Environmental Stability One great advantage of the South Pole is that once optical modules are frozen in place, the environment is extremely stable. This may not be the case in the lake or ocean. In the ocean, the site must be located well away from benthic storms (the equivalent of avalanches), which are known to occur on steep slopes near the great oceanic trenches. Thus, the abyssal plains are favored for ocean deployment. Lake Baikal is known to have seasonal variation in optical properties and backgrounds, which are not desirable but can be monitored and accounted for.

Homogeneity of Medium Homogeneity and isotropy are obviously desirable characteristics of the target/detection media. The ocean is extremely uniform on the scales that concern us, except in the few hundred meters above the bottom, where there may be turbid water from benthic flows. Ice, on the other hand, does have vertical inhomogeneity, with optical variations between presumably horizontally uniform layers. This stratification has caused difficulty in interpreting the early AMANDA data, but is claimed to be under control.

Power and Proximity to Shore Power delivery is a major determinant in site selection. Given the unavailability of ocean-bottom power sources (ocean-bottom nuclear reactors being forbidden by international treaties), power must be delivered from shore. Buoys are vulnerable to storms and human damage. Commercial fiber optic links within a power cable have adequate capacity to transmit data to the shore.

Present-day optical modules consume about 10 W per module (ocean version), not counting the overhead for control and multiplexing electronics. Future optical modules may reach 0.1 W per module, but this still implies a need for about a kilowatt of power for a cubic-kilometer array, too much for long-term batteries to provide. For the foreseeable future, power will have to be provided from shore.

In ice, the power and signal cables arrive at the surface, where the electronics and power supplies can be conveniently placed. The distance is short enough to permit use of multimode fibers, whereas the longer runs of the ocean-based arrays require single-mode fibers.

Infrastructure For any neutrino telescope installation, use of existing local infrastructure is an advantage. Desirable qualities are good transportation, locally available technology and expertise, laboratory facilities, and a hospitable political situation. Of course, location-dependent funding opportunities carry great weight, as demonstrated by the disposition of present efforts.

6.2.2 Array Design

Below, we summarize the consensus of 25 years of studies and debates about optimal array design.

Photocathode Area Many computer simulations have shown that the details of the distribution of optical sensors do not matter much in the achieving of sensitive muon detection area. Of course, spacing the modules too close together will produce many more hits per track than are needed for reconstruction. At the other extreme, as modules are spaced further and further apart, the effective area grows for some time and angular resolution improves, but the array becomes anisotropic in angular response. Configurations that do not have regularities help to suppress degenerate multiple solutions in fitting tracks. Generally, one needs hits on at least three strings to get unique track solutions. Also, spacing with some redundancy in detections helps avoid misfitted downward tracks.

The parameter most crucial to the array sensitivity is photocathode area. DUMAND studies showed that with 16-in photomultipliers, the effective area achievable with a wide variety of geometries was close to 100 m² per optical module. Thus a 1-km² ocean array with minimum threshold for through-going muons (about 200 GeV in this case) would require about 10,000 optical modules. Raising the energy threshold can permit the use of fewer modules. This scale is clearly within present experience, as Super-Kamiokande has 13,000 photomultipliers (though deployed in a more benign environment).

Triggering The problem of array triggering becomes more severe at shallow depths and increasing number of channels. For the noisy situations in the ocean or lake, suppressing single photoelectron hits greatly eases the requirements. The simplest way to implement this is to pair optical modules and form local two-hit requirements, and then use a hierarchical trigger (205). More sophisticated schemes can detect near-neighbor coincidences without close proximity. A simple array-wide multiplicity of neighbor pair triggers should suffice for even cubic-kilometer arrays in the ocean or lake, and the solution should be easier still in ice.

Vertical Strings In the early DUMAND studies, many plans for deployment were examined, including structures for fixing the array geometry and even deep ocean enclosures. Investigations of alternatives have almost always led back to the simple design of an array of multiple vertical strings of connected detectors. Kilometer-scale structures are ruled out by the high costs of their construction, deployment, and service. Because of irresistible anchoring forces, a cubic-kilometer array cannot be enclosed in a lake or ocean.

The rule applies for ice as well, since simple drilled holes seem the only practical option (though drilling on a slant is possible). Large holes in the ice are ruled out by energy costs.

The exception to this is that the towers of umbrella-like structures adopted by the Baikal and NESTOR groups do seem to work. The umbrella spines provide a way to precisely position subelements of an array, while leaving the overall structure flexible and deployable.

Photomultipliers Are Hard to Beat Many studies have searched for means to detect light with low noise levels and reasonable costs (ruling out present large-area solid-state detectors). No practical alternatives have been found, though various suggestions for cylindrical photomultipliers and liquid light detectors have been put forth. Studies have also been made of means to enhance photomultiplier light collection, and these too have proved impractical. One simple design employed by the IMB group used plastic-plate wavelength-shifting collars to increase light collection in eight-inch photomultipliers by about a factor of two. The price for this is some loss of timing, but the devices are cost-effective. These might be used in lake or ocean but are probably impractical in ice. Mirrored cones have been used in underground detectors to enhance light collection in a given solid angle, but these are probably not useful in open arrays, where isotropic response is desirable.

In sum, despite many attempts, it seems that bare photomultipliers are presently the devices of choice for large Cherenkov neutrino telescopes in water or ice. Photomultiplier costs scale with photomultiplier diameter more than area, so larger photomultipliers are more cost-effective. Also, due to the overhead costs for individual modules (electronics, housings, connectors, mechanical hardware, and cables), the largest practical photomultipliers are preferred. In ice, the overhead consideration appears to be dominated by the hole diameter, which in turn is dominated by energy costs. In the ocean, the limitation has in the past been the availability of standard (16-inch) glass pressure housings.

6.2.3 Reliability and Maintainability

Reliability has seldom concerned physicists in small laboratories. With the advent of large collider detectors and space-based experiments, that has changed. For a large neutrino telescope, many of the methods developed for space-grade reliability will be needed.

Accessibility and Service In general, of course, accessibility to the experimental elements to enable service is strongly desirable. This may not be the case, however, for optical units frozen permanently into the ice, or for deep ocean arrays. For the Lake Baikal experiment, the ability to annually retrieve the array from the winter ice covering has permitted an incremental approach. For the deep ocean, as the oil industry makes use of deeper locations, robots will become more available—and more affordable. Accessibility is worth a great deal in trade for the greater costs for a space-grade high-reliability system, but large systems still require high-reliability engineering because servicing takes so much time.

Avoiding Vulnerability to Single-Point Failure An important issue in the design of any remotely operated system is the vulnerability to single-point failure. Two approaches have been used. One is to minimize the number of active elements between sensor and shore, and the other is to make multiple paths available for data and command and control. Command and control systems can have defaults to fail-safe modes of autonomous operation in the case of command-link failure. The data link must survive. It seems the ideal situation would be for individual data links from sensors to shore station, sufficiently decoupled so that failure of one would impact no other. This has not proved practical as yet, and data multiplexing has been needed. Robustness can be won back via redundant paths. A good rule is to attempt in such designs to put the complexity at either end of the chain.

The ice situation does permit individual cable or fiber optic links to the surface, and there standard laboratory electronics can be used. Reliability and service are still issues, though, because of inaccessibility during the long polar winter and the number of holes needed for a cubic-kilometer detector.

Growth and Evolution Designs allowing growth and evolution are strongly desirable. Ocean and lake arrays can be retrieved and reconfigured as the science

evolves. The future availability of robots may make this simpler as well. In ice, the photomultipliers must be abandoned, but this may be an affordable cost.

Deployment The main challenge of putting an array in the desired location is how to deploy a multiply-connected array of strings of instruments on the ocean bottom and have a hope of getting them back if need be. Schemes have ranged from individual installation and subsequent connection by robot, to installation of completely preconnected arrays using cannisters from which strings of elements would be released to float upward after bottom placement. Another option is to have one cable to shore (or to an accessible junction box) for each string.

Deployment in ice is straightforward. A hole is drilled with hot water and the instrument string is lowered down the hole before the ice refreezes (one day). Once frozen in, it is permanent. Overpressuring during freeze-in has been a concern but seems manageable.

Focus on Connectors and Cables Connectors and cables have been the single most troublesome source of difficulty in all the neutrino experiments (and many other experiments as well) in the ocean, in ice, and in the deep mine Cherenkov detectors. The problem is most acute in the ocean due to the conductivity and corrosiveness of the seawater. Testing in situ is a must.

7. EXISTING AND PROPOSED PROJECTS

We review below the existing underground neutrino astronomy capable projects, list the larger projects now beginning that are the first dedicated to neutrino astronomy, and then briefly discuss future prospects.

7.1 Related Smaller and Lower-Energy-Threshold Projects

Table 3 lists the major past and present underground neutrino detectors, which of course have some capability for high-energy neutrino astronomy. For this purpose we list the muon detection area of the devices.

The first three instruments listed in the table were built specifically to search for natural neutrinos and to make initial forays into neutrino astronomy. The first natural neutrino was observed by the Reines group's experiment in the world's deepest (gold) mines in South Africa (CWI), on February 23, 1965. This date must be taken as the very beginning of neutrino astronomy, though it was a null subject for the next 22 years (to the day). The other pioneer project was carried out in a deep mine in the Kolar Gold Fields in India, detecting neutrinos at about the same time as CWI and continuing with a series of experiments in that mine over the next 25 years. These early instruments had little tracking ability and a rather low energy threshold (< 100 MeV), but they did set the first limits on astrophysical neutrinos.

The table neglects the radiochemical solar neutrino experiments and several small underground detectors. Borexino and KamLAND are included as

TABLE 3 Large underground instruments with high-energy detection capability, 1960s through 2000^a

Detector, location	Dates	μ Area (m^2)	Dir. sense	Technique	Primary purpose
KGF, South India	1965–70	10	N	LS + FT	obs ν s
CWI, South Africa	1965–70	110	N	LS + FT + Fe	obs ν s
Silver King, Utah	1966–70	30	Y	WC + Ctrs + Fe	obs ν s
KGF, South India	1978–88	20	N	ST	PDK
Baksan, Caucasus	1980–P	250	Y	LS tanks	ν s
IMB, Ohio	1981–90	400	Y	WC	PDK
HPW, Utah	1982–85	100	Y	WC	PDK
Kamioka, Japan	1982–94	120	Y	WC	PDK
NUSEX, Mt. Blanc	1983–88	10	N	ST + Fe	PDK
Fréjus, France	1985–88	90	N	ST + Fe	PDK
Soudan I, Minn.	1985–90	10	N	ST + Concrete	PDK
Soudan II, Minn.	1990–P	100	N	DT + Fe	PDK
MACRO, Italy	1995–(00)	800	Y	LS + ST +	monopoles
LVD, Italy	1996–?	500	Y	LS tanks + ST	SN ν s
Super-Kamiokande	1996–(10)	740	Y	WC	PDK
SNO, Canada	1999–?	300	Y	D ₂ O WC	solar ν s
Borexino, Italy	(2002–10)	<100	Y	LS	solar ν s
KamLAND, Japan	(2002–12)	100	Y	LS	reactor ν s

^aP, present; Dir., direction; WC, water Cherenkov; ST, streamer tubes; LS, liquid scintillator; PS, plastic scintillator; FT, flash tubes.

experiments under construction at present, since they will have substantial capability for a future galactic supernova observation.

The second round of experiments really began with the nucleon decay search instruments of the early 1980s, some of which continue to the present. The largest of these is the Super-Kamiokande Detector, with a gross mass of 50 kt, veto shield surrounding a fiducial volume of 22 kt, and energy threshold reaching down well into the solar neutrino regime at 5 MeV.

None of these underground experiments is likely to participate in extrasolar neutrino astronomy, but there is certainly an opportunity for serendipitous discovery (aside from galactic supernovae). A long-shot possibility would be the observation of neutrinos from GRBs.

7.2 Second-Generation Projects

Table 4 lists the high-energy neutrino telescope projects that fall into the category of second-generation instruments. By this we mean detectors specifically

TABLE 4 Second-generation initiatives in high-energy neutrino astronomy^a

Detector	Location	Status	μ Area (10^3 m^2)	Depth (mwe)	Technique	Threshold (GeV)
(DUMAND II	Hawaii	1992–95	20	4760	WC	20)
Baikal NT-200	Siberia	1996–N	3	1000	WC	10
AMANDA II	S. Pole	1996–P	30	2000	WC in ice	20
NESTOR	Greece	T/C	100	3500	WC	1
SADCO	Greece	T	1000	3500	Acoust.	$> 10^6$
RICE	S. Pole	T/C	1000	1000	μ -wave	$\sim 10^6$
ANTARES	France	T/C	30	2000	WC	?
NEMO	Italy	P	?	?	WC	?
RAMAND	US	T	?	Moon	μ -wave	10^{11}
ICECUBE	S. Pole	P	1000	2000	WC in ice	> 100
KM3	Ocean	P	1000	> 4000	WC	$> 100?$

^aN, now operating; T, testing and development; C, construction; P, proposed or under discussion; WC, water Cherenkov; μ -wave, microwave detection; Acoust., acoustic wave detection.

dedicated to neutrino astronomy, with areas large enough to allow observations. The DUMAND project, which stimulated the field and carried out a great deal of technical development, got only as far as counting muons and setting limits on UHE cascades in the deep ocean before it was cancelled in 1995 (232–234).

The Baikal (248) and AMANDA (249) projects are now both reporting observations of up-coming muon events, presumably due to atmospheric neutrinos; these observations demonstrate feasibility. NESTOR (250) has counted muons in the deep Mediterranean as well and plans to deploy a long-term installation in 2001. ANTARES (251) is doing technical development and environmental studies and plans to deploy an array by 2003. A new group, NEMO (252), located near Sicily, is still refining plans. (This is not to be confused with a double beta decay experiment with the same name.)

An expanded AMANDA collaboration is proposing a full cubic-kilometer detector, ICECUBE (253), at the South Pole, to operate within a decade. Hot-water drilling of the holes limits the rate of installation. There have been discussions about a world collaboration on a full under-ocean cubic-kilometer neutrino telescope (229), but as yet nothing firm has coalesced. It seems likely that this step will await success with at least one of the under-ocean initiatives.

7.3 Future Projects

As one may imagine, there have been very many suggestions for new and larger neutrino detectors.

On the lower-energy side, there is discussion about a follow-up experiment to the largest underground detector, the 50-kt Super-Kamiokande, but no flagship

project or even consensus has yet emerged (254). Given the US \$100 million cost of Super-Kamiokande, a leap of an order of magnitude in size will be very difficult to fund. But such a detector, with perhaps a megaton of sensitive volume and sensitivity reaching down to the solar neutrino scale, could accomplish many things: a search for nucleon decay to lifetime of $\simeq 10^{35}$ years in favored modes ($e^+\pi^0$), excellent monitoring for temporal variations of solar neutrino fluxes, a supernova search out to the nearby galaxies, a more significant search for low-energy neutrinos from GRBs, further neutrino-oscillation studies (particularly if sterile neutrinos are in the picture), and more. It is not sufficient in our view simply to make a larger version of the present water Cherenkov detectors. One scheme proposed would use the ring imaging Cherenkov technique (255).

Larger underground detectors are not only very expensive but vulnerable to problems due to their large cavity sizes. The weight of the overburden could cause the cavity to collapse. Also, cavity excavation costs in hard rock for a megaton detector are certainly intimidating and a major hurdle to overcome.

On the high-energy front, the immediate future will continue to be dominated by some of the projects cited in the previous subsection, all of which have more ambitious plans for the future, working toward the 1-km³ goal. The AMANDA group seems to have the lead at the moment, with the cubic-kilometer ICECUBE proposal on the table. Even if approved, this will take some years to implement because of the limited rate of hole drilling during limited seasonal access to the South Pole. Aside from the three present European projects in the Mediterranean and the venerable Lake Baikal project, there has been some activity in the United States even in the wake of the DUMAND demise. The goal is to form a collaboration working toward a deep ocean cubic-kilometer array, but as yet nothing has coalesced. Various groups will need to cooperate in order to achieve a real deep ocean neutrino telescope.

Certainly the evolution of technology will make a deep ocean detector more achievable, particularly as oil exploration moves to greater depths. There could also be breakthroughs in optical detection, as for example with a liquid-state photodetector that would be pressure-tolerant and could scale to large sizes. However, these breakthroughs seem at least a decade away from commercial availability.

Radio and acoustic techniques are still in development, so it is hard to speculate about their eventual success. Most likely these less developed technologies will be boosted into full-scale tests along with one or more water or ice Cherenkov detectors. Perhaps it is with these techniques that the biggest surprises may come about, as they are the least developed and there is room for significant technological innovation as well.

The future of the extensive air shower techniques for neutrino search in the EeV regime seems to be limited by the restricted solid angle. Still, if large neutrino fluxes exist at the energy of the end of the cosmic-ray spectrum, there could be wonderful results from this venue.

For the next decade, however, we should look to the large under-ice and under-water optical Cherenkov detectors to begin the era of high-energy neutrino astronomy.

8. SUMMARY AND CONCLUSIONS

High-energy neutrino astronomy, still nascent after 40 years of dreams, plans, and initial attempts, holds enormous scientific potential. Given the number of serious projects under way in ice, lake, and ocean, it would seem that success cannot be long denied.

Although the many neutrino sources we have discussed may or may not exist, if history tells us anything it is that the most interesting results will be none of the above, but something entirely unexpected. Physics beyond our current theory-biased horizon could remain unrecognized for some time. We should retain a phenomenological approach in the emergent field of high-energy neutrino astrophysics.

Visit the Annual Reviews home page at www.AnnualReviews.org

LITERATURE CITED

- Learned JG. *Proc. Neutrino '94, XVI Int. Neutrino Phys. Astrophys. Conf., May 29–June 3, Eilat, Israel*, ed. A Dar, M Gronau, *Nucl. Phys. Proc. Suppl.* 38:484–94 (1995)
- Gaissner TK, Halzen F, Stanev T. *Phys. Rev.* 258:173–236 (1998)
- Gaissner TK, Halzen F, Stanev T. *Phys. Rev.* 271:355–56 (1996)
- Gandhi R, Quigg C, Reno MH, Sarcevic I. *Nucl. Phys. Proc. Suppl.* 48:475–477 (1996)
- Protheroe RJ. *Nucl. Phys. Proc. Suppl.* 77:465–73 (1999)
- Belolaptikov IA, et al (Baikal Collaboration). *Astropart. Phys.* 7:263–82 (1997)
- Blood H, Learned JG, Reines F, Roberts A. *Proc. Int. Neutrino Conf., 688, Aachen, 1976*; DUMAND Collaboration. *Proc. Int. Cosmic Ray Conf., 25th, Durban, S. Africa, 1997*, astro-ph/9705198; Waldrop MM. *Science* 250:208 (1990)
- Halzen F, Learned J, Stanev T. *Astrophys. in Antarctica, Newark, DE 1989, AIP Conf. Proc.* 198, ed. D Mullan, M Pomerantz, T Stanev. New York: AIP (1989); Halzen F, Learned JG. *UH-511-659-88* (1988); Halzen F. *New Astron. Rev.* 42:289–99 (1988)
- Basa S, et al (ANTARES Collaboration). *Proc. Texas Symp. Relativistic Astrophys. and Cosmol., 19th, Paris, France, Dec. 14–18*, ed. J Paul, T Montmerle, E Aubourg (1998), <http://antares2.in2p3.fr/>
- Resvanis LK, et al (NESTOR Collaboration). *Proc. Workshop High Energy Neutrino Astrophys., Honolulu, March 23–26*, ed. VJ Stenger, JG Learned, S Pakvasa, X Tata, pp. 325–53. Singapore: World Sci. (1992); Sotiriou S. *Proc. Rencontres de Blois, 8th, Chateau de Blois, France, June 8–12*, ed. T Stolarczyk, J Tran Thanh Van, F Vannucci, p. 305. Ed. Frontières (1996), <http://www.uoa.gr/~nestor/intro.html>
- Halzen F. *Am. Astron. Soc. Meet.* 192:6629 (1998); proposal, Univ. Wisc., Feb. 2000
- Fichtel CE, Trombka JJ. *Gamma-Ray Astrophysics: New Insight Into the Universe. Tech. Rep. NASA-RP-1386* (1997)
- Ong RA. *Phys. Rep.* 305:93–202 (1998)
- Hoffman CM, Sinnis C, Fleury P, Punch M. *Rev. Mod. Phys.* 71:897 (1999)
- Aharonian FA. *Astropart. Phys.* 11:225–34 (1999)
- Gould RJ, Shröder G. *Phys. Rev. Lett.* 16:252 (1966)
- Svensson R, Zdziarski AA. *Ap. J.* 349:415–28 (1990)
- Salamon MH, Stecker FW. *Ap. J.* 493:547–54 (1998)

19. Mannheim K, Westerhoff S, Meyer H, Fink H-H. *Astron. Astrophys.* 315:77–85 (1996)
20. Madau P, Phinney ES. *Ap. J.* 456:124–31 (1996)
21. Primack JR, Bullock JS, Somerville RS, MacMinn D. *Astropart. Phys.* 11:93–102 (1998)
22. Kneiske TM, Mannheim K, Hartmann D. *Ap. J.* submitted (2000)
23. Markov MA. *Proc. Int. Conf. High Energy Phys., Rochester*, ed. ECG Tinlog, et al, p. 597 (1960)
24. Greisen K. *Proc. Int. Conf. Instrum. for High Energy Phys.* 1:210 (1960)
25. Roberts A, ed. *Proc. 1976 DUMAND Summer Workshop, Hawaii*. Batavia, IL: Fermilab (1976)
26. Kolb EW, Turner MS. *The Early Universe*. Reading, MA: Addison-Wesley (1990)
27. Super-Kamiokande Collaboration. *Phys. Rev. Lett.* 81:1562–67 (1998)
28. Sarkar S. *Nucl. Phys. Proc. Suppl.* 66:168–80 (1998)
29. Turner MS, Tyson JA. *Rev. Mod. Phys.* 71:S145 (1999)
30. Berezhinsky VS, et al. *Astrophysics of Cosmic Rays*. Amsterdam: North-Holland (1990)
31. Gaisser TK. *Cosmic Rays and Particle Physics*. Cambridge, UK: Cambridge Univ. Press (1990)
32. Gaisser TK, et al. *Phys. Rev. D* 54:5578 (1996); Gaisser TK. *Nucl. Phys. Proc. Suppl.* 77:133 (1999); Honda M. *Nucl. Phys. Proc. Suppl.* 77:140 (1999)
33. Volkova LV. *Yad. Fiz.* 31:1531 (1980); *Sov. J. Nucl. Phys.* 31:784 (1980); Roberts A, ed. *DUMAND 1978 Workshop Proc.*, 1:75. La Jolla, CA: DUMAND, Scripps Inst. Oceanogr. (1978)
34. Aglietta M, et al. *Phys. Rev. D* 58:92005 (1998)
35. Bugaev EV, et al. *Phys. Rev. D* 58:05401 (1998)
36. Thunman M, Ingelman G, Gondolo P. *Astropart. Phys.* 5:309 (1996); hep-ph/9505417
37. Pasquali L, Reno MH, Sarcevic I. hep-ph/9905389 (1999)
38. Gandhi R, Quigg C, Reno MH, Sarcevic I. *Astropart. Phys.* 5:81 (1996); hep-ph/9512364
39. Gandhi R, Quigg C, Reno MH, Sarcevic I. *Phys. Rev. D* 58:093009–0093024 (1998)
40. Stanev T. *Phys. Rev. Lett.* 83:5427 (1999)
41. Caldwell D, et al. *Current Aspects of Neutrino Physics*. Springer (2000)
42. Halzen F, Saltzberg D. *Phys. Rev. Lett.* 81:4305 (1998)
43. Dutta S, Reno MH, Sarcevic I. hep-ph/0005310 (2000)
44. Seckel D, Stanev T, Gaisser TK. *Ap. J.* 382:652–66 (1991)
45. Ingelman G, Thunman M. *Phys. Rev. D* 54:4385–92 (1996)
46. Bergström L. *New Astron. Rev.* 42:245–57 (1998)
47. Hettlage C, Mannheim K, Learned JG. *Astropart. Phys.* 13:45–50 (2000)
48. Hunter SD, Digel SW, de Geus EJ, Kanbach G. *Ap. J.* 436:216–28 (1994)
49. Domokos G, Elliott B, Kovesi-Domokos S. *J. Phys. Nucl. Part. Phys.* G19:899–911 (1993)
50. Berezhinsky VS, Gaisser TK, Halzen F, Stanev T. *Astropart. Phys.* 1:281–87 (1993)
51. de Paolis F, Ingrosso G, Jetzer Ph, Roncadelli M. *Phys. Rev. Lett.* 74:14–17 (1995)
52. Ingelman G, Thunman M. Uppsala Univ. Preprint TSL/ISV-96-0136 (1996); astro-ph/9604286
53. Hunter SD, et al. *Ap. J.* 481:205–40 (1997)
54. Mayer-Hasselwander HA, et al. *Astron. Astrophys.* 335:161–72 (1998)
55. Halzen F, Stanev T, Yodh GB. *Phys. Rev. D* 55:4475–79 (1997)
56. Sreekumar S, et al. *Ap. J.* 494:523–34 (1998)
57. von Montigny C, et al. *Ap. J.* 440:525–53 (1995)
58. Mukherjee R, et al. *Ap. J.* 490:116–35 (1997)
59. Mukherjee R, Chiang J. *Astropart. Phys.* 11:213–15 (1999)

60. Hasinger G. *IAU Symp.* 183:200 (1999)
61. Protheroe RJ, Johnson PA. *Astropart. Phys.* 4:253 (1996)
62. Coppi PS, Aharonian FA. *Ap. J.* 487:L9–L12 (1997)
63. Rachen JP, Meszárós P. *Phys. Rev. D* 58:123005 (1998)
64. Muecke A, et al. *Comp. Phys. Comm.* 124:290–314 (1999)
65. Mannheim K. *Astropart. Phys.* 3:295 (1995)
66. Waxman E, Bahcall J. *Phys. Rev. D* 59:023002 (1999)
67. Mannheim K, Protheroe RJ, Rachen JP. *Ap. J.* In press (2000), astro-ph/9812398 (1999)
68. Boyle BJ, Terlevich RJ. *Mon. Not. R. Astron. Soc.* 293:L49 (1998)
69. Thunman M, Ingelman G, Gondolo P. *Astropart. Phys.* 5:309–332 (1996)
70. Colafrancesco S, Blasi P. *Astropart. Phys.* 9:227–46 (1998)
71. Nellen L, Mannheim K, Biermann PL. *Phys. Rev. D* 47:5270–74 (1993)
72. Stecker FW, Salamon MH. *Space Sci. Rev.* 75:341 (1996)
73. Rachen JP, Biermann PL. *Astron. Astrophys.* 272:161 (1993)
74. Waxman E, Bahcall J. *Phys. Rev. Lett.* 78:2292–95 (1997)
75. Sigl G. *Towards the Millenium in Astrophys., Problems and Prospects. Int. School of Cosmic Ray Astrophys. 10th Course, Erice, Italy, June 16-23, 1996*, ed. MM Shapiro, R Silberberg, JP Wefel, p. 31. Singapore: World Sci. (1998)
76. Birkel M, Sarkar S. *Astropart. Phys.* 9:297–309 (1998)
77. Rhode W, et al. *Astropart. Phys.* 4:217 (1996)
78. Gorham PW, Liewer KM, Naudet CJ. *Proc. Int. Cosmic Ray Conf., 26th, Salt Lake City, UT, Aug. 1999*. Salt Lake City, UT: Univ. Utah, astro-ph/9906504 (1999)
79. Balkanov V, et al (BAIKAL Collaboration). *Proc. Int. Workshop Topics in Astroparticle and Underground Phys., 6th (TAUP99), Sept. 6–10, 1999, Paris, France*, astro-ph/0001145 (2000)
80. Bolesta JW, et al. *Proc. Int. Cosmic Ray Conf., 25th, Durban, S. Africa*, 7:29. Pochesfstroom Univ., S. Africa (1997)
81. Porrata R, et al. *Proc. Int. Cosmic Ray Conf., 25th, Durban, South Africa*, 7:9. Pochesfstroom Univ., S. Africa (1997)
82. Aglietta M, et al. *Phys. Lett.* B333:555 (1994)
83. Sreekumar P, et al (EGRET Collaboration). *Ap. J.* 494:523 (1998)
84. Lipari P. *Astropart. Phys.* 1:195 (1993)
85. Stecker FW, Salamon MH. astro-ph/9501064 (1995)
86. Protheroe RJ. astro-ph/9809144 (1998)
87. Mannheim K. *Phys. Rev. D* 48:2408–14 (1993)
88. Bednarek W, Protheroe RJ. *Phys. Rev. Lett.* 79:2616–19 (1997)
89. Gaisser TK, Protheroe RJ, Stanev T. *Ap. J.* 492:219–27 (1998)
90. Atoyan AM, Aharonian FA, Tuffs RJ, Völk HJ. *Astron. Astrophys.* 355:211–220 (2000)
91. Baring MG, Ellison DC, Reynolds SJ. *Ap. J.* 482:372–76 (1997)
92. Krymskii GF. *Dokl. Akad. Nauk. SSSR* 234:1306 (English transl. *Sov. Phys.-Dokl.* 22:327) (1977)
93. Axford WI, Leer E, Skadron G. *Proc. Int. Cosmic-Ray Conf., Plovdiv, 15th*, 11:132 (1977)
94. Fermi E. *Phys. Rev.* 75:1169 (1949)
95. Fermi E. *Ap. J.* 119:1 (1954)
96. Parker EN. *Phys. Rev.* 109:1328 (1958)
97. Drury LO'C. *Rep. Prog. Phys.* 46:973 (1983)
98. Blandford RD, Eichler D. *Phys. Rep.* 154:1 (1987)
99. Kirk JG, Melrose DB, Priest ER. *In Plasma Astrophysics: Saas-Fee Advanced Course 24 (Lecture Notes 1994)*, Swiss Society for Astrophysics and Astronomy, ed. AO Benz, TJ-L Courvoisier. Springer (1994)
100. Biermann PL, Strittmatter PA. *Ap. J.* 322:643–49 (1987)

101. Kirk JG. *Relativistic Jets in AGNs, Proc. Int. Conf.*, p. 145–52 (1997)
102. Guthmann AW, Kirk JG, Gallant YA, Achterberg A. *Proc. Huntsville GRB Symp., 5th*. In press (2000), astro-ph/0002176
103. Vietri M. astro-ph/0002269 (2000)
104. Schneider P, Kirk JG. *Astron. Astrophys.* 217:344–50 (1989)
105. Ellison DC, Drury LO'C, Meyer J-P. *Ap. J.* 487:197–217 (1997); Meyer J-P, Drury LO'C, Ellison DC. *Ap. J.* 487:182 (1997); Drury LO'C, Aharonian FA, Völk HJ. *Astron. Astrophys.* 287:959 (1994)
106. Buckley JH, et al. *Astron. Astrophys.* 329:639–58 (1998)
107. Catanese M, Weekes TC. *Proc. Astron. Soc. Pac.* 111:1193–1222 (1999)
108. Chiuderi C, Einaudi G. Plasma astrophysics: lectures held at the Astrophysics School VII in San Miniato, Italy, 3–14 October 1994, Springer (Lecture Notes in Physics; 468) (1996)
109. Lovelace RVE. *Nature* 262:649–52 (1976)
110. Goldreich P, Julian WH. *Ap. J.* 157:869–80 (1969)
111. de Gouveia dal Pino EM, Lazarian A. *Astrophysical Plasmas: Codes, Models, and Observations, Mexico City, Oct. 25–29, 1999*, ed. SJ Arthus, N Brickhaus, J Franco. *Revista Mexicana de Astronomica y Astrofisica, Serie de Conferencias*. In press (2000)
112. Biermann PL, Völk HJ. *Ap. J.* 333:L65–L68 (1988)
113. Koyama K, et al. *Nature* 378:255 (1995)
114. Tanimori T, et al. *Ap. J.* 497:L25–L28 (1998)
115. Pühlhofer G, et al. *Proc. Int. Cosmic Ray Conf., 28th, Salt Lake City, UT* 3:492. Salt Lake City: Univ. Utah Press (1999)
116. Baring MG, et al. *Ap. J.* 513:311–38 (1999)
117. Roy M. *J. Phys.* G25:129–34 (1999)
118. Biermann PL. *Space Sci. Rev.* 74:385–96 (1995)
119. Protheroe RJ, Stanev T. *Astropart. Phys.* 10:185–96 (1999)
120. Mirabel IF, Rodríguez LF. *Annu. Rev. Astron. Astrophys.* 37:409–43 (1999)
121. Peebles PJE. *Principles of Physical Cosmology*. Princeton, NJ: Princeton Univ. Press (1993)
122. Mannheim K, Schlickeiser R. *Astron. Astrophys.* 286:983–96 (1994)
123. Völk HJ, Klein U, Wiebeleski R. *Astron. Astrophys.* 213:L12–L14 (1989)
124. Fabian AC, Iwasawa K. *Mon. Not. R. Astron. Soc.* 303:L34–L36 (1999)
125. Mannheim K. *Astropart. Phys.* 11:49–57 (1999)
126. Blandford RD, Netzer H, Woltjer L. In *Active Galactic Nuclei: Saas-Fee Advanced Course 20 (Lecture Notes, 1990, Swiss Society for Astrophysics and Astronomy)*, ed. TJ-L Courvoisier, M Mayor. Springer (1990)
127. Frank J, King AR, Raine DJ. *Accretion Power in Astrophysics*. Cambridge, UK: Cambridge Univ. Press. 2nd ed. (1992)
128. Blandford RD. *Astrophys. Space Sci.* 261:245–52 (1998)
129. Antonucci R. *High Energy Processes in Accreting Black Holes, Astron. Soc. Pac. Conf. Ser. 161*, ed. J Poutanen, R Svensson, p. 193. San Francisco: Astron. Soc. (1999)
130. Fabian AC, et al. *Mon. Not. R. Astron. Soc.* 277:L11–L15 (1995)
131. Miyoshi M, et al. *Nature* 373:127 (1995)
132. Kazanas D, Protheroe RJ. *Nature* 302:228–30 (1983); Protheroe RJ, Kazanas D. *Ap. J.* 265:620 (1978)
133. Sikora M, Kirk JG, Begelman MC, Scheider P. *Ap. J.* 320:L81–L85 (1987)
134. Mannheim K, Biermann PL. *Astron. Astrophys.* 221:211–20 (1989)
135. Stecker F, Done C, Salamon M, Sommers P. *Phys. Rev. Lett.* 66:2697 (1991)
136. Szabo AP, Protheroe RJ. *Astropart. Phys.* 2:375–92 (1994)
137. Svensson R. *Mon. Not. R. Astron. Soc.* 227:403–51 (1987)

138. Zdziarski AA. *Mon. Not. R. Astron. Soc.* 281:L9–L13 (1996)
139. Stecker FW, Salamon MH. *Space Sci. Rev.* 75:341 (1996)
140. Blandford RD, Königl A. *Ap. J.* 232:34–48 (1979)
141. Aharonian F (HEGRA Collaboration). *Astron. Astrophys.* 349:11–28 (1999)
142. Mannheim K. *Science* 279:684–86 (1998)
143. Mannheim K. *Astron. Astrophys.* 269:67–76 (1993)
144. Protheroe RJ. *Accretion Phenomena and Related Outflows, IAU Colloquium 163. Astron. Soc. Pac. Conf. Ser.*, ed. DT Wickramasinghe, GV Bicknell, L Ferrario, 121:585 (1997)
145. Bednarek W, Protheroe RJ. *Mon. Not. R. Astron. Soc.* 287:L9–L13 (1997)
146. Dar A, Laor A. *Ap. J.* 478:L5–L8 (1997)
147. Ensslin T, Biermann PL, Kronberg PP, Wu X–P. *Ap. J.* 477:560–67 (1997)
148. Dar A, Shaviv NJ. *Astropart. Phys.* 4:343–49 (1996)
149. Völk HJ, Atoyan AM. *Astropart. Phys.* 11:73–82 (1999)
150. Berezhinsky VS, Blasi P, Ptuskin VS. *Ap. J.* 487:529–35 (1997)
151. Meszáros P, Rees MJ. *Ap. J.* 405:278–84 (1993); Meszáros P, Laguna P, Rees MJ. *Ap. J.* 415:181–90 (1993); Meszáros P, Rees MJ. *Mon. Not. R. Astron. Soc.* 269:L41 (1994); Meszáros P, Rees MJ. *Ap. J.* 482:L29 (1997)
152. Ruffert M, Janka H–T. *Astron. Astrophys.* 338:535–55 (1998)
153. Paczynski B, Xu G. *Ap. J.* 427:708–13 (1994)
154. Ostrowski M, Zdziarski AA. *Adv. Space Sci.* 231:339–41 (1995)
155. Milgrom M, Usov V. *Ap. J.* 449:L37–L40 (1995)
156. Stecker FW. *Astropart. Phys.*, in press, astro-ph/9911269 (1999)
157. Waxman E, Bahcall J. *Phys. Rev. Lett.* 78:2292–95 (1997)
158. Vietri M. *Phys. Rev. Lett.* 80:3690–93 (1998); Vietri M. *Ap. J.* 507:40–45 (1998)
159. Plaga R. *Ap. J.* 424:L9–L12 (1994)
160. Gallant YA, Achterberg A, Kirk JG. *Astron. Astrophys. Suppl.* 138:549–50 (1999)
161. Totani T. *Astropart. Phys.* 11:451–55 (1999)
162. Boettcher M, Dermer CD. *Ap. J.* 499:L131–34 (1998)
163. Atkins R (Milagro Collaboration). astro-ph/0001111 (2000)
164. Mannheim K, Hartmann D, Funck B. *Ap. J.* 467:532–36 (1996)
165. Jungman G, Kamionkowski M, Griest K. *Phys. Rep.* 267:195 (1996)
166. Bergstrom L, Edso J, Gondolo P. *Phys. Rev. D* 58:103519 (1998)
167. Gondolo P, Silk J. hep-ph/0001070 (2000)
168. Hawking SW. *Nature* 248:30 (1974)
169. Page DN, Hawking SW. *Ap. J.* 206:1 (1976)
170. Carr BJ, MacGibbon JH. *Phys. Rep.* 307:141 (1998)
171. Barrau A. *Astropart. Phys.* In press (2000), astro-ph/9907347
172. Rubakov VA. *JETP Lett.* 33:644 (1981)
173. Bezrukov L, et al (Baikal Collaboration). *Proc. Workshop on the Dark Side of the Universe: Experimental Efforts and Theoretical Framework, 2nd, Rome, Italy, Nov. 13–14, 1995*, astro-ph/9601160 (1996), astro-ph/0001151 (2000)
174. Belolaptikov IA, et al (Baikal Collaboration). astro-ph/9802223 (1998)
175. Hill CT. *Nucl. Phys.* B224:469 (1983)
176. Aharonian FA, Bhattacharjee P, Schramm DN. *Phys. Rev. D* 46:4188 (1992)
177. Bhattacharjee P, Hill CT, Schramm DN. 1992. *Phys. Rev. Lett.* 69:567 (1992)
178. Gill AJ, Kibble TWB. *Phys. Rev. D* 50:3660 (1994)
179. Protheroe RJ, Stanev T. *Phys. Rev. Lett.* 77:3708 (1996)
180. Sigl G, Lee S, Schramm D, Coppi P. *Phys. Lett.* B392:129 (1997)
181. Yoshida S, Dai H, Jui CCH, Sommers P. *Astropart. Phys.* 479:547 (1997)
182. Birkel M, Sarkar S. hep-ph/9804285 (1998)

183. Morris DA, Ringwald A. *Proc. Nestor Int. Conf., 3rd, Oct. 1993, Pylos, Greece*, ed. L. Resvanis, astro-ph/94032214 (1994); Morris DA, Ringwald A. *Proc. Int. Cosmic Ray Conf., 23rd, Calgary, Canada, July 1993*, hep-ph/9308358 (1993)
184. Bergstrom L, Liotta R, Rubinstein H. *Phys. Lett. B* 276:231 (1992)
185. Jain P, McKay DW, Panda S, Ralston JP. hep-ph/0001031 (2000)
186. Weiler TJ. *Phys. Rev. Lett.* 49:234 (1982); *Ap. J.* 285:495 (1982); Roulet E. *Phys. Rev. D* 47:5247 (1993)
187. Weiler TJ. *Astropart. Phys.* 11:303 (1999), hep-ph/9710431
188. Fargion D, Mele B, Salis A. astro-ph/9710029 (1997)
189. Weiler T. *Proc. Beyond the Desert 99*, ed. H Klapdor-Kleingrothaus, hep-ph/9910316 (1999)
190. Ashour-Abdalla M, et al. *Phys. Rev. A* 23:1906 (1981); Tajima T. *Laser Part. Beams* 3:351 (1985); Kruer WL. *The Physics of Laser Plasma Interactions*. Reading, MA: Addison-Wesley (1998)
191. Gelmini G, Kusenko A. hep-ph/9908276 (1999)
192. Learned JG, Pakvasa S. *Astropart. Phys.* 3:267 (1995); hep-ph/9408296
193. Husain A. 1999. *Proc. Lomonosov Conf. Elementary Particle Phys., 9th, Sept. 20–26, 1999, Moscow, Russia*, ed. A Studeniken, hep-ph/0001128
194. Bento L, Keraanen P, Maalampi. 1999. *Phys. Lett. B* 476:203–12 (2000)
195. Rosner J, Wilkerson J. hep-ex/9702008 (1997)
196. Gorham PW. Submitted; hep-ex/0001041 (2000)
197. Beacom JF. hep-ph/9909231 (1999); Beacom JF, Vogel P. *Phys. Rev. D* 58:053010,093012 (1998); Zatsepin GT. *JETP Lett.* 8:205 (1968)
198. Stodolsky L. astro-ph/9911167 (1999)
199. DUMAND Collaboration. *Proposal for a deep ocean neutrino detector*, July 1988, HDC-2-88. Honolulu: Univ. Hawaii Press (1998)
200. Jackson JD. *Classical Electrodynamics*. New York: Wiley. 638 pp. 3rd ed. (1996)
201. Djilkibaev Zh. *Proc. Workshop Simulations and Analysis Methods for Large Neutrino Telescopes, DESY Zeuthen, Germany, July 6–9, 1998*, ed. C Spiering, DESY-PROC-1999-01:132 (1999)
202. Price PB. *Proc. Workshop Simulations and Analysis Methods for Large Neutrino Telescopes, DESY Zeuthen, Germany, July 6–9, 1998*, ed. C Spiering, DESY-PROC-1999-01:120, astro-ph/9501073
203. Spiering C. *Int Workshop Neutrino Telescopes, 8th, Venezia, 1999*, ed. M Baldo-Ceolin, II:63. Padova, Italy: Univ. Padova (1999)
204. Halzen F, Zas E, Stanev T. *Proc. Int. Cosmic Ray Conf., 22nd, Dublin, 1991*, ed. M Cawley, et al 4:686 (1992)
205. Camerini U, et al. *Proc. Int. Cosmic Ray Conf., 23rd, Calgary, July 1993*. DUMAND-4-93 (1993)
206. Learned JG. *Phys. Rev. D* 1:19, 3293 (1979), and Ref. 208
207. Price B. *Nucl. Instrum. Methods A* 325:346–56 (1993)
208. Hunter SD, et al. *J. Acoust. Soc. Am.* 69:1557 (1981)
209. Dedenko LG, et al. *Proc. Int. Cosmic Ray Conf., 25th, Durban, S. Africa, Aug., 7:89 (1997)*
210. Halzen F, Learned JG, Stanev T. *Astrophys. in Antarctica, Bartol, AIP Conf. Proc.* 198:39. New York: AIP (1990)
211. Deleted in proof
212. Kotzer P, ed. *Proc. DUMAND 1975 Summer Study, Bellingham, WA, July*. Bellingham, WA: W. Washington State College (1976)
213. Roberts A, ed. *Proc. 1976 DUMAND Summer Workshop, Honolulu, HI, Sept. 1976*. Batavia, IL: Fermilab (1977)
214. Roberts A. *Rep. 1977 Summer Workshop, Moscow, June 1977, ESN, 31-9, Sept.*

- 1977, p. 370. London: Off. Naval Res. (1977)
215. Bradner H, ed. *Proc. La Jolla 1977 Workshop Signal Processing*. La Jolla, CA: Scripps Inst. Oceanogr. (1978)
 216. Wilkins G, ed. *Proc. San Diego Summer Workshop Ocean Eng., Aug. 1977*. San Diego, CA: Naval Ocean Systems Cent. (1978)
 217. Roberts A, et al, eds. *Proc. 1978 DUMAND Summer Study, La Jolla, CA. Vol. 1: Array Studies*, La Jolla, CA: DUMAND, Scripps Inst. Oceanogr., 351 pp. (1978); Roberts A, ed. *Vol. 2: UHE Interactions and Neutrino Astronomy*, 213 pp. (1978); Wilkins G, ed. *Vol. 3: Oceanographic and Ocean Engineering Studies*, 213 pp. (1978)
 218. Learned JG, ed. *Proc. Khabarovsk Lake Baikal DUMAND Meet., Sept. 1979*, 376 pp. Honolulu, HI: Hawaii DUMAND Cent. (1980)
 219. Roberts A, ed. *Proc. DUMAND Signal Processing Workshop, Honolulu, February 1980*. Honolulu, HI: Hawaii DUMAND Cent. (1981)
 220. Stenger VJ, ed. *Proc. 1980 DUMAND Summer Symp., Honolulu, HI, July–Aug.*, 2 vols. Honolulu, HI: Hawaii DUMAND Cent. (1981)
 221. Roberts A, ed. *Proc. DUMAND 1980 Deployment Workshop, La Jolla, CA, Dec. 1980*. Honolulu, HI: Hawaii DUMAND Cent. (1981)
 222. Roberts A, ed. *Proc. DUMAND 1982 Signal Processing Workshop, Honolulu, HI, Feb. 1982*. Honolulu, HI: Hawaii DUMAND Cent. (1982)
 223. Roberts A, Wilkins G, eds. *Proc. 1984 DUMAND Workshop Ocean Eng. and Deployment, La Jolla, CA, Aug. 1984*. Honolulu, HI: Hawaii DUMAND Cent. (1984)
 224. Roberts A, ed. *Proc. 1988 DUMAND Workshop Ocean Eng. and Deployment, January 1988, and Proc. 1988 DUMAND Workshop Signal Processing, March 1988*. Honolulu, HI: Hawaii DUMAND Cent. (1988)
 225. Wilkes J, Young K, eds. *Proc. 1990 DUMAND Trigger Workshop, July 1990*. Seattle, WA: Univ. Washington Dep. Phys. (1990), Rep. HDC-17-90
 226. Tanaka S, Yamaguchi A. *Proc. 1990 DUMAND Optical Module Workshop, Sendai, Jpn., Oct. 1990*. Sendai, Jpn.: Bubble Chamber Phys. Lab., Tohoku Univ. (1990), Rep. HDC-16-90
 227. Resvanis L, ed. *NESTOR Int. Workshops, Pylos, Greece, 1991, 1992, 1993*. Athens: NESTOR Lab., Univ. Athens (1992, 1993, 1994)
 228. Baldo-Ceolin M, ed. *Int. Workshop on Neutrino Telescopes, Palazzo Loredan, Campo Santo Stefano, Venezia*. Padova, Italy: Univ. Padova. 8 workshops (1988, 1990, 1991, 1992, 1993, 1994, 1997, 1999)
 229. Chaloupka V, et al. LBL-38321, Feb. 1996. 62 pp. (1996)
 230. Spiering C, ed. *Simulation and Analysis Methods for Large Telescopes, DESY, Zeuten, Germany July 6–9, 1998*. DESY-PROC-1999-01
 231. Hauptman J, et al. *Proc. Int. Cosmic Ray Conf., 23rd, Calgary, July 1993*. DUMAND-5-93 (1993).
 232. Wilkes RJ, et al. *Proc. Int. Symp. UHE Cosmic Ray Interactions, 7th, Ann Arbor, MI, June 1992*. UWSEA PUB 92-15, DUMAND-9-92 (1992)
 233. Hanada H, et al. *Nucl. Instrum. Methods A*, 408A:2,3,425 (1998)
 234. Bolesta J. *Upper limits to neutrino emission from active galactic nuclei and quasars*. PhD thesis. Univ. Hawaii, Honolulu (1998)
 235. Krabi J, et al. Zeuthen preprint PHE 91-013, 12/91 (1991)
 236. Resvanis LK, et al. *Proc. Workshop on High Energy Neutrino Astronomy, HENA '92, Mar. 23–26*, ed. V Stengh, J Learned, S Pakvasa, X Tata. Singapore: World Sci. (1992)

237. Bosetti PS. In *Observational Neutrino Astronomy*, ed. D Cline, p. 249. Singapore: World Sci. (1988)
238. Adams A, et al. GRANDE Proposal, GRANDE 90-005, UCI (1990)
239. Nishikawa K. *Proc. Venice Workshop. Neutrino Telescopes, 4th, Padova*, ed. M Baldo-Ceolin. Padova, Italy: Univ. Padova (1991)
240. Moscoso L, et al. NET Proposal, Padova, 3/92 (1992)
241. Bergstrom L, Johansson S. See Ref. 235
242. Reid J, et al. See Ref. 204, 4:678
243. Auriemma G. See Ref. 204, 4:682
244. Atkins R, et al (Milagro Collaboration). astro-ph/0001111, astro-ph/9909090 (2000)
245. Provorov A, et al. See Ref. 235, p. 337 (1991)
246. Deleted in proof
247. Cervera A, et al. hep-ph/0002108 (2000); McDonald KT, et al. physics/9911009 (1999)
248. Balkanov VA, et al (Baikal Collaboration). astro-ph/0001145. <http://www.ifh.de/baikal/baikalhome.html>
249. Andres E, et al (AMANDA Collaboration). astro-ph/9906203. <http://alizarin.physics.wisc.edu/>
250. Trasatti L, et al (NESTOR Collaboration). *Nucl. Phys. Proc. Suppl.* 70:442 (1999). <http://www.uoa.gr/~nestor/intro.html>
251. Montanet F, et al (ANTARES Collaboration). astro-ph/0001380 (2000). <http://antares2.in2p3.fr/>
252. Montaruli T for NEMO Collaboration. See Ref. 246, 2:448, hep-ex/9905019
253. Halzen F, et al (AMANDA Collaboration). Prepared for *Int. Cosmic Ray Conf., 26th, Salt Lake City, UT, Aug 17-25, 1999*. <http://alizarin.physics.wisc.edu/karle/icecube/>
254. Diwan M, ed. *NNN99 and NNN2000, Proc. Int. Workshop Next Generation Nucleon Decay and Neutrino Detector, Sept. 23-25, 1999, Stony Brook, NY*. In press (2000). <http://k2k.physics.sunysb.edu/NNN99/>
255. Antonioli P, et al. CERN-SPSC-98-37 (1998); Ypsilantis T, et al. *Nucl. Instrum. Methods A* 371:330 (1996)



CONTENTS

Various Researches in Physics, <i>Vernon W. Hughes</i>	0
The Shears Mechanism in Nuclei, <i>R. M. Clark, A. O. Macchiavelli</i>	1
Energy Loss in Perturbative QCD, <i>R. Baier, D. Schiff, B. G. Zakharov</i>	37
The CDF and DO Upgrades for Run II, <i>T. LeCompte, H. T. Diehl</i>	71
Precision Nuclear Measurements with Ion Traps, <i>G. Savard, G. Werth</i>	119
The Quantum Physics of Black Holes: Results from String Theory, <i>Sumit R. Das, Samir D. Mathur</i>	153
Precision Measurements of the W Boson Mass, <i>Douglas A. Glenzinski, Ulrich Heintz</i>	207
Developments in Rare Kaon Decay Physics, <i>A.R. Barker, S.H. Kettell</i>	249
Strangeness Production in Heavy-Ion Collisions, <i>Spyridon Margetis, Karel Safarik, Orlando Villalobos Baillie</i>	299
Random Matrix Theory and Chiral Symmetry in QCD, <i>J.J.M. Verbaarschot, T. Wettig</i>	343
On the Production of Superheavy Elements, <i>P. Armbruster</i>	411
Recent Progress in Neutron Star Theory, <i>Henning Heiselberg, Vijay Pandharipande</i>	481
Prospects for Spin Physics at RHIC, <i>Gerry Bunce, Naohito Saito, Jacques Soffer, Werner Vogelsang</i>	525
B Mixing, <i>Colin Gay</i>	577
The QCD Coupling Constant, <i>Ian Hinchliffe, Aneesh Manohar</i>	643
High-Energy Neutrino Astrophysics, <i>John G. Learned, Karl Mannheim</i>	679